

THE UNIVERSITY OF CHICAGO

ENGINEERING THE IMMUNE SYSTEM TO IMPROVE VACCINES: FROM
MOLECULAR PROBE DESIGN TO TRANSLATIONAL APPLICATIONS

A DISSERTATION SUBMITTED TO
THE FACULTY OF THE PRITZKER SCHOOL OF MOLECULAR ENGINEERING
IN CANDIDACY FOR THE DEGREE OF
DOCTOR OF PHILOSOPHY

BY
BRITTANY ANNE MOSER

CHICAGO, ILLINOIS

JUNE 2019

Portions of Chapter 1 have been reproduced in part with permission from: Tom, J.; Albin, T.; Manna, S.; Moser, B.; Steinhardt, R.; Esser-Kahn, A. Application of immunomodulatory immune synergies to adjuvant discovery and vaccine development. *Trends Biotechnol.* 37 (4) 373-388, 2019. © 2019 Elsevier Inc.

Portions of Chapter 2 have been reproduced in part with permission from: Moser, B.; Steinhardt, R.; Escalante-Buendia, Y.; Boltz, D.; Barker, K.; Yoo, S.; McGonnigal, B.; Esser-Kahn, A. Immune potentiator for increased safety and improved protection of vaccines by NF- κ B modulation. *BioRxiv*<https://doi.org/10.1101/489732> © 2018 Brittany A. Moser & Aaron P. Esser-Kahn

Portions of Chapter 4 have been reproduced in part with permission from: Moser, B.*; Steinhardt, R.*; Esser-Kahn, A. Surface coating of nanoparticles reduces background inflammatory activity while increasing particle uptake and delivery. *ACS Biomater. Sci. Eng.*, 3(2), 206-213, 2017. © 2017 American Chemical Society

Portions of Chapter 5 have been reproduced in part with permission from: Moser, B. & Esser-Kahn, A. A Photoactivatable innate immune receptor for optogenetic inflammation. *ACS Chem. Biol.*, 12 (3), 347-350, 2017. © 2017 American Chemical Society

All other materials © 2019 Brittany A. Moser
All rights reserved.

Table of Contents

List of Tables.....	vii
List of Figures.....	viii
List of Schemes.....	xii
Acknowledgements.....	xiii
Abstract.....	xiv
1 Introduction.....	1
1.1 Introduction.....	1
1.2 Innate and Adaptive Immune System.....	2
1.3 Effect of PRR Activation.....	3
1.4 Importance of NF-κB in innate and adaptive immune activation.....	4
1.5 History of Vaccines.....	5
1.6 Vaccine Types.....	6
1.7 Vaccine adjuvant types and discovery.....	8
1.8 Strategies and progress for adjuvant development.....	9
1.9 Current State of Vaccine Adjuvants.....	10
1.10 High Throughput Screening of Immune Agonist Synergies for Adjuvant Discovery.....	16
1.11 Chemically Conjugated Synergistic Adjuvants.....	18
1.12 Particulate Delivery Systems for Immune Synergies.....	20
1.13 Synergistic Adjuvants in Vaccination Models.....	22

1.14	Clinical Synergistic Adjuvants.....	24
1.15	Applying Synergistic Studies to Adjuvant Design.....	25
1.16	Characterizing Synergistic Vaccine Efficacy.....	28
1.17	Future Perspective of synergies in vaccines.....	29
1.18	Challenges of using TLR agonists as vaccine adjuvants.....	30
1.19	Understanding synergies.....	31
1.20	Vaccine side effects.....	31
1.21	References.....	32
2	Immune potentiator for increased safety and improved protection of vaccines by NF-κB modulation.....	50
2.1	Summary.....	50
2.2	Introduction.....	50
2.3	Results and Discussion.....	52
2.3.1	Selection of Immune Potentiator.....	52
2.3.2	Examination of CpG-induced inflammation and resulting immune response.....	54
2.3.3	Immune potentiation in in vivo influenza challenge model.....	57
2.3.4	Examination of immune potentiator on Dengue neutralization.....	62
2.3.5	Analysis of influence of immune potentiator of HIV vaccination.....	62
2.3.6	Improvement of adjuvant responses across a variety of TLRs and Species.....	64
2.3.7	Exploration of the mechanism of action.....	66
2.4	Conclusion.....	70
2.5	Materials and methods.....	72
2.6	References.....	82

3	Small molecule NF-κB inhibitors as immune potentiators for enhancement of vaccine adjuvants.....	89
	3.1 Summary.....	89
	3.2 Introduction.....	89
	3.3 Results and discussion.....	90
	3.3.1 Exploration of small molecule NF- κ B inhibitors in vitro.....	90
	3.3.2 Exploration of small molecule NF- κ B inhibitors in vivo.....	92
	3.3.3 Dose-dependence of capsaicin and honokiol.....	93
	3.3.4 Determining the TRPV1-mediated effects of capsaicin.....	94
	3.3.5 Synthesis of honokiol derivative library.....	96
	3.4 Conclusion.....	99
	3.5 Materials and methods.....	99
	3.6 References	102
4	Surface Coating of Nanoparticles Reduces Background Inflammatory Activity while Increasing Particle Uptake and Delivery.....	106
	4.1 Summary.....	106
	4.2 Introduction.....	106
	4.3 Design of polymeric delivery system.....	107
	4.4 Results and Discussion.....	108
	4.4.1 Synthesis of coated polystyrene particles.....	108
	4.4.2 Physical properties of coated microparticles.....	109
	4.4.3 Immune response to core-shell constructs.....	111
	4.4.4 Agonist loading.....	115

4.4.5	Biomimimetic Nature of Core-Shell Particles.....	119
4.5	Conclusion.....	123
4.6	Materials and methods.....	123
4.7	References.....	127
5	A Photoactivatable Innate Immune Receptor for Optogenetic Inflammation.....	134
5.1	Summary.....	134
5.2	Introduction.....	134
5.3	Results and Discussion.....	136
5.3.1	Design of photoactivated receptor.....	136
5.3.2	Blue light-induced Photo-DAI activation.....	137
5.4	Conclusion.....	139
5.5	Materials and methods.....	140
5.6	References.....	143
	Appendix A.....	146
	Appendix B.....	156
	Appendix C.....	157
	Appendix D.....	179

List of Tables

Table 1.1 Adjuvants Used in FDA Approved Vaccines.....	11
Table 1.2 Natural Pathogens that Activate Multiple PRRs.	15
Table 1.3 Synergistic PRR Combinations Activated by Adjuvants in Vaccination Models.	23
Table 1.4 Synergistic Adjuvants Employed in Clinical Trials.....	25
Table 4.1 qPCR panel of immune genes.....	114
Table C1. Table of DLS, Zeta potential and EDS data.....	174

List of Figures

Figure 1.1 Overview of Innate and Adaptive Immune Activation by a Pathogen.....	13
Figure 2.1 In vivo vaccination with model antigen ovalbumin and immune adjuvant SN50.....	53
Figure 2.2 Influenza Challenge Model.....	56
Figure 2.3 In vivo vaccination against dengue and HIV.....	61
Figure 2.4 In vivo vaccinations across a broad range of adjuvants.....	64
Figure 2.5 Exploration of SN50 mechanism of action.....	68
Figure 3.1 Small molecule NF- κ B inhibitor screen in vitro.....	91
Figure 3.2 Small molecule inhibitor screen in vivo.....	92
Figure 3.3 Dose effects of honokiol and capsaicin.....	94
Figure 3.4 Role of TRPV1 of capsaicin induced anti-inflammatory and immune potentiation...96	
Figure 3.5 Honokiol derivatives and their inhibitory activity on IL-6 expression.....	98
Figure 4.1 Schematic of cellular outcomes of particle exposure.....	108
Figure 4.2 Microscopy of particles.....	110
Figure 4.3 Light microscopy of particles in media.....	111
Figure 4.4 NF- κ B activity of coated and uncoated particles.....	112
Figure 4.5 IL-1 β expression in THP-1 cells.....	113

Figure 4.6 Cell activation and endocytosis of coated and uncoated particles.....	116
Figure 4.7 Cell internalization of particles.....	118
Figure 4.8 Cell uptake of particles.....	121
Figure 4.9 Fluorescence microscopy of sorted cells.....	122
Figure 5.1 Schematic of photo-DAI activation.....	135
Figure 5.2 Photo-DAI activity in HEK Blue cells.....	136
Figure 5.3 Fluorescent reporting of dimerization from cells expressing photo-DAI.....	137
Figure 5.4 Biological activity of RAW Blue ISG cells transduced with photo-DAI system....	138
Figure A1. NF- κ B activity in mouse and human cells.....	146
Figure A2. Gating strategy for BMDC flow cytometry.....	147
Figure A3. Proinflammatory Cytokine Analysis Time Course.....	148
Figure A4. Weight Loss Post-Vaccination.....	149
Figure A5. Gating strategy for antigen specific splenocyte assay.....	150
Figure A6. Serum IgG2a, IgG2b, IgG3, IgM, IgA Antibody concentrations.....	151
Figure A7. Safety vs. Protection score.....	152
Figure A8. Gating strategy for THP-1 cell surface staining CD86 (FITC), CD40 (PE).....	153
Figure A9. Gating strategy for NHP PBMC cell surface staining, CD86 (FITC).....	154
Figure A11. Lymph node flow cytometry gating strategy.....	155

Figure C1. SEM image of coated PS particle with histogram of particle size distribution.....	157
Figure C2. SEM image of coated PS particle 80,000x.....	158
Figure C3. SEM image of coated PS particle 500,000x.....	159
Figure C4. EDS data of coated PS particles sputtered with Au/Pd.....	159
Figure C5. SEM image of PS particle 5,000x with histogram of particle size distribution.....	160
Figure C6. EDS data of PS particles sputtered with Ir.....	161
Figure C7. SEM image of coated PMMA particle with histogram of particle size distribution.	162
Figure C8. SEM image of coated PMMA particle 1,999x.....	163
Figure C9. EDS data for coated PMMA particles.....	163
Figure C10. SEM image of PMMA particle with histogram of particle size distribution.....	164
Figure C11. SEM image of PMMA particle 25,000x.....	165
Figure C12. EDS data of PMMA particles sputtered with Ir.....	165
Figure C13. SEM image of coated PLGA particle with histogram of particle size distribution.....	166
Figure C14. SEM image of coated PLGA particles 1,857x.....	167
Figure C15. EDS data of coated PLGA particles prepared in a solution of PBS.....	167
Figure C16. SEM image of PLGA particle 1,200x with histogram of particle size Distribution.....	168
Figure C17. SEM image of PLGA particles 10,833x.....	169

Figure C18. EDS data of PLGA particles sputtered with Ir.....	169
Figure C19. SEM image of coated PE particles with histogram of particle size distribution....	170
Figure C20. SEM image of coated PE particles 1,700x.....	171
Figure C21. EDS data of coated PE particles.....	171
Figure C22. SEM image of PE particles with histogram of particle size distribution.....	172
Figure C23. SEM image of PE particles 1,993x.....	173
Figure C24. EDS of PE particles sputtered with Ir.....	173
Figure C25. Confocal microscopy image of PS-CpG bead.....	175
Figure C26. Flow cytometry plot of unlabeled PS particle.....	176
Figure C27. Flow cytometry gating for cells vs. beads using forward scatter vs. side scatter...	176
Figure C28. Gating strategy for cells vs. beads.....	177
Figure C29. Flow cytometry histograms.....	178
Figure D1. Photo-DAI activity in HEK Blue cells.....	179
Figure D2. Flow cytometry analysis of mCherry fluorescence from photo-DAI activation using light or 100 ng/ mL poly(dA:dT).....	180

List of Schemes

Scheme 3.1. Honokiol derivative synthesis.....	97
--	----

Acknowledgements

I am so grateful to have had the opportunity to work in the Esser-Kahn lab. To my PhD advisor, Prof. Aaron Esser-Kahn I cannot thank you enough for the support and guidance you've given me the last five years. Thank you for believing in me and my ideas (long before I believed in myself) and always encouraging me to think bigger. I have learned so much from you.

To the rest of my thesis committee Prof. Jun Huang and Prof. Jeffery Hubbell, thank you so much for your support and exceptional scientific guidance. To Prof. Jennifer Prescher and Prof. Chang Liu thank you for your support over the years. Your insight and guidance during the preliminary stages of this work helped shape what it is today.

I want to thank the entire Esser-Kahn lab for being an amazing place to do science and enjoy life. Rachel, thank you for being an incredible colleague, mentor and friend. I will never forget our fun brainstorming sessions and toaster oven lunches. To Britteny, Matt, Liza, Alfred, Flora, and Jainu thank you for being amazing to work with and even better friends. To Yoseline, Ngoctran, Minh, Tina and Jenny, thank you so much for being incredible undergraduate researchers. Thank you for sharing my passion and enthusiasm for the work. To Tyler and Seong-min, thank you for being in this with me from the beginning and hitting all the milestones with me. I am so grateful for your friendship. Thank you to Tim for being a great friend and always getting the lab together. To Yoseline, JingJing, Beth and Troy thank you for all of your help! None of this work would be possible without you.

Thank you to Brandon, Alana, Hanh, Sam, Caleb, Christian and Stan for getting me through first year and beyond. I will never forget our french fri-days and w(h)ine nights. Thank you to Dr. Alfredo Freitas for believing in me, encouraging me and always giving good advice.

To my parents who have been a huge support through this entire process (and long before), thank you. Your encouragement and support mean the world to me.

Dan, thank you for being the best partner to walk this journey with. I am so grateful for your love and support.

Abstract

Vaccines are one of the greatest achievements to public health allowing almost complete eradication of small pox and polio and dramatically reducing the incidence of a variety of other diseases. However, many diseases still exist without a vaccine. To create vaccines for these diseases we need to understand and create enhanced responses that enable proper immune activation. This organized activation can be achieved using adjuvants, components added to the vaccine to enhance the immune response. Typically, vaccines have been empirically derived, leading to expensive and lengthy development periods. Our lab is focused on creating tools to enable rational and optimized vaccine design. My work focuses on two main areas: creating tools to probe immune responses on the single-cell level, leading to a greater understanding of immune activation and applying this understanding to create more effective vaccines to challenging diseases.

One of the biggest challenges of creating new vaccines is attaining an adequate safety profile. Many vaccines can provide protection but do not translate to the clinic due to the high levels of inflammation they induce. CpG, a synthetic bacterial DNA mimic, has demonstrated great promise as an adjuvant, however most vaccines that include CpG do not make it through clinical trials. Using an NF- κ B inhibitor, we demonstrate that we can enhance the safety and protection afforded by CpG and many other common adjuvants.

Many of the most effective vaccines stimulate multiple innate immune pathways. When this combination of pathways leads to enhancement of the immune response this is known as an immune synergy. Although the existence of immune synergies is well understood, the mechanism of enhanced activity is still unknown. Few tools exist to directly examine spatial and temporal elements of immune activation and synergies. Described here are two tools to elucidate

the spatiotemporal aspects of innate immune responses. The first is a particle-based system allowing effective agonist presentation and tracking of activated cells. The second is an optogenetic innate immune receptor allowing the receptor to be activated with the spatial and temporal precision of light.

1 Introduction

1.1 Introduction

Vaccines are one of the most effective forms of disease prevention available to humans and animals providing extended survival and improved quality of life.¹ Vaccines educate the immune system to recognize target pathogens without ever being at risk for the disease.^{2,3} To date, effective vaccines have been designed empirically, usually relying on inactivated or attenuated forms of the pathogen.⁴⁻⁷ This approach has enabled several successful vaccines, leading to the eradication of small pox and near eradication of polio.⁸ Although this approach is successful for a handful of diseases, it presents challenges for others.^{9,10} Some weakened or inactivated pathogens are not immunogenic enough on their own to produce a robust and life-long immune response and therefore do not lead to protection.¹¹ Additionally, the amount of pathogen needed, storage conditions and side effects are all important factors that could cause a vaccine to fail during clinical trials, leaving the public without protection.^{3,12-16} Overcoming these challenges requires a deep understanding of the mechanistic framework that underlies the immune response and unique, adaptable and scalable tools to effectively tune the protective nature of the vaccine.

By exploring the mechanisms by which the immune system is ultimately governed and applying that knowledge to vaccine formulation, we hope to improve vaccine efficacy and safety and widen the scope of diseases that can be prevented by prophylaxis. By utilizing tools from optogenetics, we can build immune receptors from the ground up, enabling precise spatiotemporal precision over activation. Employing single-cell technology will provide key insights into immune activation. Lastly, analyzing key pathways involved in immune activation and modulating them accordingly will lead to breakthroughs in vaccine technology.

1.2 The Innate and Adaptive Immune System

The immune system has two branches, the innate immune system that acts quickly and non-specifically and the adaptive immune system that takes time to develop, but is specific to a particular pathogen.⁷ Both responses are important in fighting disease and are intrinsically linked through feedback mechanisms. In response to infection, innate immune cells which express pattern recognition receptors (PRRs) recognize pathogen associated molecular patterns (PAMPs) on the invader and are the first to respond, sending out chemical signals such as cytokines and chemokines to the surrounding environment.¹⁷ Antigen presenting cells (APCs) such as dendritic cells, macrophages and B cells infiltrate the area, become activated by PAMPs and begin engulfing pathogens and cellular debris and processing them for expression on the major histocompatibility complex (MHC) for display on the cell surface.⁷ This surface presentation signifies what antigens the cell has encountered. This surface presentation is the link between the innate and adaptive immune system and is incredibly important for creating successful vaccines. After activation, the APCs express other surface receptors important for costimulation, such as CD40 and CD86. This key step of activating the APC is an important link between the innate and adaptive immune system.

The APCs then travel to the lymphnode where eventually they will encounter a T cell with a T cell receptor (TCR) that recognizes the MHC-peptide complex on the APC.⁷ Additionally, the costimulatory molecules on the APC are recognized by the T cell and signal to the T cell to expand, creating more T cells expressing the same TCR. This expanding T cell population is created to increase the probability of discovering a B cell that has engulfed antigen and is presenting the same MHC-peptide as the APC that originally activated the T cell. Upon activation by the T cell, the B cell will proliferate and differentiate into memory B cell and

plasma B cells. Memory B cells remain in circulation and provide a memory response to a particular pathogen. Plasma B cells produce antibodies.

1.3 Effect of PRR activation

There are several subclasses of pattern recognition receptors such as retinoic acid-inducible (RIG) receptors, C-type lectin, dectins, nucleotide-binding oligomerization domain (NOD) -like receptors and toll like receptors (TLRs).¹⁸ TLRs are the most well-characterized PRRs. TLRs are an actively being explored as vaccine adjuvants because this class of receptors natively recognizes the most common pathogen associated molecular patterns present on bacteria viruses, etc. Responses of PRRs to PAMPs lead to strong and effective immune responses. There are ten types of TLRs in humans that recognize different classes of PAMPs. TLRs contain a horseshoe-shaped motif comprising of several leucine-rich repeat units (LRRs). Two TLRs come together around LRRs to form a constitutive dimer. TLR dimers can be homodimers between two of the same TLR or TLR heterodimers where two different TLR types come together. TLRs can signal either from the cell surface or from the endosome. TLRs that signal from the cell surface include: TLR 1, 2, 4, 5, and 6. These receptors activate in response to molecules located on the surface on pathogens. TLRs that activate in the endosome are TLR3, 7, 8, and 9. These TLRs recognize molecules that are located within a pathogen such as RNA or DNA. In response to PRR activation transcription factors such as NF- κ B and IR3 are activated priming the transcription of a variety of cytokines, chemokines and cell surface receptors. Downstream responses to PRRs such as TLRs lead to lasting immunity.

1.4 Importance of NF- κ B in innate and adaptive immune activation

NF- κ B is a transcription factor that resides in every single cell in the human body, at all times.¹⁹ This transcription factor remains in the cytoplasm until intracellular signaling pathways uncover its nuclear localization sequence enabling it to migrate to the nucleus where it can prime the transcription of more than 400 immune genes.²⁰ This process begins with activation of a receptor, either a PRR such as a TLR or a cytokine receptor.²¹ The downstream transcription is tailored to the particular type of receptor activation. NF- κ B accomplishes this variety of gene profiles through subunit diversity.¹⁹ NF- κ B is a family of transcription factors made up of two subunits- a DNA binding domain and a transcriptional activator domain. Together these subunits form a dimer that can both bind specific DNA sequences, called promoters, and can activate transcription. Each DNA binding domain has a unique affinity for a particular promoter leading to select gene transcription in response to specific subunit activation. Each transcriptional activator has different affinities for other transcription factors leading to large complexes that either upregulate or downregulate transcription. Additionally, dimers can form between DNA binding domain subunits, leading to promoter binding, but not transcription—essentially blocking transcription of specific genes. The variety of subunits and their functions leads to diversity in the results gene profile and immune response. As NF- κ B is a master regulator of a significant number of immune genes, the immune system has evolved to balance the expression of immune genes. Although the work has been pursued to identify the significance of each subunit, more studies need to be conducted to fully elucidate the functions of each subunit and how they work together.

1.5 History of vaccines

Throughout history vaccines have taken a variety of forms beginning with smallpox inoculation. As early as 430 BC it was identified that those who had survived smallpox did not contract the disease again and survivors were called upon to nurse the ill. From this it became clear that our bodies have complex mechanisms that enable us to remember past infections.²² This understanding led to the innovation of the first “vaccine” where a small amount of material from a smallpox pustule was transferred from a patient with the disease to a non-immune patient, this process was termed inoculation. The material was scratched into the skin with the hope that a mild, but still protective infection would result. Typically, patients would develop a less severe infection than naturally acquired smallpox, however after inoculation the illness would last weeks to months.²² The second generation of a vaccine came in the 1700s from Edward Jenner. Jenner noticed that milkmaids who had previously been ill with cowpox, did not show symptoms upon infection with smallpox. This interesting connection led to an improvement in the inoculation procedure. Instead of inoculating with smallpox, Jenner inoculated with cowpox, a much less severe disease.²² From this we learned that some less harmful diseases could protect against more severe and devastating diseases. This eventually led to the idea that pathogens could be attenuated by adapting them to other species making them less infectious to humans. Albert Sabin used a rodent-adapted polio virus to use as a vaccine against polio. Later, it was discovered by Jonas Salk that inactivating the virus by chemical means could lead to long-lasting immunity while enhancing the safety of the vaccine.^{23,24} These instances paved the way for empirical design of many modern vaccines.

1.6 Vaccine Types

There are four main categories of vaccines recognized by the World Health Organization (WHO): Live attenuated, inactivated, toxoid and subunit vaccines.^{7,25} Each vaccine type has found use against select pathogens delivering safe and effective protection from disease.

Live attenuated vaccines are vaccines that use a weakened form of a live virus. The attenuation is achieved by passage through a foreign host.^{6,25,26} This can be done in vitro using tissue culture, or in vivo through embryonated eggs or live animals.^{6,25,26} The foreign host acts as a selection for host-optimized virus, eventually becoming so optimized for the host that it is not infectious to humans. The attenuation process makes it easier for the human immune system to eliminate, but keeps necessary components for effective immune response. Vaccines of this type are advantageous because they activate all phases of the immune system. Because the intact virus is administered, it contains PAMPs that are recognized by the innate and adaptive immune systems. The virus will replicate very slowly enabling typical host-pathogen interactions and adaptations, leading to a robust innate and adaptive immune response.^{7,25} These vaccines are generally low cost because they contain only the virus and no additional manufactured components are required. The potential for the virus to mutate back to the infectious variant is a disadvantage of this vaccine especially for immunocompromised patients.²⁷ Typically, immunocompromised individuals are cautioned not to receive vaccines of this type causing them to rely on herd immunity for protection. These vaccines need to be stored at proper environments for the virus to remain viable which can sometimes present problems in shipping and maintenance of vaccine lots.^{15,28} Vaccines of this type currently administered in the clinic are: tuberculosis, measles vaccine, yellow fever and the live-attenuated vaccine for seasonal influenza.

Inactivated vaccines consist of a virus, bacteria or other pathogen that have been rendered inactivated using a method such as heat or formaldehyde.²⁵ This inactivation leads to a non-infectious pathogen that can safely be used in vaccination. This is advantageous for immune compromised patients because they can safely be vaccinated without fear of infection. This type of vaccine often requires booster vaccines because the inactivation process interferes with full establishment of immunity. Pertussis and the most commonly used seasonal flu vaccine are inactivated vaccines.

Toxoid vaccines are another class with inactivated components. The toxin produced by the pathogen is inactivated by heat or formaldehyde. In this case, immunity is being formed to the toxin produced by the pathogen, rather than to the pathogen itself. Tetanus and diphtheria are an example of this type of vaccine.

Subunit vaccines consist of one of (or subset of) the proteins or sugars responsible for infection. This antigen can either be expressed in a different virus or bacteria creating a recombinant pathogen or the components for this vaccine are expressed and purified enabling more intentional and repeatable dosage. This type of vaccine is favorable due to the increased control over purity, dosage and reproducibility in antibody formation. Each subunit consists of a particular antigen that is important to providing immunity. By controlling which subunits and the amount of each subunit is in the vaccine, the resulting immunity is more reproducible. Typically, these vaccines are more shelf-stable enabling efficacy to be maintained in a variety of environmental conditions. Current clinical vaccines of this type include hepatitis B, some seasonal flu vaccines, and pneumonia vaccine. The subunits typically are not immunogenic enough on their own, so adjuvants are added to increase the immune response.

1.7 Vaccine adjuvant types and discovery

Adjuvants are components added to vaccines to increase the immune response, leading to protection. Adjuvants are required when vaccine formulations are not immunogenic enough to elicit protection.²⁹ Ideally adjuvants are stable with a long shelf life, biodegradable or easy to metabolize, inexpensive to produce on large scales, do not induce immune responses to themselves and promote the desired cellular or humoral immune response against the antigen of interest.^{29,30}

Currently, very few adjuvants are approved for use in humans in the United States.³¹ The most common adjuvant is aluminum formulated as amorphous aluminum hydroxyphosphate sulfate (AAHS), aluminum hydroxide, aluminum phosphate or potassium aluminum sulfate (Alum). The adjuvanting power of aluminum salts was discovered in 1920 when it was observed that variations in batches led to significant changes in the effectiveness of the vaccines. This variability was determined to be due to contamination of the reaction vessels, where “dirty” vessels demonstrated and increased effectiveness. From then on a variety of salts and substances were combined with vaccines to assess how effectively they boost the immune response. Although many substances boosted immune responses, for decades alum was the only adjuvant approved for use in humans.

In the last decade, a few other adjuvants have been approved for use in humans in the United States.³¹ MF59 is an oil-in-water emulsion composed of squalene. This adjuvant improves immune cell infiltration and aids in transport of antigen to the lymphnode, improving presentation to adaptive immune cells.³² Other adjuvants use synthetic PAMP-like derivatives that activate TLRs. AS04 which consists of Monophosphoryl lipid A (MPLA) combined with alum.³³ MPLA activates TLR4 leading to improved innate immune response.³⁴ AS01B consists

of MPLA and QS-21, a natural compound found in the tree *Quillaja Saponaria*. The mechanism of QS-21 has not yet been fully elucidated but membrane lysis has been noted to be involved.³⁵ Lastly, CpG ODN 1018 has been approved for use in a single vaccination, HepB. CpG is a synthetic DNA mimic consisting of cytosine phosphoguanine that mimics bacterial genetic material.³⁷ While these approved adjuvants have enabled protection against a variety of diseases, many diseases cannot be prevented with current vaccine technologies and therefore new and improved adjuvants need to be created.

1.8 Strategies and progress for adjuvant development

The need to develop new vaccines for diseases that continue to threaten public health, such as HIV and malaria, as well as emerging diseases, like Ebola and Zika virus still exists. However, most vaccines are empirically derived, with little understanding of their mechanism of action. This lack of understanding makes it difficult to rationally and rapidly develop new vaccines toward prevalent diseases.

The effectiveness of a vaccine is influenced by its composition, where vaccines are composed of an antigen and an adjuvant.³⁸ Treatment with antigens alone can suffer from low immunogenicity, so an adjuvant is required to enhance the immune response toward the antigen of interest³⁹. Adjuvants are typically formulated using a single immune agonist, aluminum salts, and/or in an oil-in-water emulsion. Recently, developing adjuvants that are composed of multiple types of immune agonists has shown promise. This strategy aims to elicit an enhanced immune response, known as an “immune synergy,” potentially providing a more effective vaccine^{40,41}. Here, we provide an overview of immune synergies present in pathogens and successful synergistic combinations used in the clinic. The techniques and topics discussed here can provide future direction and guidance toward advancing synergistic adjuvant and vaccine development.

1.9 Current State of Vaccine Adjuvants

Adjuvants greatly influence the activation and direction of immune signaling pathways and the body's protective response toward infection^{39,42}. Therefore, choosing the appropriate adjuvant is crucial to vaccine efficacy. Alum has been used to adjuvant clinical vaccines for almost a century⁴², followed by oil-in-water emulsions (complete Freund's adjuvant³⁹, MF59-Novartis⁴³, and AS03⁴⁴) and adjuvants containing a mixture of Alum and TLR agonists (AS04, RC529-lipid A mimetic⁴⁵). Alum and Freund's adjuvant, have been successful in enhancing the immune response, but these adjuvants also result in unwanted systemic and local side effects.^{16,46} Since there are few FDA approved adjuvants (e.g. Alum, MPLA - Monophosphoryl Lipid A, CpG-ODN) (Table 1)^{47,48}, there is a greater interest in developing new adjuvants with improved safety profiles that elicit targeted immune responses⁴⁹⁻⁵¹.

Table 1.1 Adjuvants Used in FDA Approved Vaccines.

Adjuvant	FDA Approved Vaccine/Treatment	Ref.
Alum (Aluminum salts)	Hepatitis A, Hepatitis B, Diphtheria-Tetanus-Pertusis (DTaP, Tdap), Haemophilus influenzae type b (Hib), Human Papillomavirus (HPV) - Gardasil, Pneumococcal Infection	42 ^a
AS03 (Tocopherol oil-in-water emulsion)	H5N1 Influenza vaccine	44 ^a
AS04 (Al(OH) ₃ & MPLA)	Cervarix - HPV	45 ^a
MF59 (Squalene oil-in-water emulsion)	Fluad Flu vaccine	43 ^b
RC529 (Lipid A mimetic)	Hepatitis B	45
Al(OH) ₃ & Outer Membrane Vesicles (OMVs – TLR2 & TLR4)	Bexsero - Meningococcal	48 ^c
Amorphous Aluminum Hydroxyphosphate Sulfate (AAHS) & Outer Membrane Protein Complex (OMPC – TLR2)	Pedvax-HIB – Hib, Meningococcal	48 ^d
Imiquimod R837 (TLR7 small molecule agonist)	Carcinoma (topical treatment)	51 ^e
CpG-ODN (TLR9 oligonucleotide agonist)	Hepatitis B	47 ^f

^a<https://www.fda.gov/biologicsbloodvaccines/safetyavailability/vaccinesafety/ucm187810.htm>;

<https://www.fda.gov/biologicsbloodvaccines/vaccines/approvedproducts/ucm101572.htm>;

<https://www.fda.gov/biologicsbloodvaccines/vaccines/approvedproducts/ucm094042>

^b<https://www.fda.gov/BiologicsBloodVaccines/Vaccines/ApprovedProducts/ucm473989.htm>;

<https://www.ncbi.nlm.nih.gov/pmc/articles/PMC5806633/>

^c<https://www.fda.gov/biologicsbloodvaccines/vaccines/approvedproducts/ucm431374.htm>

^d<https://www.fda.gov/downloads/BiologicsBloodVaccines/Vaccines/ApprovedProducts/UCM315680.pdf>

^e<https://www.fda.gov/downloads/Drugs/DevelopmentApprovalProcess/DevelopmentResources/UCM428714.pdf>

^f<https://www.fda.gov/BiologicsBloodVaccines/Vaccines/ApprovedProducts/ucm584752.htm>;

<https://www.fda.gov/downloads/BiologicsBloodVaccines/Vaccines/ApprovedProducts/UCM590189.pdf>

With the need for new adjuvants that generate a specific immune response, PAMPs are being utilized as adjuvants to activate specific PRRs and increase immunogenicity without systemic toxicity. PAMPs inherently activate the immune system in an effective manner (**Fig. 1.1**). This natural efficacy has led to the utilization of native or synthetically optimized PAMP derivatives as adjuvants in vaccines to enhance and elicit specific immune responses against co-administered antigens ⁴⁵. TLR agonists are at the forefront of adjuvant development because TLRs are well characterized and their administration can elicit a strong cellular T_H1 response, which many vaccines lack. ^{39,45} Additional classes of PAMPs, such as nucleotide-binding oligomerization domain (NOD/NLR), stimulator of interferon genes (STING), retinoic acid-inducible gene I (RIG-I), and C-type lectin (CLR) agonists, are also starting to be employed as potential adjuvants. ^{52,53} Targeting specific PRRs from different classes provides a wide range of immune responses because each receptor activates a distinct signaling pathway, thereby influencing innate and subsequent adaptive immune responses to produce defined cellular and antibody responses. ^{54,55}

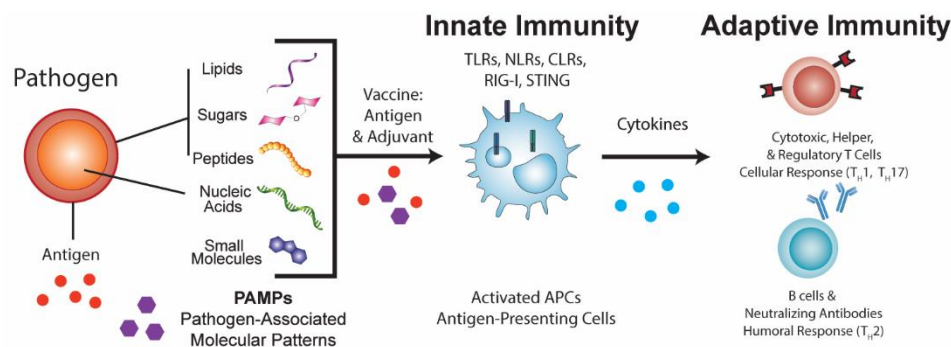


Figure 1.1 Overview of Innate and Adaptive Immune Activation by a Pathogen.

Immunotherapies, including vaccines, eliminate and prevent infection by activating the host immune system against a target pathogen. Effective vaccines stimulate the innate immune system, the rapid response of the body to pathogens, which subsequently interacts with the adaptive immune system to provide a long-term response. The innate immune system is comprised of APCs, such as dendritic cells and macrophages, which express PRRs. PRRs are activated by immunostimulatory molecules (PAMPs) such as ssDNA, lipoproteins, and small molecules that are present in native pathogens. The innate immune system evolved to sense defined sets of pathogen-associated molecules that are potential molecular codes. Each specific code or combination of molecules corresponds to a specific pathogen and elicits a defined immune response (i.e., distinct cytokine production and antigen presentation). The specificity of pathogen recognition and the ability to sense multiple PAMPs are intrinsic to the defense and homeostasis-maintaining mechanisms of the immune system. These immune agonists not only control the initial innate immune response but also influence the downstream adaptive immune response to a target antigen. The adaptive immune response includes cellular (TH1) and antibody (TH2) responses, by T and B cells, respectively. Both cellular and antibody responses are necessary to provide an effective and prolonged immune response against pathogens. Abbreviations: ssDNA, single-stranded DNA; TH1/2/17, type 1/2/17 T helper cell.

Many adjuvant formulations consist of a single type of PAMP. Unfortunately, a single immune agonist is not always as effective as a whole pathogen at eliciting an efficacious immune response. Natural pathogens, such as *Neisseria meningitidis* and the yellow fever virus, contain more than one type of PAMP (Table 1.2)^{56–83}. Due to this innate efficacy, there has been greater use of multiple ligands to synergistically enhance the immune response. These improved responses can provide reduced adjuvant and antigen dosing, also known as “dose sparing”^{40,41}. In addition, response amplification through immune synergies aids in differentiating foreign antigens from self-antigens, thus working to prevent autoimmune responses. Immune synergies can also dictate

the type of response generated, which depends on the specific combination of PRRs targeted, ensuring that the protective immune responses produced are tailored to the pathogen of interest.^{84,85} The use of multiple classes of PAMPs as adjuvants in clinical models has demonstrated positive vaccination results, suggesting considerable potential for these molecules as new adjuvants.

Table 1.2 Natural Pathogens that Activate Multiple PRRs.

Disease/Pathogen	PRRs Activated	Type of Pathogen	Ref.
<i>Mycobacterium tuberculosis</i>	TLR2, TLR4, TLR9, NOD1, NOD2	Bacteria	56-58
<i>Mycobacterium paratuberculosis</i>	TLR2, TLR4, NOD2	Bacteria	59
<i>Neisseria meningitidis</i>	TLR2, TLR4, TLR9	Gram Neg. Bacteria	60
<i>Streptococcus pneumoniae</i>	TLR2, TLR4, TLR9	Gram Pos. Bacteria	60
<i>Haemophilus influenzae</i> type b	TLR2, TLR4, TLR9	Gram Neg. Bacteria	60
Yellow fever virus	TLR2, TLR7, TLR8, TLR9	Virus	61-64
Herpes simplex virus	TLR2, TLR9	Virus	65-68
<i>Helicobacter pylori</i>	TLR2, TLR4, TLR5	Gram Neg. Bacteria	69
Respiratory syncytial virus (RSV)	TLR2/6, TLR3, TLR4, TLR7, RIG-I, MDA5, NOD2	Virus	70-71
<i>Candida albicans</i>	TLR2, TLR1, TLR6, TLR4, TLR9, CLRs	Fungus	72-73
Flaviviruses (Dengue, West Nile, Zika virus)	TLR3, MDA5, RIG-I	Virus	74-75
<i>Taxoplasma gondii</i>	TLR2, TLR9, TLR11, TLR12	Parasite	76
<i>Plasmodium</i>	TLR9, MDA5, TLR7, TLR1, TLR2, TLR4, TLR6	Parasite	77-78
<i>Leishmania</i>	TLR2, TLR6, TLR4, TLR7, TLR9	Parasite	79
<i>Salmonella</i>	TLR2, TLR4, TLR5	Bacteria	80
Murine cytomegalovirus	TLR2, TLR3, TLR7, TLR9	dsDNA	81-82
<i>Trypanosoma cruzi</i>	TLR2/6, TLR4, TLR7, TLR9	Parasite	83-84
Rhinovirus	TLR2, TLR3, TLR7, TLR8, RIG-I, MDA5	Virus	85-86

1.10 Technologies for Synergistic Adjuvant Development

Recent discoveries have prompted collaboration between different scientific disciplines, leading to the development of new methods to improve the adjuvanticity of native and synthetic PRR agonists as well as the delivery of synergistic adjuvants. Innovative chemical, biological, and

engineering methods are being utilized to rapidly screen and analyze synergistic immune responses for adjuvant discovery, determine dosing, localize delivery of multi-agonist adjuvants, and deliver vaccine cargo to specific immune cell subtypes and cellular compartments. We will touch on each of these points with regards to adjuvant discovery and vaccine development.

1.10 High Throughput Screening of Immune Agonist Synergies for Adjuvant Discovery

High throughput screening (HTS) has recently been utilized as a method to analyze multiple cytokines when screening different immune synergy combinations and choosing the best adjuvant for a vaccine^{84,86}. HTS is widely used in drug discovery to rapidly screen compound libraries for biologically active molecules. Several TLR small molecule immune potentiators (SMIPs) (e.g. TLR2 and TLR7 small molecule agonists) have recently been discovered by HTS, which has allowed screening of millions of compounds for adjuvanticity, and these SMIPs have been used as vaccines adjuvants.^{49,50} The efficiency of HTS allows rapid determination of potential adjuvant hits, making this platform a powerful tool for adjuvant discovery.

Since not all TLRs have small molecule agonists (e.g. TLRs 3, 5, and 9), HTS can quickly determine what types of chemical structures activate specific TLRs. A multiplexed high throughput method was used to screen several compound libraries (>100,000 compounds) for specific PRR activity with the aim to discover new small molecule adjuvants.⁸⁶ From the molecule screen, amphotericin B (AmpB) was discovered to elicit TLR2 and TLR4 immune activity, with an immune response profile similar to MPLA, suggesting the potential of AmpB as a new adjuvant. Zhang and colleagues also used HTS technology to screen a library of compounds for activity against TLR3.⁸⁷ With one hit compound, they performed structure activity relationship (SAR) studies leading to one molecule that activates TLRs 3, 8, and 9. All three TLRs are activated by virus-derived nucleic acids, which may explain how this one molecule can activate all three TLRs.

The HTS platform provided analysis of 59 different compounds and subsequent derivatives of the hit small molecule. These processes would be laborious and time consuming without high throughput technology. Applying medicinal chemistry approaches and high throughput screening to adjuvant discovery can lead to other synergistic small molecule adjuvants, where pharmacokinetics, pharmacodynamics, and biodistribution properties can all be optimized.

In addition, HTS has been applied to the analysis and characterization of synergistic immune responses from specific agonist combinations. Immune synergies typically have been studied using standard cytokine readouts, such as ELISA.⁸⁵ However, ELISA is not the most efficient method to analyze multiple cytokines, since only one cytokine can be measured at a time. The invention of multiplexed screens, like Luminex assays, improved the screening process, providing the ability to analyze a larger number of samples or multiple cytokines in a single sample. Unfortunately, this type of technology still suffers from a detection limit of pg/mL, resulting in the requirement for high volumes of supernatant or sera.^{54,86} To circumvent these challenges, Garcia-Cordero and colleagues developed a nanoscale high throughput immunoassay chip using soft lithography techniques to analyze synergistic activity between PRR agonist combinations.⁸⁴ Their data provided results comparable to that obtained by traditional ELISAs. Their microfluidic device can detect four different biomarkers using only nanoliters of sera in a 384 well plate format. They can also reach a lower detection limit of 100 fM with *in vitro* cell media and *in vivo* sera. Using their technology, they identified agonist combinations from 10 different TLR agonists that resulted in synergistic or inhibitory cytokine production. They validated their synergistic *in vitro* observations in an *in vivo* model system. The ability to screen a large quantity of PRR agonist combinations in a dose dependent manner provides a faster and more cost-efficient readout to determine effective immune responses from distinct agonist combinations for adjuvant discovery. Multiplex assays

still face challenges with non-specific binding and cross reactivity when analyzing complex biological samples, but this technology is a step toward developing platforms that solve analytical challenges and screen for compounds that elicit desired immune responses.

1.11 Chemically Conjugated Synergistic Adjuvants

The discovery of synergistic interactions between multiple types of PRRs has led to the covalent conjugation of PAMPs to develop new multi-agonist adjuvants that improve vaccine immunogenicity. PAMPs are spatially associated with one another due to the natural structure of pathogens. Although unconjugated mixtures of multiple PRR agonists elicit synergistic immune activity, this approach does not mimic the spatial component of PRR activation by a pathogen. Adjuvants that are mixtures of unconjugated agonists can diffuse through the immune system and may get cleared more readily. To address this issue, a panel of dimeric TLR agonists was synthesized, containing combinations of TLR2, TLR4, and TLR9 agonists, which were separated by PEG₆, PEG₁₂, and PEG₂₄ linkers^{88,89}. These single molecular entities aimed to mimic the spatial proximity of immunostimulatory components in natural pathogens with initial inspiration from the herpes simplex virus⁶³. Evaluation of these compounds' immunostimulatory activity provided evidence that the immunogenicity was dependent on the linker length, the specific combination of conjugated TLR agonists, and the sizes of the agonists due to possible steric interactions, all important considerations for adjuvant development. Chimeric molecules with potent immunostimulatory capabilities provide new adjuvant options and potentially lower adjuvant doses in vaccines.

Developing more potent and effective immunostimulants *via* covalent conjugation has led to the application of these tools as adjuvants in vaccination models. The first example of this was CL429, a chimeric molecule containing the agonists Pam₂C and Murabutide, which stimulates

TLR2 and NOD2, respectively⁹⁰. CL429 was used as an adjuvant in a HIV-1 subunit vaccine and increased HIV-1 p-24 antigen specific IgG and IgA antibody titers when compared to either the individual agonists or a mixture of the unconjugated TLR2 and NOD2 agonists. The ability to induce specific and high antibody titers of different subtypes further demonstrated the utility of PRR agonist conjugation in modulating the immune response and improving adjuvant potency. Covalently linked PRR agonist research was further explored to the development of a trimeric agonist adjuvant, since many pathogens contain agonists for 3-5 different PRRs^{60,62,91}. The trimeric molecule is composed of TLR4, 7, and 9 agonists linked to a triazine core. The tri-agonist increased antibody breadth and depth to vaccinia virus antigens in a vaccinia model vaccination study and elicited a more balanced T_H1/T_H2 immune response compared to its unconjugated counterparts or the corresponding conjugated di-agonists. This balanced and enhanced antigen specific response may elicit unique and potentially protective cellular and antibody immune responses, compared to solely a T_H1 or T_H2 response. The covalently linked PRR agonists demonstrate that spatial components play an important role in effective immune system activation.

The synthetic systems discussed are also modular, so that PRR agonists can be exchanged to test different immune synergies. The specific combination of covalently linked agonists is crucial to obtain the desired immune response, as each agonist stimulates characteristic immune signaling pathways and cytokine production. Looking forward, this technology can also be used to conjugate antigens to synergistic agonist combinations. Single agonist-antigen conjugates have been successful in enhancing the immune response, possibly due to efficient antigen presentation that results from colocalization of the antigen and adjuvant in the same endosome^{92,93}. Therefore, synergistic adjuvant-antigen conjugates should be considered for future vaccine development and formulation. As an example, synergistic TLR agonist combinations have been conjugated to whole

tumor cell antigens and exhibited enhanced activation marker and cytokine responses⁹⁴. Further probing synergistic agonist-antigen combinations may provide valuable information to help design improved vaccines in a more methodical manner.

1.12 Particulate Delivery Systems for Immune Synergies

In addition to covalent localization of multi-agonist adjuvants, particulate vaccine delivery systems have been synthesized that mimic pathogens in size and spatial organization^{95,96}. Particulate systems, including nanoparticles, nanodiscs, and liposomes, that range from sub- to low micron in diameter provide cargo delivery at sizes similar to that of a virus or bacteria^{97,98}. These delivery systems have shown enhanced antigen uptake by APCs, which can lead to increased antigen presentation and immune activation^{99,100}. Biodegradable PLGA particles (~300 nm in diameter) have been developed to encapsulate or adsorb dual or triple combinations of TLR agonists, imitating the size and composition of a pathogen^{101,102}. Mice immunized with multi-TLR agonist adjuvant formulations have demonstrated distinct changes in the immune response compared to the use of one agonist or antigen alone. These immune responses include the production of the highest avidity antibody titers toward the target antigen and balanced T_H1/T_H2 responses *via* increased IgG1 and IgG2c levels¹⁰¹. While targeting the antigen and adjuvant to the same endosome is known to increase antigen presentation, stronger humoral responses were observed when the antigen and adjuvant were in separate nanoparticles, requiring more mechanistic investigation¹⁰². Even so, delivering antigen and adjuvant in different particles would provide a platform system for vaccine formulation development. Nanodiscs are another novel adjuvant delivery system developed to encapsulate dual TLR agonist combinations⁹⁸. Immunizations with this scaffold led to a reduction in plasma cholesterol levels and potent anti-tumor activity in two different model systems, presenting another efficacious platform that can

easily combine synergistic adjuvants with a range of antigens.

Other techniques, such as mesoporous silica templating and agonist adsorption to particles *via* electrostatic and non-covalent interactions, have also been used to synthesize multi-PRR adjuvant delivery systems. Mesoporous silica templating provides uniform particles with high surface area for agonist loading. In an *in vivo* OVA model, NOD2 and TLR9 agonist-loaded mesoporous silica particles exhibited synergistic increases in cytokine production and enhanced CD4⁺ and humoral T_H1 responses when compared to either NOD2 or TLR9 agonist-loaded particles¹⁰³. Tukhvatulin and colleagues also studied NOD/TLR synergies by adsorbing TLR4 (MPLA) and NOD2 (MDP) agonists to alum particles¹⁰⁴. By activating TLR4 instead of TLR9, both T_H1 and T_H2 responses were enhanced as well as OVA specific IgG antibodies across multiple subsets (IgG1, IgG2, and IgG3), demonstrating an increased breadth in the immune response. These results show how activating multiple PRRs can tune the immune response depending on the PRRs activated and how an agonist's role can change depending on the agonist pairing.

Another advantage of particle delivery systems is that their physiochemical properties can be tuned to target cargo delivery, alter release kinetics, and direct the immune response. Particulate delivery vehicles that traffic to specific locations *in vivo* and depot in tissues to provide slow drug release have had a significant impact on vaccine efficacy. Lynn and colleagues synthesized a nanoparticulate adjuvant that exemplified targeted biodistribution¹⁰⁰. A TLR7/8 agonist was conjugated to a polymer scaffold at different densities and with varying polymer attributes, such as linker length and composition. Increased density of the TLR agonist on the polymer scaffold resulted in particle formation (~700 nm) of the polymer. The particulate form of the adjuvant led to higher cytokine production in the lymph nodes, promoted local lymph node retention and APC uptake, limited systemic toxicity, and enhanced protective T cell responses. They have since

shown the broad applicability of this idea to a number of proteins and adjuvants.^{105,106} Applying this technology to multiple PRR agonists and immune synergy studies may provide targeted delivery, specific biodistribution, and mechanistic insight into immune activation.

1.13 Synergistic Adjuvants in Vaccination Models

Currently, a number of experimental adjuvants interact with multiple families of PRRs, synergistically stimulating several immune signaling pathways, and have been used in model vaccination studies, including *M. tuberculosis* and HIV (**Table 1.3**).^{56,76,90,91,97,101–104,107–115} These newly developed adjuvant formulations have led to enhanced immunogenicity and prolonged responses *via* the increase in magnitude, avidity, and breadth of specific cellular and antibody subtypes as well as reduced disease burden, providing protection in challenge studies. Shifts in T_H2 (IgG1) to T_H1 (IgG2c) antibody subtypes and cellular responses have also been observed and resulted in reduced parasite burden¹¹⁶. Multi-PRR adjuvant systems have resulted in lower reactogenicity and local inflammation compared to commercial adjuvant systems, demonstrating safety improvements from current adjuvants^{117–120}. These types of distinct molecular adjuvants will be necessary to achieve defined immunogenicity and safety profiles, affording more straightforward vaccine characterization that can guide future vaccine development.

Table 1.3 Synergistic PRR Combinations Activated by Adjuvants in Vaccination Models.

PRR Synergistic Combination	Ligands	Cellular Location	Vaccination Model	Ref.
TLR4, TLR7/8	GLA, Resiquimod R848	Cell surface, Endosome	PvRII (<i>Plasmodium vivax</i> antigen)	107
TLR4, TLR9	GLA, CpG-ODN MPLA, CpG-ODN	Cell surface, Endosome	<i>M. tuberculosis</i> <i>Leishmania</i> , TC-1 tumor, OVA	58, 108 78, 100, 103, 109
TLR4, TLR7	1Z105 (Pyrimido-indole), 1V270 (Imidazoquinoline) MPLA, Imiquimod R837 GLA, Imiquimod R837	Cell surface, Endosome	Influenza virus (hemagglutinin) Influenza H1N1 PbCSP (recombinant malaria antigen)	110 104 99
TLR7/8, TLR9	3M-052 Imidazoquinoline, CpG-ODN Resiquimod R848, CpG-ODN	Endosome	CT26 colon cancer cells HIV-1, Malaria	111 113, 114-115
TLR3, TLR9	Poly(I:C), CpG-ODN	Endosome	B16-F10 pulmonary metastases	114
TLR2/6, TLR3, TLR9	MALP2, Poly(I:C), CpG-ODN	Cell surface, Endosome	HIV	115
TLR2, NOD2	Pam2C, Murabutide	Cell surface, Cytosolic	HIV-1	92
TLR4, TLR7, TLR9	Pyrimido-indole, Loxoribine, CpG-ODN MPLA, Imiquimod R837, CpG-ODN	Cell surface, Endosome	Vaccinia Virus OVA	93 103
TLR9, NOD2	CpG-ODN, Muramyl dipeptide (MDP)	Endosome, Cytosolic	OVA	105
TLR4, NOD2	MPLA, Muramyl dipeptide (MDP)	Cell surface, Cytosolic	OVA	106
STING, TLR9	cGAMP, CpG-ODN	Cytosolic, Endosome	B16 F10 melanoma	145
Mincle, TLR3	TDB or MMG, Poly(I:C)	Cell surface, Endosome	<i>M. paratuberculosis</i>	54
Mincle, TLR7/8	TDB, R848	Cell surface, Endosome	N/A	148

1.14 Clinical Synergistic Adjuvants

Several synergistic clinical adjuvant systems (AS01, AS02, and AS15) developed by GlaxoSmithKline (GSK) show promise in clinical applications (Table 4)^{121,122}. AS01 and AS02 adjuvant formulations, composed of MPLA (TLR4) and saponin QS21 (NLRP3), have been utilized in malaria vaccines and can elicit strong T cell responses¹²³. Currently, these adjuvants are being tested with experimental vaccines for a variety of disease models, including HIV and tuberculosis^{117,118,124}. AS15 is composed of QS21, MPLA, and CpG oligonucleotide in a liposomal formulation and has been efficacious in anti-cancer vaccines¹²⁴. Higher antibody titers and stronger T cell responses were obtained with vaccine formulations containing AS15 adjuvant compared to AS02B adjuvant. The higher efficacy may be attributed to the addition of CpG oligonucleotide in AS15. GSK also performed a comparative study of their Adjuvant System (AS) formulations using a hepatitis B model antigen¹²⁵. They observed differences in the magnitude (i.e. antibody titers), but not the quality (i.e. functional cytokine profiles) of the immune response. Their findings were surprising due to the different adjuvant compositions, but warrant more extensive readouts to compare.

CAF09 is an emerging synergistic adjuvant that targets the Mincle (C-type lectin) and TLR3 receptors with monomycoloyl glycerol (MMG) and Poly(I:C), respectively⁵². It is a cationic adjuvant formulation that is starting to be used in the clinic. Favorable immune responses have been observed, including robust CD8⁺ T cell responses, higher cytokine release per T cell, and efficacious responses with lower antigen doses, thus demonstrating the importance of targeting alternative PRRs and their respective activation pathways^{126,127}. Another interesting synergy is the combination of trehalose-6,6-dibehenate (also a C-type lectin agonist) with TLR7/8 agonist for activation of neonatal immune cells.¹²⁸ With these multi-PRR activating adjuvants in the

pipeline exhibiting promising protection and efficacy, we can learn from the successes of these synergistic adjuvants and apply our findings to the design of next generation adjuvants for commercial applications.

Table 1.4 Synergistic Adjuvants Employed in Clinical Trials.

Synergistic Adjuvant in Clinical Trials	Adjuvant Components (PRRs Activated)	ClinicalTrials.gov Identifier
AS01	MPLA, Q21 saponin (TLR4, NLRP3 inflammasome)	NCT00397943
AS02	MPLA, Q21 saponin (TLR4, NLRP3 inflammasome)	NCT00307528 / NCT01767402
AS15	MPLA, CpG (TLR4, TLR9)	NCT00086866
CAF09	MMG – monomycoloyl glycerol, Poly(I:C) (Mincle receptor (C type lectin), TLR3)	NCT03412786

1.15 Applying Synergistic Studies to Adjuvant Design

With these promising synergistic adjuvants in the clinic, new adjuvant development should employ the knowledge gained from clinical and fundamental synergistic studies. Researchers have started to apply the immunogenicity profiles from pathogens to develop improved vaccines. Understanding how natural pathogens function and utilizing known mechanisms of infection are also important factors when designing adjuvants. For example, *M. tuberculosis* activates the immune system through TLRs 2, 4, and 9⁵⁶. Combining all three TLR agonists to create a multi-agonist adjuvant system may further improve *M. tuberculosis* vaccines. Applying similar strategies to fight other diseases will be important to design effective adjuvants.

Improved adjuvant design and vaccine efficacy will also need approaches that control the dose and time release of synergistic cargo, target specific cellular compartments and cell types, and study single cell expression profiles *in vivo*. Napolitani and colleagues examined synergistic

immune activation over time at specific doses and the order in which distinct PRRs were activated¹²⁹. Analyzing the temporal aspect of synergistic immune responses displayed when specific cytokine responses peaked. They also observed that enhanced immune responses depended on the order in which two distinct TLR agonists were administered. The ability to control the timing of the immune response and dictate the order in which PRRs are activated are both important considerations for vaccine development. These capabilities can be incorporated into new technologies, including covalent chemistries, nanoparticulate systems, or photocaged agonists. Designing molecules with distinct pharmacokinetic and pharmacodynamic properties as well as defined formulations can temporally control immune activation to provide desired drug release kinetics and immune activation profiles.

Targeting particular cellular compartments is another important factor because PRRs are expressed in distinct cellular locations based on the chemical identity of the PAMP, the signaling pathways activated, and the types of responses produced¹³⁰. The chemical identity of immune agonists and their corresponding receptors have been determined to be key contributors to the synergistic immune response^{84,85}. Directing drugs to specific cellular compartments has been demonstrated by many groups¹³¹. Agonists formulated with cationic lipids and lipidated immunostimulants have been synthesized to allow for longer residence times within the endosome as well as target the draining lymph nodes to improve antigen presentation^{130,132}.

Beyond cellular compartments, specific immune cell subtypes play an essential role in the types of immune responses elicited based on different PRR expression profiles^{133–135}. Several researchers have characterized PRR expression on different types of immune cells using RT-PCR. Specific cell subtypes and lymphatic organs can be directly targeted based on unique cell surface receptors or markers, such as DEC-205 and DC-SIGN^{136,137}. Designing synergistic adjuvants with

directing ligands (e.g. multivalent ligands) or covalent inhibitor properties will allow targeting toward specific cellular locations and cell subtypes. As a result, distinct PRR combinations and subsequent synergistic signaling pathways can be activated and potentially reduce systemic toxicity and clearance. When studying PRR expression and activation of various immune subsets, the challenge in analysis continues to be with the differences between species and tissue types. This information should be kept in mind when designing vaccination models.

While examining overall cellular responses is crucial for studying immune synergies, single cell analysis has emerged as a powerful tool that permits the extraction of critical data from individual cells that is obscured in bulk assays. Many single cell analysis studies utilize single cell RNA sequencing (RNA-Seq) technology in order to quantify RNA transcription levels across the genome ^{138,139}. Utilization of techniques, such as RNA-Seq, may lead to new insight into the mechanism of immune agonist synergies. The data obtained can also potentially provide new and essential information regarding cell signaling and the efficacy of targeting agonist synergies to specific tissues, cell subtypes, or subcellular compartments ^{140,141}. Analyses of such single cell data have shown that there are rare subsets of cells that may initiate immune responses ¹⁴². The integration of detailed single cell data into the population context may provide a deeper understanding of the mechanism behind immune synergies. This data may, in turn, inform the development of more potent and precisely targeted synergistic adjuvants. Single cell techniques will also be invaluable in characterizing the downstream effects of adjuvants. Characterizing the type of antibody producing B-cells, the T-cell composition and overall lymphnode response to specific adjuvants.¹⁴³

1.16 Characterizing Synergistic Vaccine Efficacy

The yellow fever vaccine, a live, attenuated version of the virus, acts through TLRs 2, 7, 8, and 9 and is one of the most successful vaccines developed^{61,62}. The high efficacy of the vaccine is a result of the polyvalent immune response elicited, comprised of a wide range of critical cellular and antibody responses (i.e. CD8⁺ and CD4⁺ T cells, IgG, IgM). The cooperation of this broad set of immune responses results in responses that are rapidly produced and peak at different times post immunization. In addition, protective antibodies are present up to 40 years after the initial vaccination, where all of these aspects are crucial to the overall robustness of the vaccine. The yellow fever vaccine demonstrates the significant role of a prolonged immune response and the production of different types of immune responses at specific times. Therefore, analyzing the robustness of the immune response from synergistic vaccines over time will be of utmost importance. Depending on the disease, there are clear readouts, such as bacterial clearance, reduced parasite burden, and tumor volume. In addition, vaccines can be tracked, using techniques such as luminescence and PET imaging, to visualize vaccine biodistribution and correlate a vaccine's biophysicochemical properties to its efficacy. These measures of vaccine efficacy need to be monitored to ensure sustained protective responses in challenge studies and clearance of the target pathogen.

The kinetic profile of different branches of the immune response and dose response curves should be characterized for synergistic vaccines. The types of immune responses and the corresponding times elicited are critical to communication within the immune system and the efficacy of the vaccine^{61,129,134,144}. Also, dose response curves for synergistic adjuvants do not always exhibit the expected peak shape and can display a Gaussian-like curve, providing crucial information about the proper administration dose^{145,146}. Correlating synergistic vaccine

formulations to pathogen clearance, response robustness, and specific cytokine, cellular, and antibody responses over time will provide a more comprehensive understanding of the relationship between vaccine composition, resulting immune responses, and adjuvant and vaccine efficacy. High throughput technology can aid in analyzing large amounts of data and determining trends. Even so, it will be imperative to carefully examine large data sets to arrive at accurate conclusions.

1.17 Future Perspective of synergies in vaccines

Applying synergistic combinations of PRR agonists to vaccine adjuvant design has led to more effective immune responses and higher protective efficacy *via* increases in titers and breadth of cellular and antibody responses. Inspiration for new and simple to manufacture adjuvants may be attained from some of the emerging PRR agonists (see Outstanding Questions), such as STING and C-type lectin agonists that stimulate other signaling pathways, including TBK1-IRF3 and Syk-CARD9, and may access immune responses that other adjuvants cannot. Recently, STING agonists have gained considerable attention as adjuvants for immunotherapy applications (<https://cen.acs.org/articles/96/i9/STING-fever-sweeping-through-cancer.html>). Although synergy studies have been limited, synergistic effects have been observed between STING and TLR9 to reduce tumor growth *via* potent T_H1 responses¹⁴⁷, demonstrating the potential to expand the adjuvant toolbox with other effective PRR synergies. However, most STING agonists are cyclic-dinucleotides, which have poor drug properties and are difficult to formulate, and small molecule agonists have only been reported for murine STING^{148,149}. Thus, similar to other TLR agonists, potential therapies involving STING activation could greatly benefit from HTS and SAR studies to determine human STING agonists with improved pharmacological properties. C-type lectins are another attractive target for future immune synergies, where enhanced polyfunctional and age-dependent immune responses have been observed with TLR3 and TLR7/8 agonists^{52,150}.

Although, not all PRR combinations enhance the immune response, rather this cross talk can inhibit immune activation^{84,150}. But inhibitory responses can potentially be used as an advantage to down regulate undesired immune responses (e.g. autoimmune diseases).

The novel technologies discussed have aided in the development of new synergistic adjuvants and delivery systems as well as analytical platforms for synergistic immune responses. Looking forward, improved model systems and analytical readouts will be crucial to design and develop future vaccines. Vaccines perform differently depending on the adjuvant and result in varying degrees of efficacy, as observed in a head-to-head comparison of several clinical adjuvants in a standard set of vaccination models⁵⁵. From this study, the proper adjuvant and corresponding immune responses could be determined for a target disease, thus characterizing novel adjuvants in a similar manner should be considered. It will also be imperative to use the most comparable model system, which may involve human tissue or whole blood assays, in order to streamline vaccine development and avoid misleading conclusions. The challenge in using human samples results from high costs and lack of supply – receiving enough material to perform studies in an efficient time frame. *In silico* modeling may provide a cost effective alternative to predict vaccine efficacy and address the aforementioned challenges. Systems vaccinology and immunoinformatics can be powerful tools to improve vaccine design (i.e. predict pathogen epitope changes for elusive diseases that are constantly mutating)¹⁵¹. Computational modeling has its limitations and is based on certain assumptions, but these approaches show great promise if validated properly *in vivo* and with the proper inputs from current data sets to build the model.

1.18 Challenges of using TLR agonists as vaccine adjuvants

With all of these new adjuvant and formulation technologies, it is crucial to consider the safety profile of the vaccination materials¹⁵². For example, the amount of systemic cytokines produced,

cell viability, and off targets effects should all be monitored. Several considerations, including formulation and administration route, can drastically alter the immune response, potentially providing synergistic or inhibitory responses. Particulate formulation or additives, such as squalene oil-in-water emulsions, can synergistically enhance the immune response and may be an alternative approach to develop potent adjuvants, while avoiding toxic side effects^{153,154}. In addition, simply changing the administration route can change what immune cells are targeted and the responses elicited, providing another method to obtain improved immune responses (e.g. intraperitoneal versus subcutaneous injections)¹⁵⁴. With these considerations in mind, the application of immune synergies to modulate the immune response is and will be a powerful tool for novel and more rational adjuvant discovery, thereby impacting future development of safer and more effective vaccines.

1.19 Understanding synergies

Although it is clear that immune synergies can both quantitatively enhance the magnitude of the immune response and qualitatively modify the expression pattern of a variety of genes, the mechanistic understanding of how this occurs remains elusive.⁴¹ Our lab is designing tools to allow us to probe these synergies while gaining a mechanistic understanding of how PRRs work together to provide enhanced immunity. This fundamental understanding will lead to improved vaccine formulations.

1.20 Vaccine side effects

While combinations of TLR agonists or single TLR agonists have demonstrated immense promise as vaccine adjuvants, many induce high and unsafe levels of systemic inflammation. Often the dose of TLR agonist required to acquire adequate immunity is above the threshold that induces extreme levels of inflammatory cytokines leading to failed clinical trials. CpG DNA is potent

adjuvant that produces enhanced antigen-specific immune responses with less toxicity than many other adjuvants.¹⁵⁵ However this adjuvant has only been approved for use in the last year in one vaccine, Heplisiv-B.¹⁵⁶ All other clinical trials including CpG DNA in vaccines have failed to complete clinical trials, many due to the safety.^{157,158}

1.21 References

1. Mäkelä, P. H. Vaccines, coming of age after 200 years. *FEMS Microbiol Rev* 24, 9–20 (2000).
2. Burton, D. R. Antibodies, viruses and vaccines. *Nature Reviews Immunology* 2, 706–713 (2002).
3. Plotkin, S. A., & Plotkin, S. L. (2011). The development of vaccines: how the past led to the future. *Nature Reviews Microbiology*, 9(12), 889.
4. Rueckert, C. & Guzmán, C. A. Vaccines: From Empirical Development to Rational Design. *PLOS Pathogens* 8, e1003001 (2012).
5. Pulendran, B. & Ahmed, R. Immunological mechanisms of vaccination. *Nat Immunol* 12, 509–517 (2011).
6. Saluzzo, J.-F. Empirically Derived Live-Attenuated Vaccines Against Dengue and Japanese Encephalitis. in *Advances in Virus Research* (eds. Chambers, T. J. & Monath, T. P.) 61, 419–443 (Academic Press, 2003).
7. Ada, G. Vaccines and Vaccination. *New England Journal of Medicine* 345, 1042–1053 (2001).
8. Lane, J. M. The current and future landscape of smallpox vaccines. *Global Biosecurity* 1, 106–112 (2019).
9. Silva, J. V. J. *et al.* Current status, challenges and perspectives in the development of

- vaccines against yellow fever, dengue, Zika and chikungunya viruses. *Acta Tropica* 182, 257–263 (2018).
10. Vetter, V., Denizer, G., Friedland, L. R., Krishnan, J. & Shapiro, M. Understanding modern-day vaccines: what you need to know. *Annals of Medicine* 50, 110–120 (2018).
 11. Bhurani, V., Mohankrishnan, A., Morrot, A. & Dalai, S. K. Developing effective vaccines: Cues from natural infection. *International Reviews of Immunology* 37, 249–265 (2018).
 12. Pickering, L. K., Wallace, G. & Rodewald, L. Too Hot, Too Cold: Issues With Vaccine Storage. *Pediatrics* 118, 1738–1739 (2006).
 13. Hurley, L. P. Barriers to the Use of Herpes Zoster Vaccine. *Annals of Internal Medicine* 152, 555 (2010).
 14. Tan, L. J. *et al.* From refrigerator to arm: Issues in vaccination delivery. *Vaccine* 32, 2389–2393 (2014).
 15. Chen, D., & Kristensen, D. (2009). Opportunities and challenges of developing thermostable vaccines. *Expert review of vaccines*, 8(5), 547-557.
 16. Petrovsky, N. & Aguilar, J. C. Vaccine adjuvants: Current state and future trends. *Immunol Cell Biol* 82, 488–496 (2004).
 17. Chow, J., Franz, K. M. & Kagan, J. C. PRRs are watching you: Localization of innate sensing and signaling regulators. *Virology* 479–480, 104–109 (2015).
 18. Mancini, R. J., Stutts, L., Ryu, K. A., Tom, J. K. & Esser-Kahn, A. P. Directing the Immune System with Chemical Compounds. *ACS Chemical Biology* 9, 1075–1085 (2014).
 19. Hoffmann, A., & Baltimore, D. (2006). Circuitry of nuclear factor κ B signaling. *Immunological reviews*, 210(1), 171-186.
 20. Basagoudanavar, S. H. *et al.* Distinct Roles for the NF- κ B RelA Subunit during Antiviral

- Innate Immune Responses. *Journal of Virology* 85, 2599–2610 (2011).
21. Gilmore, T. D. Introduction to NF- κ B: players, pathways, perspectives. *Oncogene* 25, 6680–6684 (2006).
 22. Riedel, S. Edward Jenner and the History of Smallpox and Vaccination. *Baylor University Medical Center Proceedings* 18, 21–25 (2005).
 23. Baicus, A. History of polio vaccination. *World J Virol* 1, 108–114 (2012).
 24. Blume, S. & Geesink, I. A Brief History of Polio Vaccines. *Science* 288, 1593–1594 (2000).
 25. Dai, X., Xiong, Y., Li, N., & Jian, C. (2019). Vaccine Types. In *Vaccines*. IntechOpen.
 26. Minor, P. D. Live attenuated vaccines: Historical successes and current challenges. *Virology* 479–480, 379–392 (2015).
 27. Ljungman, P. Vaccination of immunocompromised patients. *Clinical Microbiology and Infection* 18, 93–99 (2012).
 28. Reyes, M. A., De Borrero, M. F., Roa, J., Bergonzoli, G. & Saravia, N. G. Measles vaccine failure after documented seroconversion. *The Pediatric Infectious Disease Journal* 6, 848 (1987).
 29. Pashine, A., Valiante, N. M. & Ulmer, J. B. Targeting the innate immune response with improved vaccine adjuvants. *Nat Med* 11, S63–S68 (2005).
 30. Rabinovich, N. R., McInnes, P., Klein, D. L. & Hall, B. F. Vaccine technologies: view to the future. *Science* 265, 1401–1404 (1994).
 31. Mbow, M. L., De Gregorio, E., Valiante, N. M. & Rappuoli, R. New adjuvants for human vaccines. *Current Opinion in Immunology* 22, 411–416 (2010).
 32. O’Hagan, D. T., Ott, G. S., De Gregorio, E. & Seubert, A. The mechanism of action of

- MF59 – An innately attractive adjuvant formulation. *Vaccine* 30, 4341–4348 (2012).
33. Didierlaurent, A. M. *et al.* AS04, an Aluminum Salt- and TLR4 Agonist-Based Adjuvant System, Induces a Transient Localized Innate Immune Response Leading to Enhanced Adaptive Immunity. *The Journal of Immunology* 183, 6186–6197 (2009).
 34. Schülke, S. *et al.* MPLA shows attenuated pro-inflammatory properties and diminished capacity to activate mast cells in comparison with LPS. *Allergy* 70, 1259–1268 (2015).
 35. Barclay, T., & Petrovsky, N. (2017). Vaccine Adjuvant Nanotechnologies. In *Micro and Nanotechnology in Vaccine Development* (pp. 127-147). William Andrew Publishing.
 36. Schillie, S. *et al.* Recommendations of the Advisory Committee on Immunization Practices for Use of a Hepatitis B Vaccine with a Novel Adjuvant. *MMWR Morb Mortal Wkly Rep* 67, 455–458 (2018).
 37. Hartmann, G., & Krieg, A. M. (2000). Mechanism and function of a newly identified CpG DNA motif in human primary B cells. *The Journal of Immunology*, 164(2), 944-953.
 38. Orr, M. T. *et al.* Adjuvant formulation structure and composition are critical for the development of an effective vaccine against tuberculosis. *J Control Release* 172, (2013).
 39. Reed, S. G., Orr, M. T. & Fox, C. B. Key roles of adjuvants in modern vaccines. *Nat Med* 19, 1597–1608 (2013).
 40. Cao, X. Self-regulation and cross-regulation of pattern-recognition receptor signalling in health and disease. *Nat Rev Immunol* 16, 35–50 (2016).
 41. Tan, R. S. T., Ho, B., Leung, B. P. & Ding, J. L. TLR Cross-talk Confers Specificity to Innate Immunity. *Int Rev Immunol* 33, 443–453 (2014).
 42. Bergmann-Leitner, E. S. & Leitner, W. W. Adjuvants in the Driver’s Seat: How Magnitude, Type, Fine Specificity and Longevity of Immune Responses Are Driven by Distinct Classes

- of Immune Potentiators. *Vaccines* 2, 252–296 (2014).
43. Calabro, S. *et al.* The adjuvant effect of MF59 is due to the oil-in-water emulsion formulation, none of the individual components induce a comparable adjuvant effect. *Vaccine* 31, 3363–3369 (2013).
 44. Garçon, N., Vaughn, D. W. & Didierlaurent, A. M. Development and evaluation of AS03, an Adjuvant System containing α -tocopherol and squalene in an oil-in-water emulsion. *Expert Rev Vaccines* 11, 349–366 (2012).
 45. Toussi, D. N. & Massari, P. Immune Adjuvant Effect of Molecularly-defined Toll-Like Receptor Ligands. *Vaccines (Basel)* 2, 323–353 (2014).
 46. Fontes, J. A. *et al.* Complete Freund's adjuvant induces experimental autoimmune myocarditis by enhancing IL-6 production during initiation of the immune response. *Immun Inflamm Dis* 5, 163–176 (2017).
 47. Jackson, S. *et al.* Immunogenicity of a two-dose investigational hepatitis B vaccine, HBsAg-1018, using a toll-like receptor 9 agonist adjuvant compared with a licensed hepatitis B vaccine in adults. *Vaccine* 36, 668–674 (2018).
 48. Oh, D.-Y. *et al.* Adjuvant-induced Human Monocyte Secretome Profiles Reveal Adjuvant- and Age-specific Protein Signatures. *Mol Cell Proteomics* 15, 1877–1894 (2016).
 49. Santone, M. *et al.* A new TLR2 agonist promotes cross-presentation by mouse and human antigen presenting cells. *Human Vaccines & Immunotherapeutics* 0, 00–00 (2015).
 50. Wu, T. Y.-H. *et al.* Rational design of small molecules as vaccine adjuvants. *Science Translational Medicine* 6, 263ra160-263ra160 (2014).
 51. Buonsanti, C. *et al.* Novel adjuvant Alum-TLR7 significantly potentiates immune response to glycoconjugate vaccines. *Scientific Reports* 6, 29063 (2016).

52. Thakur, A. *et al.* Targeting the Mincle and TLR3 receptor using the dual agonist cationic adjuvant formulation 9 (CAF09) induces humoral and polyfunctional memory T cell responses in calves. *PLoS ONE* 13, e0201253 (2018).
53. Temizoz, B., Kuroda, E. & Ishii, K. J. Combination and inducible adjuvants targeting nucleic acid sensors. *Curr Opin Pharmacol* 41, 104–113 (2018).
54. Fischetti, L., Zhong, Z., Pinder, C. L., Tregoning, J. S. & Shattock, R. J. The synergistic effects of combining TLR ligand based adjuvants on the cytokine response are dependent upon p38/JNK signalling. *Cytokine* 99, 287–296 (2017).
55. Knudsen, N. P. H. *et al.* Different human vaccine adjuvants promote distinct antigen-independent immunological signatures tailored to different pathogens. *Sci Rep* 6, (2016).
56. Kleinnijenhuis, J., Oosting, M., Joosten, L. A. B., Netea, M. G. & Van Crevel, R. Innate immune recognition of *Mycobacterium tuberculosis*. *Clin. Dev. Immunol.* 2011, 405310 (2011).
57. Lee, J.-Y. *et al.* The role of nucleotide-binding oligomerization domain 1 during cytokine production by macrophages in response to *Mycobacterium tuberculosis* infection. *Immunobiology* 221, 70–75 (2016).
58. Ferwerda, G. *et al.* NOD2 and Toll-Like Receptors Are Nonredundant Recognition Systems of *Mycobacterium tuberculosis*. *PLOS Pathogens* 1, e34 (2005).
59. Ferwerda, G. *et al.* *Mycobacterium paratuberculosis* is recognized by Toll-like receptors and NOD2. *J Leukoc Biol* 82, 1011–1018 (2007).
60. Mogensen, T. H., Paludan, S. R., Kilian, M. & Østergaard, L. Live *Streptococcus pneumoniae*, *Haemophilus influenzae*, and *Neisseria meningitidis* activate the inflammatory response through Toll-like receptors 2, 4, and 9 in species-specific patterns. *J Leukoc Biol*

- 80, 267–277 (2006).
61. Pulendran, B. Learning immunology from the yellow fever vaccine: innate immunity to systems vaccinology. *Nat Rev Immunol* 9, 741–747 (2009).
 62. Querec, T. *et al.* Yellow fever vaccine YF-17D activates multiple dendritic cell subsets via TLR2, 7, 8, and 9 to stimulate polyvalent immunity. *Journal of Experimental Medicine* 203, 413–424 (2006).
 63. Sato, A., Linehan, M. M. & Iwasaki, A. Dual recognition of herpes simplex viruses by TLR2 and TLR9 in dendritic cells. *PNAS* 103, 17343–17348 (2006).
 64. Sørensen, L. N. *et al.* TLR2 and TLR9 synergistically control herpes simplex virus infection in the brain. *J. Immunol.* 181, 8604–8612 (2008).
 65. Uno, K. *et al.* Toll-like receptor (TLR) 2 induced through TLR4 signaling initiated by *Helicobacter pylori* cooperatively amplifies iNOS induction in gastric epithelial cells. *American Journal of Physiology - Gastrointestinal and Liver Physiology* 293, G1004–G1012 (2007).
 66. Jensen, S. & Thomsen, A. R. Sensing of RNA Viruses: a Review of Innate Immune Receptors Involved in Recognizing RNA Virus Invasion. *J Virol* 86, 2900–2910 (2012).
 67. Marr, N., Turvey, S. E. & Grandvaux, N. Pathogen recognition receptors crosstalk in respiratory syncytial virus sensing: host and cell type perspective. *Trends Microbiol* 21, 568–574 (2013).
 68. Inoue, M. & Shinohara, M. L. Clustering of Pattern Recognition Receptors for Fungal Detection. *PLoS Pathog* 10, e1003873 (2014).
 69. Plato, A., Willment, J. A. & Brown, G. D. C-Type Lectin-Like Receptors of the Dectin-1 Cluster: Ligands and Signaling Pathways. *International Reviews of Immunology* 32, 134–

- 156 (2013).
70. Castillo Ramirez, J. A. & Urcuqui-Inchima, S. Dengue Virus Control of Type I IFN Responses: A History of Manipulation and Control. *J Interferon Cytokine Res* 35, 421–430 (2015).
 71. Errett, J. S., Suthar, M. S., McMillan, A., Diamond, M. S. & Gale, M. The essential, nonredundant roles of RIG-I and MDA5 in detecting and controlling West Nile virus infection. *J. Virol.* 87, 11416–11425 (2013).
 72. Hamel, R. *et al.* Biology of Zika Virus Infection in Human Skin Cells. *J. Virol.* 89, 8880–8896 (2015).
 73. Sher, A., Tosh, K. & Jankovic, D. Innate recognition of *Toxoplasma gondii* in humans involves a mechanism distinct from that utilized by rodents. *Cell Mol Immunol* 14, 36–42 (2017).
 74. Sharma, S. *et al.* Innate immune recognition of an AT-rich stem-loop DNA motif in the *Plasmodium falciparum* genome. *Immunity* 35, 194–207 (2011).
 75. Kalantari, P. *et al.* Dual engagement of the NLRP3 and AIM2 inflammasomes by plasmodium-derived hemozoin and DNA during malaria. *Cell Rep* 6, 196–210 (2014).
 76. Raman, V. S. *et al.* Applying TLR Synergy in Immunotherapy: Implications in Cutaneous Leishmaniasis. *J Immunol* 185, 1701–1710 (2010).
 77. Tukhvatulin, A. I. *et al.* Combined stimulation of Toll-like receptor 5 and NOD1 strongly potentiates activity of NF- κ B, resulting in enhanced innate immune reactions and resistance to *Salmonella enterica* serovar Typhimurium infection. *Infect. Immun.* 81, 3855–3864 (2013).
 78. Szomolanyi-Tsuda, E., Liang, X., Welsh, R. M., Kurt-Jones, E. A. & Finberg, R. W. Role

- for TLR2 in NK Cell-Mediated Control of Murine Cytomegalovirus In Vivo. *J. Virol.* 80, 4286–4291 (2006).
79. Tabeta, K. *et al.* Toll-like receptors 9 and 3 as essential components of innate immune defense against mouse cytomegalovirus infection. *Proc. Natl. Acad. Sci. U.S.A.* 101, 3516–3521 (2004).
80. Rodrigues, M. M., Oliveira, A. C. & Bellio, M. The Immune Response to *Trypanosoma cruzi*: Role of Toll-Like Receptors and Perspectives for Vaccine Development. *J Parasitol Res* 2012, (2012).
81. Bafica, A. *et al.* Cutting Edge: TLR9 and TLR2 Signaling Together Account for MyD88-Dependent Control of Parasitemia in *Trypanosoma cruzi* Infection. *The Journal of Immunology* 177, 3515–3519 (2006).
82. Triantafilou, K. *et al.* Human rhinovirus recognition in non-immune cells is mediated by Toll-like receptors and MDA-5, which trigger a synergetic pro-inflammatory immune response. *Virulence* 2, 22–29 (2011).
83. Slater, L. *et al.* Co-ordinated role of TLR3, RIG-I and MDA5 in the innate response to rhinovirus in bronchial epithelium. *PLoS Pathog.* 6, e1001178 (2010).
84. Garcia-Cordero, J. L., Nembrini, C., Stano, A., Hubbell, J. A. & Maerkl, S. J. A high-throughput nanoimmunoassay chip applied to large-scale vaccine adjuvant screening. *Integr Biol (Camb)* 5, 650–658 (2013).
85. Timmermans, K. *et al.* Blueprints of Signaling Interactions between Pattern Recognition Receptors: Implications for the Design of Vaccine Adjuvants. *Clin. Vaccine Immunol.* 20, 427–432 (2013).
86. Salyer, A. C. D. *et al.* Identification of Adjuvant Activity of Amphotericin B in a Novel,

- Multiplexed, Poly-TLR/NLR High-Throughput Screen. *PLoS ONE* 11, e0149848 (2016).
87. Zhang, L., Dewan, V. & Yin, H. Discovery of Small Molecules as Multi-Toll-like Receptor Agonists with Proinflammatory and Anticancer Activities. *J. Med. Chem.* 60, 5029–5044 (2017).
 88. Mancini, R. J., Tom, J. K. & Esser-Kahn, A. P. Covalently coupled immunostimulant heterodimers. *Angew. Chem. Int. Ed. Engl.* 53, 189–192 (2014).
 89. Ryu, K. A., Slowinska, K., Moore, T. & Esser-Kahn, A. Immune Response Modulation of Conjugated Agonists with Changing Linker Length. *ACS Chem. Biol.* 11, 3347–3352 (2016).
 90. Pavot, V. *et al.* Cutting Edge: New Chimeric NOD2/TLR2 Adjuvant Drastically Increases Vaccine Immunogenicity. *J Immunol* 1402184 (2014). doi:10.4049/jimmunol.1402184
 91. Tom, J. K. *et al.* Modulation of Innate Immune Responses via Covalently Linked TLR Agonists. *ACS Cent Sci* 1, 439–448 (2015).
 92. Kramer, K., Shields, N. J., Poppe, V., Young, S. L. & Walker, G. F. Intracellular Cleavable CpG Oligodeoxynucleotide-Antigen Conjugate Enhances Anti-tumor Immunity. *Mol. Ther.* 25, 62–70 (2017).
 93. Blander, J. M. & Medzhitov, R. Toll-dependent selection of microbial antigens for presentation by dendritic cells. *Nature* 440, 808–812 (2006).
 94. Tom, J. K., Mancini, R. J. & Esser-Kahn, A. P. Covalent Modification of Cell Surfaces with Immune Agonists Improves & Directs Immune Stimulation. *Chem. Commun.* (2013). doi:10.1039/C3CC45468A
 95. Ali, O. A. *et al.* Identification of immune factors regulating anti-tumor immunity using polymeric vaccines with multiple adjuvants. *Cancer research* 74, 1670 (2014).

96. Gutjahr, A. *et al.* Biodegradable Polymeric Nanoparticles-Based Vaccine Adjuvants for Lymph Nodes Targeting. *Vaccines (Basel)* 4, (2016).
97. Fox, C. B. *et al.* A nanoliposome delivery system to synergistically trigger TLR4 AND TLR7. *Journal of Nanobiotechnology* 12, 17 (2014).
98. Kuai, R. *et al.* Dual TLR agonist nanodiscs as a strong adjuvant system for vaccines and immunotherapy. *Journal of Controlled Release* 282, 131–139 (2018).
99. Junkins, R. D. *et al.* A robust microparticle platform for a STING-targeted adjuvant that enhances both humoral and cellular immunity during vaccination. *J Control Release* 270, 1–13 (2018).
100. Lynn, G. M. *et al.* In vivo characterization of the physicochemical properties of polymer-linked TLR agonists that enhance vaccine immunogenicity. *Nat Biotech* 33, 1201–1210 (2015).
101. Madan-Lala, R., Pradhan, P. & Roy, K. Combinatorial Delivery of Dual and Triple TLR Agonists via Polymeric Pathogen-like Particles Synergistically Enhances Innate and Adaptive Immune Responses. *Sci Rep* 7, 2530 (2017).
102. Kasturi, S. P. *et al.* Programming the magnitude and persistence of antibody responses with innate immunity. *Nature* 470, 543–547 (2011).
103. Gause, K. T. *et al.* Codelivery of NOD2 and TLR9 Ligands via Nanoengineered Protein Antigen Particles for Improving and Tuning Immune Responses. *Adv. Funct. Mater.* 26, 7526–7536 (2016).
104. Tukhvatulin, A. I. *et al.* Powerful Complex Immunoadjuvant Based on Synergistic Effect of Combined TLR4 and NOD2 Activation Significantly Enhances Magnitude of Humoral and Cellular Adaptive Immune Responses. *PLOS ONE* 11, e0155650 (2016).

105. Zhu, G. *et al.* Albumin/vaccine nanocomplexes that assemble in vivo for combination cancer immunotherapy. *Nat Commun* 8, 1954 (2017).
106. Francica, J. R. *et al.* Thermoresponsive Polymer Nanoparticles Co-deliver RSV F Trimers with a TLR-7/8 Adjuvant. *Bioconjug. Chem.* 27, 2372–2385 (2016).
107. Wiley, S. R. *et al.* Targeting TLRs Expands the Antibody Repertoire in Response to a Malaria Vaccine. *Science Translational Medicine* 3, 93ra69-93ra69 (2011).
108. Orr, M. T. *et al.* A Dual TLR Agonist Adjuvant Enhances the Immunogenicity and Protective Efficacy of the Tuberculosis Vaccine Antigen ID93. *PLoS One* 9, (2014).
109. Ebrahimian, M. *et al.* Co-delivery of Dual Toll-Like Receptor Agonists and Antigen in Poly(Lactic-Co-Glycolic) Acid/Polyethylenimine Cationic Hybrid Nanoparticles Promote Efficient In Vivo Immune Responses. *Front. Immunol.* 8, (2017).
110. Goff, P. H. *et al.* Synthetic Toll-Like Receptor 4 (TLR4) and TLR7 Ligands as Influenza Virus Vaccine Adjuvants Induce Rapid, Sustained, and Broadly Protective Responses. *J. Virol.* 89, 3221–3235 (2015).
111. Zhao, B. G., Vasilakos, J. P., Tross, D., Smirnov, D. & Klinman, D. M. Combination therapy targeting toll like receptors 7, 8 and 9 eliminates large established tumors. *J Immunother Cancer* 2, 12 (2014).
112. Moody, M. A. *et al.* Toll-like receptor 7/8 (TLR7/8) and TLR9 agonists cooperate to enhance HIV-1 envelope antibody responses in rhesus macaques. *J. Virol.* 88, 3329–3339 (2014).
113. Mitchell, R. A., Altszuler, R., Frevert, U. & Nardin, E. H. Skin scarification with *Plasmodium falciparum* peptide vaccine using synthetic TLR agonists as adjuvants elicits malaria sporozoite neutralizing immunity. *Scientific Reports* 6, 32575 (2016).

114. Whitmore, M. M. *et al.* Synergistic Activation of Innate Immunity by Double-Stranded RNA and CpG DNA Promotes Enhanced Antitumor Activity. *Cancer Res* 64, 5850–5860 (2004).
115. Zhu, Q. *et al.* Using 3 TLR ligands as a combination adjuvant induces qualitative changes in T cell responses needed for antiviral protection in mice. *J Clin Invest* 120, 607–616 (2010).
116. Mitchell, R. A., Altszuler, R., Frevert, U. & Nardin, E. H. Skin scarification with *Plasmodium falciparum* peptide vaccine using synthetic TLR agonists as adjuvants elicits malaria sporozoite neutralizing immunity. *Scientific Reports* 6, 32575 (2016).
117. Leroux-Roels, I. *et al.* Improved CD4⁺ T cell responses to *Mycobacterium tuberculosis* in PPD-negative adults by M72/AS01 as compared to the M72/AS02 and Mtb72F/AS02 tuberculosis candidate vaccine formulations: a randomized trial. *Vaccine* 31, 2196–2206 (2013).
118. Leroux-Roels, I. *et al.* Strong and persistent CD4⁺ T-cell response in healthy adults immunized with a candidate HIV-1 vaccine containing gp120, Nef and Tat antigens formulated in three Adjuvant Systems. *Vaccine* 28, 7016–7024 (2010).
119. Casella, C. R. & Mitchell, T. C. Putting endotoxin to work for us: Monophosphoryl lipid A as a safe and effective vaccine adjuvant. *Cellular and Molecular Life Sciences* 65, 3231–3240 (2008).
120. Hyer, R., McGuire, D. K., Xing, B., Jackson, S. & Janssen, R. Safety of a two-dose investigational hepatitis B vaccine, HBsAg-1018, using a toll-like receptor 9 agonist adjuvant in adults. *Vaccine* 36, 2604–2611 (2018).
121. Didierlaurent, A. M. *et al.* Adjuvant system AS01: helping to overcome the challenges of

- modern vaccines. *Expert Rev Vaccines* 16, 55–63 (2017).
122. Leroux-Roels, I. *et al.* Adjuvant system AS02V enhances humoral and cellular immune responses to pneumococcal protein PhtD vaccine in healthy young and older adults: Randomised, controlled trials. *Vaccine* 33, 577–584 (2015).
123. Garçon, N. & Di Pasquale, A. From discovery to licensure, the Adjuvant System story. *Hum Vaccin Immunother* 13, 19–33 (2016).
124. Kruit, W. H. J. *et al.* Selection of Immunostimulant AS15 for Active Immunization With MAGE-A3 Protein: Results of a Randomized Phase II Study of the European Organisation for Research and Treatment of Cancer Melanoma Group in Metastatic Melanoma. *JCO* 31, 2413–2420 (2013).
125. Leroux-Roels, G. *et al.* Impact of adjuvants on CD4(+) T cell and B cell responses to a protein antigen vaccine: Results from a phase II, randomized, multicenter trial. *Clin. Immunol.* 169, 16–27 (2016).
126. Espinosa, D. A. *et al.* Robust antibody and CD8 + T-cell responses induced by P. falciparum CSP adsorbed to cationic liposomal adjuvant CAF09 confer sterilizing immunity against experimental rodent malaria infection. *npj Vaccines* 2, 10 (2017).
127. Billeskov, R. *et al.* Low Antigen Dose in Adjuvant-Based Vaccination Selectively Induces CD4 T Cells with Enhanced Functional Avidity and Protective Efficacy. *J. Immunol.* 198, 3494–3506 (2017).
128. Haren, S. D. van *et al.* Age-Specific Adjuvant Synergy: Dual TLR7/8 and Macrophage-Inducible C-Type Lectin Activation of Human Newborn Dendritic Cells Enables Th1 Polarization. *The Journal of Immunology* 1600282 (2016). doi:10.4049/jimmunol.1600282
129. Napolitani, G., Rinaldi, A., Bertoni, F., Sallusto, F. & Lanzavecchia, A. Selected Toll-like

- receptor agonist combinations synergistically trigger a T helper type 1-polarizing program in dendritic cells. *Nat. Immunol.* 6, 769–776 (2005).
130. Honda, K. *et al.* Spatiotemporal regulation of MyD88–IRF-7 signalling for robust type-I interferon induction. *Nature* 434, 1035–1040 (2005).
131. Rajendran, L., Knölker, H.-J. & Simons, K. Subcellular targeting strategies for drug design and delivery. *Nat Rev Drug Discov* 9, 29–42 (2010).
132. Liu, H., Kwong, B. & Irvine, D. J. Membrane Anchored Immunostimulatory Oligonucleotides for In Vivo Cell Modification and Localized Immunotherapy. *Angew Chem Int Ed Engl* 50, 7052–7055 (2011).
133. Kadowaki, N. *et al.* Subsets of human dendritic cell precursors express different toll-like receptors and respond to different microbial antigens. *J. Exp. Med.* 194, 863–869 (2001).
134. Kwissa, M., Nakaya, H. I., Oluoch, H. & Pulendran, B. Distinct TLR adjuvants differentially stimulate systemic and local innate immune responses in nonhuman primates. *Blood* 119, 2044–2055 (2012).
135. Lundberg, K., Rydnert, F., Greiff, L. & Lindstedt, M. Human blood dendritic cell subsets exhibit discriminative pattern recognition receptor profiles. *Immunology* 142, 279–288 (2014).
136. Dhodapkar, M. V. *et al.* Induction of antigen-specific immunity with a vaccine targeting NY-ESO-1 to the dendritic cell receptor DEC-205. *Sci Transl Med* 6, 232ra51 (2014).
137. van Kooyk, Y., Unger, W. W. J., Fehres, C. M., Kalay, H. & García-Vallejo, J. J. Glycan-based DC-SIGN targeting vaccines to enhance antigen cross-presentation. *Molecular Immunology* 55, 143–145 (2013).
138. Wu, A. R. *et al.* Quantitative assessment of single-cell RNA-sequencing methods. *Nat Meth*

- 11, 41–46 (2014).
139. Saliba, A.-E., Westermann, A. J., Gorski, S. A. & Vogel, J. Single-cell RNA-seq: advances and future challenges. *Nucleic Acids Res* 42, 8845–8860 (2014).
140. Satija, R., Farrell, J. A., Gennert, D., Schier, A. F. & Regev, A. Spatial reconstruction of single-cell gene expression data. *Nat Biotech* 33, 495–502 (2015).
141. Achim, K. *et al.* High-throughput spatial mapping of single-cell RNA-seq data to tissue of origin. *Nat Biotech* 33, 503–509 (2015).
142. Patil, S. *et al.* Single-cell analysis shows that paracrine signaling by first responder cells shapes the interferon- β response to viral infection. *Sci Signal* 8, ra16 (2015).
143. Chen, Y.-Q. *et al.* Influenza Infection in Humans Induces Broadly Cross-Reactive and Protective Neuraminidase-Reactive Antibodies. *Cell* 173, 417-429.e10 (2018).
144. Schreibelt, G. *et al.* Commonly used prophylactic vaccines as an alternative for synthetically produced TLR ligands to mature monocyte-derived dendritic cells. *Blood* 116, 564–574 (2010).
145. Douglass, E. F., Miller, C. J., Sparer, G., Shapiro, H. & Spiegel, D. A. A Comprehensive Mathematical Model for Three-Body Binding Equilibria. *J Am Chem Soc* 135, 6092–6099 (2013).
146. Shukla, N. M. *et al.* Toll-Like Receptor (TLR)-7 and -8 Modulatory Activities of Dimeric Imidazoquinolines. *J. Med. Chem.* 55, 1106–1116 (2012).
147. Temizoz, B. *et al.* TLR9 and STING agonists synergistically induce innate and adaptive type-II IFN. *Eur. J. Immunol.* 45, 1159–1169 (2015).
148. Li, L. *et al.* Hydrolysis of 2'3'-cGAMP by ENPP1 and design of nonhydrolyzable analogs. *Nature Chemical Biology* 10, 1043–1048 (2014).

149. Kim, S. *et al.* Anticancer Flavonoids Are Mouse-Selective STING Agonists. *ACS Chem. Biol.* 8, 1396–1401 (2013).
150. van Haren, S. D. *et al.* Age-Specific Adjuvant Synergy: Dual TLR7/8 and Mincle Activation of Human Newborn Dendritic Cells Enables Th1 Polarization. *J. Immunol.* 197, 4413–4424 (2016).
151. Negahdaripour, M. *et al.* A novel HPV prophylactic peptide vaccine, designed by immunoinformatics and structural vaccinology approaches. *Infection, Genetics and Evolution* 54, 402–416 (2017).
152. Ko, E.-J., Lee, Y.-T., Lee, Y., Kim, K.-H. & Kang, S.-M. Distinct Effects of Monophosphoryl Lipid A, Oligodeoxynucleotide CpG, and Combination Adjuvants on Modulating Innate and Adaptive Immune Responses to Influenza Vaccination. *Immune Netw* 17, 326–342 (2017).
153. Seydoux, E. *et al.* Effective Combination Adjuvants Engage Both TLR and Inflammasome Pathways To Promote Potent Adaptive Immune Responses. *J. Immunol.* 201, 98–112 (2018).
154. Schmidt, S. T. *et al.* The administration route is decisive for the ability of the vaccine adjuvant CAF09 to induce antigen-specific CD8⁺ T-cell responses: The immunological consequences of the biodistribution profile. *J Control Release* 239, 107–117 (2016).
155. Weeratna, R. D., McCluskie, M. J., Xu, Y. & Davis, H. L. CpG DNA induces stronger immune responses with less toxicity than other adjuvants. *Vaccine* 18, 1755–1762 (2000).
156. Lai, C.-Y., Yu, G.-Y., Luo, Y., Xiang, R. & Chuang, T.-H. Immunostimulatory Activities of CpG-Oligodeoxynucleotides in Teleosts: Toll-Like Receptors 9 and 21. *Front Immunol* 10, (2019).

157. Klinman, D. M. *et al.* Activation of the innate immune system by CpG oligodeoxynucleotides: immunoprotective activity and safety. *Springer Semin Immunopathol* 22, 173–183 (2000).
158. Vollmer, J. & Krieg, A. M. Immunotherapeutic applications of CpG oligodeoxynucleotide TLR9 agonists. *Advanced Drug Delivery Reviews* 61, 195–204 (2009).

2 Immune potentiator for increased safety and improved protection of vaccines by NF- κ B modulation

2.1 Summary

Many modern vaccines include adjuvants that activate the immune system and provide an enhanced humoral or cellular response. Current approved adjuvants are unable to provide desired responses against some pathogens (e.g. HIV or dengue). Many new adjuvants have been developed and demonstrate promising results, but side effects from the inflammatory response induced by these adjuvants have resulted in limited FDA approvals. No adjuvants yet possess the capability to independently modulate inflammation and protection. Here we demonstrate a method to limit inflammation and side effects associated with vaccination while retaining the protective responses using a variety of promising adjuvants. To accomplish this, we combined a selective NF- κ B inhibitor with the immune adjuvant. The resulting vaccines reduce systemic inflammation and boost antibody responses. In an influenza challenge model, we demonstrate that this approach enhances protection. This method is generalizable across a broad range of adjuvants and antigens. We anticipate these studies will lead to a novel approach to vaccine formulation design that may prove general across a wide range of adjuvants, enabling their greater use in the public realm.

2.2 Introduction

Vaccines are considered one of the most effective global health interventions against infectious diseases. Despite their success, current and future vaccines face contradictory challenges of increasingly stringent safety margins and more effective and diverse protective responses. A major challenge in developing new vaccine approaches is striking a balance between effective

immune activation, leading to protective responses, and limiting the excess inflammation and side effects. To boost the immune response, toll-like receptor (TLR) agonists have been explored as vaccine adjuvants because they activate the innate immune system, promoting the expression of a wide variety of immune genes including inflammatory cytokines and cell surface receptors important for T cell interactions.¹⁻⁶ Effective TLR agonists stimulate the desired cellular or humoral adaptive responses; however, the excessive inflammation induced by many of these compounds has made it challenging to transition them into new clinical vaccines.⁷ For example, CpG DNA, a TLR 9 agonist, has wide-ranging promise as a vaccine adjuvant and provides protection for diseases currently without a vaccine, such as HIV.⁸ CpG DNA also enables vaccines to be produced with less antigen⁹, induces protective responses faster¹⁰, and produces effective anti-tumor activity.^{11,12} CpG has demonstrated great promise in increasing seroprotective antibody titers in human clinical trials.^{13,14} However, the excessive inflammatory response induced by this adjuvant has resulted in many clinical trial failures and is cited as limiting its therapeutic promise.^{15,16} CpGs are only a fraction of the hundreds of TLR agonists.¹⁷ However due to the unsafe side effects, only a handful of TLR agonists are approved for limited use in humans.¹⁸ Studies indicate that side effects are mediated through excessive and systemic distribution of TNF- α and IL-6.^{19,20} Here we demonstrate a method to decouple part of the inflammatory response from the antigen presenting actions of several adjuvants using an immune potentiator. Using a broad range of TLR agonists, we demonstrate both in vitro and in vivo that using an immune potentiator decreases proinflammatory cytokines while maintaining adaptive immune function. In vivo, we find that co-administering the immune potentiator with the 2017-2018 flu vaccine (Fluzone) decreases side effects associated with vaccination and increases protection. Co-administration of the immune potentiator with CpG-ODN1826 (CpG) and dengue capsid protein leads to elimination

of systemic proinflammatory cytokines post-vaccination and yields sustained neutralizing antibodies. Additionally, administering the immune potentiator with CpG and gp120, a HIV viral coat protein, increased serum IgG and vaginal IgA antibodies and shifted IgG antibody epitope recognition. Lastly, we observed immune potentiation and improved safety for several TLR agonists – implying a general approach. Immune potentiation may find use in reducing the systemic side effects associated with inflammation for many adjuvanted vaccines²¹– creating the potential for many PRR agonists to be used safely, increasing the diversity of adaptive immune profiles and widening the scope of disease prevention and treatment.

2.3 Results and discussion

2.3.1 Selection of Immune Potentiator

In seeking a method of immune potentiation, we explored the extensive research on the TLR activation pathway. This powerful mechanistic framework let us hypothesize about how TLR activation directs inflammatory cytokines and antigen presentation. As TLR pathways converge with NF- κ B activation, and inflammatory and adaptive responses diverge upon which NF- κ B subunit is activated, we hypothesized that we could decouple these processes via selective inhibition – leading to reduced side effects but maintaining the adaptive response. Upon TLR activation, the transcription factor NF- κ B primes the transcription of pro-inflammatory cytokines such as IL-6 and TNF- α , and cell surface receptors such as MHC-II, CD40, CD80 and CD86.^{22–}

²⁴ The NF- κ B family is a family of transcription factors, consisting of two subunits: a DNA binding domain and a transcriptional activator.^{25,26} Each NF- κ B dimer controls expression of a different set of genes for distinct cellular processes – broadly, some dimers control inflammatory

expression while others control antigen presentation.^{25–27} Selectively modulating a pathway, we conjectured, might lead to increased antigen presentation, while decreasing inflammation. NF- κ B inhibitors have been widely explored for reducing cytokine expression in cancer^{28–31}, autoimmune disorders,^{32,33} and sepsis,^{34–36} yet they have not been explored as vaccine potentiators. This lack of experimentation may be because it is broadly understood that NF- κ B activation is necessary in mounting an adequate adaptive immune response.^{31,37} However, only certain subunits direct antigen presentation³⁸. As a proof-of-concept immune potentiator we chose SN50, a cell permeable peptide that consists of the nuclear localization sequence (NLS) of the NF- κ B subunit, p50 which blocks the import of p50 containing dimers into the nucleus.³⁹

First, we sought to determine if SN50 enables inhibition of NF- κ B of innate immune cells. We validated that SN50 reduced total NF- κ B activity in human (THP-1 monocytes) and mouse (RAW macrophages) cells in a dose dependent manner. (**Fig. A1**).

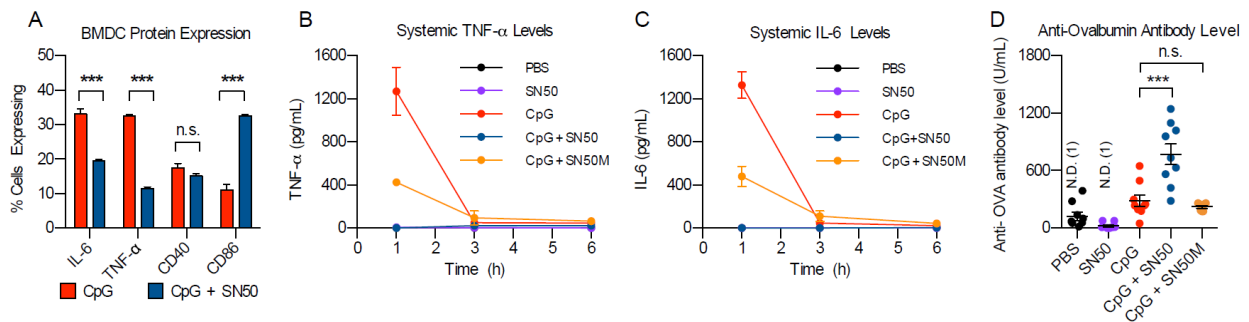


Figure 2.1. In vivo vaccination with model antigen ovalbumin and immune adjuvant SN50. (A) Intracellular cytokine staining of BMDCs treated with CpG (red bars) or CpG + SN50 (blue bars), n=3. (B) Systemic cytokine levels of TNF- α measured at 1h, 3h, 6h post-injection with: PBS (black line), SN50 alone (purple line), CpG (red line), CpG + SN50 (blue line), CpG + SN50M (yellow line), n = 4 for each time point. (C) Systemic cytokine levels of IL-6. (D) Anti-ovalbumin antibody level, day 28, n = 8. *p < 0.05, **p < 0.01, ***p < 0.001.

2.3.2 Examination of CpG-induced inflammation and resulting immune response

We sought to verify that SN50 could enable antigen presenting cells to upregulate cell surface receptors, while limiting pro-inflammatory cytokine production. We incubated murine bone marrow- derived dendritic cells (BMDCs) with SN50 and CpG or CpG alone for 6h and analyzed how the potentiator altered cytokine production and cell surface receptor expression (**Fig. 2.1a, Fig. A2**). Intracellular cytokine staining revealed that cells treated with SN50 demonstrated a 21% decrease in cells expressing TNF- α and a 13% decrease in cells expressing IL-6. Meanwhile, CD86 was upregulated by 22% and CD40 was only down regulated by 2.5%. Because the p65-p50 dimer is the most abundant dimer found in resting cells and involved in inflammatory cytokine production, we conjecture that by inhibiting this dimer, we enable the transcription and translation of cell surface receptors while limiting inflammatory cytokines. This is consistent with previous knockout experiments that demonstrate the significance of the p65 subunit in increasing inflammatory cytokine production and inhibition of CD40 and CD86.³⁸ The result is lower inflammatory responses while priming effective adaptive immune communication.

After observing that SN50 can limit inflammation without decreasing cell surface receptor expression in vitro, we next wanted to examine the effect in vivo. To determine if inhibition of NF- κ B could decrease the systemic levels of pro-inflammatory cytokines associated with CpG vaccination, we vaccinated mice intramuscularly (i.m.) with 100 μ g ovalbumin (OVA) and: PBS, SN50 (500 μ g), CpG (50 μ g), SN50 + CpG, or SN50M (500 μ g) + CpG. SN50M is a physical control for SN50 as it is a much weaker inhibitor. We chose to measure systemic levels of proinflammatory cytokines TNF- α and IL-6 because high levels are unsafe and lead to side

effects.^{19,20,40} We measured these pro-inflammatory cytokines at 1h, 3h, 6h, 24h and 48h post-injection in all groups to determine the timepoint where cytokines peak in response to CpG vaccination (**Fig. 2.1b, 1.1c, Fig. A3**). Mice vaccinated with OVA and PBS or SN50 alone elicited no systemic cytokine response. CpG demonstrated the highest response of both TNF- α (1325 pg/mL) and IL-6 (1269 pg/mL) at the 1h timepoint. The CpG + SN50 group showed complete elimination of cytokines for both cytokines. The CpG + SN50M group showed a decrease in cytokine levels, although not as large as observed with CpG + SN50. We confirmed that this decrease in inflammatory cytokines is due to the high local inhibition of injected SN50M and not physical aggregation (**Fig. A3**). To determine how SN50 would affect the humoral response, we analyzed serum antibody levels on day 28 (**Fig. 2.1d**). We chose to use an ELISA that measures total Ig(G+A+M).⁴¹ The CpG group demonstrated a 2.4-fold increase in anti-OVA antibodies compared to PBS alone. Mice vaccinated with CpG + SN50 demonstrated a 5.9-fold increase over the PBS group and 2.7-fold increase over the CpG group. These data confirmed our hypothesis that high levels of systemic TNF- α and IL-6 can be decoupled from the humoral, adaptive immune response. We were surprised to find that addition of SN50 boosted the downstream adaptive response, leading to immune potentiation. Due to this increase in adaptive response and improved safety profile after vaccination we consider SN50 to be an immune potentiator.

¹ In humans, systemic TNF- α correlate with local side effects (e.g. swelling, pain at injection site) and systemic IL-6 has been correlated with system-wide side effects (e.g. fatigue, headache, etc.) in response to vaccination.^{19,20} Additionally, both of these cytokines act as pyrogens when distributed systemically, leading to a fever response.⁴⁰

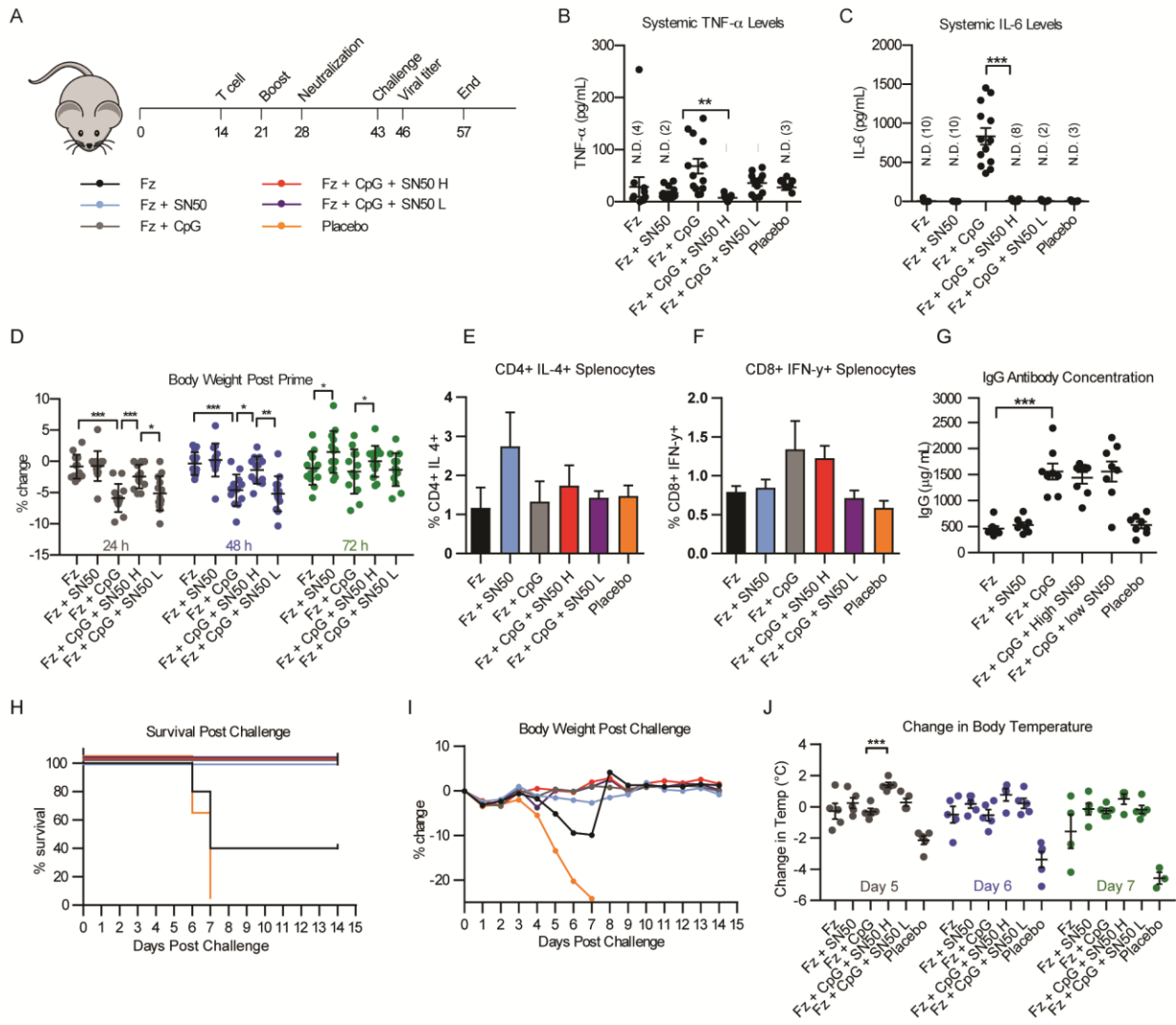


Figure 2.2. Influenza Challenge Model (A) Schematic of influenza challenge study. (B) Systemic TNF- α levels 1h post-vaccination with Fz, Fz + SN50, Fz + CpG, Fz + CpG + SN50 H, Fz + CpG + SN50 L, Placebo. n = 13 (C) Systemic IL-6 levels 1h post-vaccination. n =13 (D) Percent change in body weight 24h (grey), 48h (blue) and 72h (green) post-vaccination, n =13. (E) Antigen specific CD4+ cells. (F) Antigen specific CD8+ cells. (G) Day 28 IgG antibody concentration, n =8. (H) Survival 1-14 days post challenge, n = 5. Groups: Fz (black), Fz + SN50 (blue), Fz + CpG (grey), Fz + CpG + SN50 H (red), Fz + CpG + SN50 L (purple), Placebo (orange). n = 5 (I) Percent change in body weight 1-14 days, n = 5. (J) Body temperature 1-14 days post challenge, n=5. * $p < 0.05$, ** $p < 0.01$, *** $p < 0.001$.

2.3.3 Immune potentiation in in vivo influenza challenge model

We next wanted to focus on how SN50 might transition to a vaccine with challenge. We selected influenza vaccine as a proof-of-concept vaccination both due to its universality and the relative ease of running animal challenges with multiple parameters. We sought to determine if SN50 would reduce side effects associated with strong adjuvanticity and to see what effect this alteration on systemic cytokines would have on protection. We vaccinated mice i.m. with Fluzone® quadrivalent vaccine (Fz) for the 2017/2018 influenza season, with or without CpG (50 µg) as an immune adjuvant and 500 µg SN50 (SN50 H) or 50 µg SN50 (SN50 L) as an immune potentiator. The Fz + SN50 group demonstrated lower levels of TNF- α than Fz alone (**Fig. 2.2b, 2.2c**). Across all groups, the addition of SN50 reduced levels of TNF- α and IL-6 to levels consistent with the placebo group. To examine whether SN50 can mitigate side effects from vaccination, we analyzed the percent change in body weight 24, 48 and 72h post-vaccination (**Fig. 2.2d, A4**). Weight loss is the easiest and most objective measure of side effects in mice. Mice vaccinated with Fz and Fz + SN50 lost an average of 0.85% and 0.75%, respectively by the 24h timepoint. The Fz + CpG group lost an average of 5.9%. Adding SN50 H decreased the amount of weight loss to 2.4% and SN50 L to 5.1%. At 72h the Fz group were -1.1% of the starting weight whereas mice vaccinated with Fz + SN50 gained +1.5%. The Fz + CpG group lost -1.6% of the starting weight and adding SN50 H lead to a reduction in weight loss (0% change) and adding SN50 L lead to -1.3% change. Overall, mice with SN50 lost less weight than mice without SN50, demonstrating that SN50 lowered side effects associated with vaccination.

We next wanted to see if the addition of SN50 would change the T cell responses or antibody production. On day 14, we analyzed splenocytes for antigen specific CD4+ and CD8+ T cells. We observed no statistically significant differences between samples with and without SN50

(**Fig. 2.2e, 2.2f, Fig. A5**). On day 28, we analyzed the serum for antibody levels in the blood (**Fig. 2.2g and A6**). There was no significant difference in serum IgG concentration between Fz and Fz + SN50. There was a significant difference between Fz samples and Fz + CpG of 2.9 fold. There was no significant difference between groups vaccinated with CpG, implying that the addition of SN50 reduces inflammation and side effects from vaccination, while maintaining the antibody concentration.

We next sought to determine if SN50 would increase the protection of Fluzone. Mice were lethally challenged intranasally with 10^5 PFU A/Michigan/45/2015. On day 3 post-challenge we analyzed the lungs of three mice for viral titer (**Fig. A4**). Survival was analyzed for 14 days post-challenge (**Fig. 2.2h**). By day 7, all placebo mice and 60% of the Fz mice had reached the humane endpoint and were euthanized. All other mice survived. The Fz + SN50 group was significantly more protected than the Fz alone group. The addition of SN50 to Fz + CpG confers equal protection, while improving side effects from the initial vaccination. Surprisingly, simply adding SN50 to Fz conferred enhanced protection equal to Fz + CpG group.

Mice were analyzed for change in body weight and body temperature for 14 days post-challenge (**Fig. 2.2i, 2.2j, Fig. A4**). The peak average weight loss between Fz (-9.9%) and Fz + SN50 (-2.67%) was statistically significant. Greater weight loss is associated with a more intense infection, these data demonstrate that adding SN50 to Fz improves the response to infection. Addition of SN50 to Fz + CpG demonstrates no significant change in weight loss indicating that the SN50 can reduce systemic cytokines and side effects from vaccination with no detrimental effects to the protective response.

As an additional parameter of disease pathology, we examined body temperature post-challenge. Unlike in humans, mice demonstrate a reduction in body temperature upon infection.⁴²

The placebo has the largest peak drop in temperature (-4.57 °C), followed by the Fz group (-1.58 °C) (**Fig. 2.2j**). Adding SN50 to Fz or Fz + CpG mitigated the decrease in temperature across all groups.

Safety and protection of new vaccine adjuvants are typically considered two interdependent variables with an inverse relationship, where adequate protection is acquired by limiting safety or vice versa. As this potentiator makes the vaccine both safer and more protective, we sought a single way to analyze how SN50 was changing the safety and protection profile. As these variables are considered inversely related, there are few precedents for correlation. However, a common scoring system used widely across fields is a quartile-based scoring system.⁴³⁻⁴⁶ Following precedent for scoring systems, we developed a safety vs protection plot (**Fig. A7**). This plot is meant only to serve as a visual representation of all data collected within this study. All groups that included SN50 in the vaccination increased both the safety and the protection of the vaccine. When all data is taken together, we conclude that SN50 acts as an immune potentiator by both increasing the safety profile and improving the protective outcome of the vaccination.

Next, we wanted to examine if this type of immune potentiator could improve safety and maintain the adaptive response across a broader range of diseases and antigens. We chose to vaccinate against dengue and HIV because they represent additional, important diseases with active vaccine research. In each case, challenges with current methods have been identified and we wanted to see if SN50 could help address those challenges, as well as maintain the current function of vaccination strategies. For dengue, the main challenge is producing antibodies that neutralize the virus, inhibiting cellular uptake. For HIV, a key challenge is in generating IgA antibodies at the mucosal interface as well as eliciting broadly neutralizing antibodies targeted to

select epitopes. To explore how adding an immune potentiator affects each of these responses, we analyzed each antigen set in greater detail.

2.3.4 Examination of immune potentiator on Dengue neutralization

To explore dengue further, we vaccinated mice with the capsid protein of dengue serotype 2 (DENV-2C) and: CpG (50 µg), CpG + 500 µg SN50. SN50 completely eliminated expression of systemic cytokines (**Fig. 2.3a, 2.3b**). On day 28 we analyzed the difference in antibody concentration (**Fig. 2.3c**). Antibody concentration in CpG + SN50 mice were almost two-fold higher than the CpG group.

To determine if SN50 alters the neutralization potential, we analyzed the neutralizing titer for four strains of dengue (**Fig. 2.3d**). We tested four serum samples against one strain representative of each dengue serotype. The differences in neutralization potential were not significantly different between the two groups implying that, similar to our flu results, SN50 improves the safety while maintaining the protective responses of vaccination.

2.3.5 Analysis of influence of immune potentiator on HIV vaccination

To further test the efficacy of vaccines with SN50 and to attain a broader picture of the induced humoral immune response, we vaccinated mice with gp120, a viral coat protein from HIV necessary for infection and a target of many HIV vaccines, using CpG as the immune adjuvant. Mice vaccinated with CpG demonstrated high levels of both TNF- α and IL-6, whereas all other groups including mice vaccinated with CpG + SN50 demonstrated non-detectable levels of systemic cytokines at the 1h time point (**Fig. 2.3e, 2.3f**). On day 28, we analyzed the serum anti-gp120 antibody concentration. The CpG + SN50 group induced a 4.7 fold higher anti-gp120 IgG antibody level than the CpG group in the serum (**Fig. 2.3g, 2.3h**). This demonstrates that the addition of SN50 increases IgG antibody levels across multiple antigens and suggests that it may serve as a general immune potentiator. Because mucous membranes are particularly susceptible to

HIV infection, we also measured the anti-gp120 IgG and IgA antibody concentration in vaginal secretions (**Fig. 2.3i, 2.3j**). The CpG + SN50 group demonstrated a 4.4 fold increase in anti-gp120 IgA antibodies than mice vaccinated with CpG alone. These results suggest that SN50 with gp120 may help induce class-switching to IgA antibody isotype.

We next chose to determine if there were any alterations in the gp120 epitopes recognized by the resulting antibodies, using an overlapping peptide microarray. Interestingly, the number of epitopes recognized by CpG alone was higher than antibodies collected from CpG + SN50 mice; however, the fluorescent mean intensity of recognized epitopes is higher in the CpG + SN50 mice (**Fig. 2.3k, 2.3l**) – implying a higher concentration of antibodies against those epitopes. Upon closer inspection of particular epitopes recognized, we saw that adding the immune potentiator to the formulation shifts the epitope recognition, as different epitopes are recognized in the CpG alone and CpG + SN50, often exclusively in one condition or the other (**Fig. 2.3m**). The most highly recognized epitope in the CpG + SN50 group corresponds to the epitope recognized by the recently isolated 35O22 monoclonal antibody.⁴⁶ Antibodies isolated from mice vaccinated with CpG + SN50 also recognize the CD4 binding site recognized by several potent, broadly neutralizing antibodies (VRC01, VRC03, b12). Based on the epitopes recognized by the serum samples, we hypothesize that these antibodies may be beneficial to protection. From these data we demonstrate that the addition of SN50 shifts the epitope selectivity in the case of gp120. This may prove valuable with diseases where the current recognized epitopes are not effective enough to provide protection.

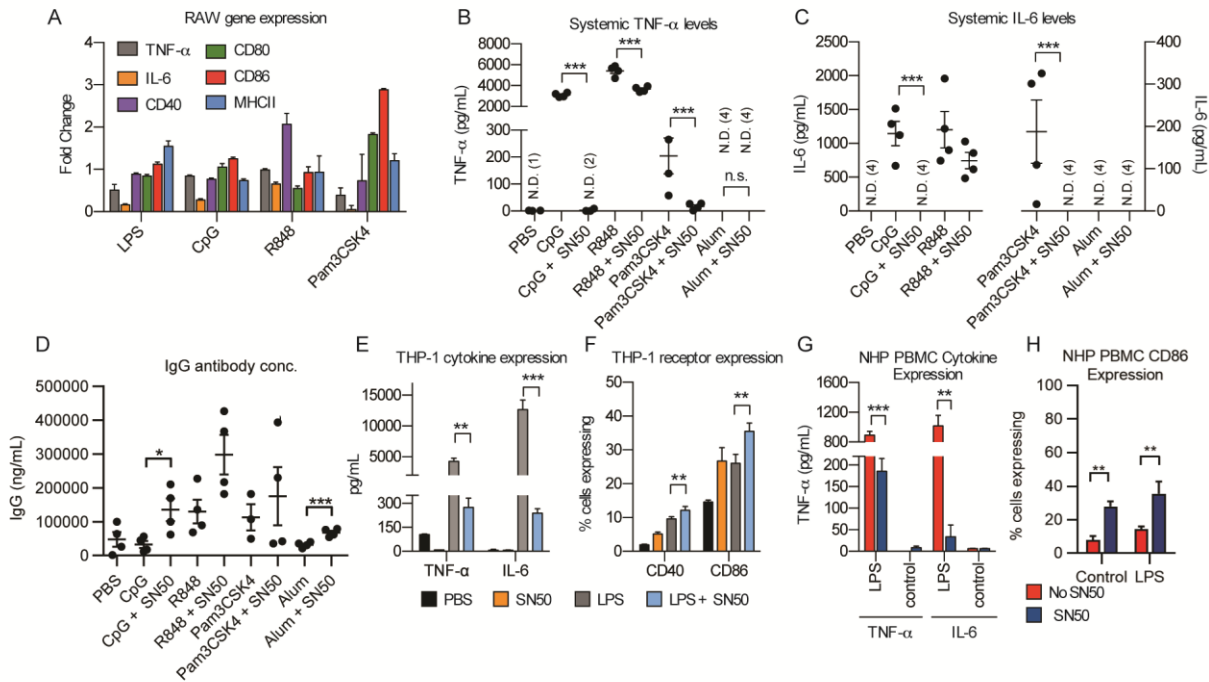


Figure 2.4. In vivo vaccinations across a broad range of adjuvants. (A) qPCR gene expression analysis of RAW macrophages stimulated with SN50 and TLR agonists compared to cells stimulated with TLR agonist alone. Pro-inflammatory cytokines TNF- α (grey bars) and IL-6 (orange bars) and cell surface receptors CD40 (purple bars), CD80 (green bars), CD86 (red bars) and MHCII (blue bars). (B) Systemic TNF- α cytokine levels of TNF- α measured at 1h post-injection with gp120 and: PBS, CpG, CpG + SN50, Pam3CSK4, Pam3CSK4 + SN50, R848, R848 + SN50, Alum, Alum + SN50, n =4. (C) Systemic IL-6 cytokine levels measured at 1h post-injection. (D) Serum IgG antibody concentrations, day 28. (E) Human THP-1 cell pro-inflammatory cytokines TNF- α and IL-6 in cell supernatant after treatment with PBS (black bars), SN50 (orange bars), LPS (grey bars), or LPS + SN50 (blue bars). (F) Cell surface receptor expression on human THP-1 cell after treatment with PBS (black bars), SN50 (orange bars), LPS (grey bars), or LPS + SN50 (blue bars). (G) Cytokine expression analysis of TNF- α and IL-6 in cell supernatant of NHP PBMCs 6h. No SN50 (red bars), SN50 (blue bars). LPS 1 μ g /mL (H) CD86 expression of NHP PBMCs 18h. No SN50 (red bars), SN50 (blue bars). *p < 0.05, **p < 0.01, ***p < 0.001.

2.3.6 Improvement of adjuvant responses across a variety of TLRs and Species

To examine the effects of the SN50 across a broad range of TLR agonists, we performed qPCR on RAW macrophages treated with SN50 followed by stimulation with agonists of different TLRs. We stimulated cells with SN50 and LPS (10 ng/mL), CpG (5 μ g/mL), R848 (1 μ g/mL) and

Pam3CSK4 (100 ng/mL) and compared transcript levels to cells treated with TLR agonist alone (**Fig. 2.4a**). We chose these TLR agonists because they represent a subset of the compounds with promising potential for commercial use if the inflammatory side effects can be controlled. In RAW macrophages, we observed downregulation of TNF- α and IL-6 pro-inflammatory cytokine transcript levels. Across all agonists, the cell surface receptors CD86 and MHCII transcript levels were upregulated, compared to agonist alone, implying that cellular communication of the APC to the T cell may not be attenuated by the addition of SN50 and subsequent reduction in cytokine production.

To examine how this would translate in vivo, we vaccinated mice with CpG (50 μ g), Pam3CSK4 (20 μ g) and R848 (50 μ g) using gp120 as the antigen. We chose to run these adjuvants alongside the most widely employed adjuvant, alum (250 μ g).

With CpG, we observed complete elimination of systemic TNF- α and IL-6 proinflammatory cytokines (**Fig. 2.4b, 2.4c**). With R848 and Pam3CSK4 we saw a significant decrease in systemic cytokines. We hypothesize that SN50 is less effective at decreasing cytokines with R848 due to the low molecular weight of the R848 molecule, enabling more rapid systemic distribution. Alum alone did not evoke a systemic cytokine response and the addition of SN50 did not alter the cytokine profile. The addition of SN50 increased the antibody levels for all adjuvants, including alum, demonstrating the broad potential use of this system to a large number of immune adjuvants (**Fig. 2.4d**).

To understand how this effect may translate to human vaccinations, we treated THP-1 monocytes with 1 μ g/mL LPS with or without SN50. Cells treated with SN50 and LPS expressed dramatically lower levels of TNF- α and IL-6 (**Fig. 2.4e, A8**). We also observed increased levels

of CD40 and CD86 (**Fig. 2.4f, Fig. A8**). Additionally, we examined the effects of SN50 on non-human primate rhesus macaque (NHP) primary peripheral blood mononuclear cells (PBMCs). We stimulated NHP PBMCs with SN50 and LPS or LPS alone for 6h and analyzed the cell supernatant for pro-inflammatory cytokines. Cells stimulated with LPS demonstrated high levels of TNF- α and IL-6 in the cell supernatant, cells with SN50 demonstrated significant reduction in cytokine levels (**Fig. 2.4g**). We observed that CD86 expression was upregulated 2-fold in cells stimulated with SN50 and LPS compared to cells stimulated with LPS alone (**Fig. 2.4h, Fig. A9**). This implies that SN50 may work similarly in NHP and humans as it does in mice.

2.3.7 Exploration of the mechanism of action

We next wanted to more directly examine how early systemic expression of TNF- α and IL-6 impact the immediate inflammatory response and downstream adaptive immune response. We vaccinated mice with CpG and either TNF- α neutralizing antibody (TNF- α N) or IL-6 neutralizing antibody (IL-6N) and measured the systemic cytokines (**Fig. 2.5**). The CpG + IL-6N group demonstrated a 1.4 -fold decrease in TNF- α expression and a complete reduction of systemic IL-6 expression. The CpG + TNF- α N group demonstrated complete elimination of systemic TNF- α and a 3-fold reduction of IL-6 expression. This result was confirmed by a control isotype antibody to rule out any nonspecific interactions. Although both IL-6N and TNF- α N groups demonstrated higher average antibody levels, these differences were not statistically significant (**Fig. 2.5**). This indicates that reducing inflammation from CpG with the initial vaccination is not detrimental to antibody production. Initially it may seem surprising that decreasing the excessive systemic inflammatory response leads to a sustained adaptive response, however, adequate immunity to specific diseases has been acquired from a variety of FDA

approved immune adjuvants (e.g. alum, MPLA) without unsafe levels of pro-inflammatory cytokines.^{47,48} Additionally, a variety of studies have demonstrated that physical sequestration of non-approved immune adjuvants by conjugation to antigens^{49,50}, polymers^{51,52}, phospholipids^{52,53} or inclusion in particles⁵⁴ lead to dramatically reduced systemic pro-inflammatory cytokines without negatively affecting the adaptive response. Therefore, it is not entirely surprising that simply limiting excessive systemic inflammation from CpG adjuvanted vaccination (while enabling all other signaling) is not detrimental to the downstream adaptive response.

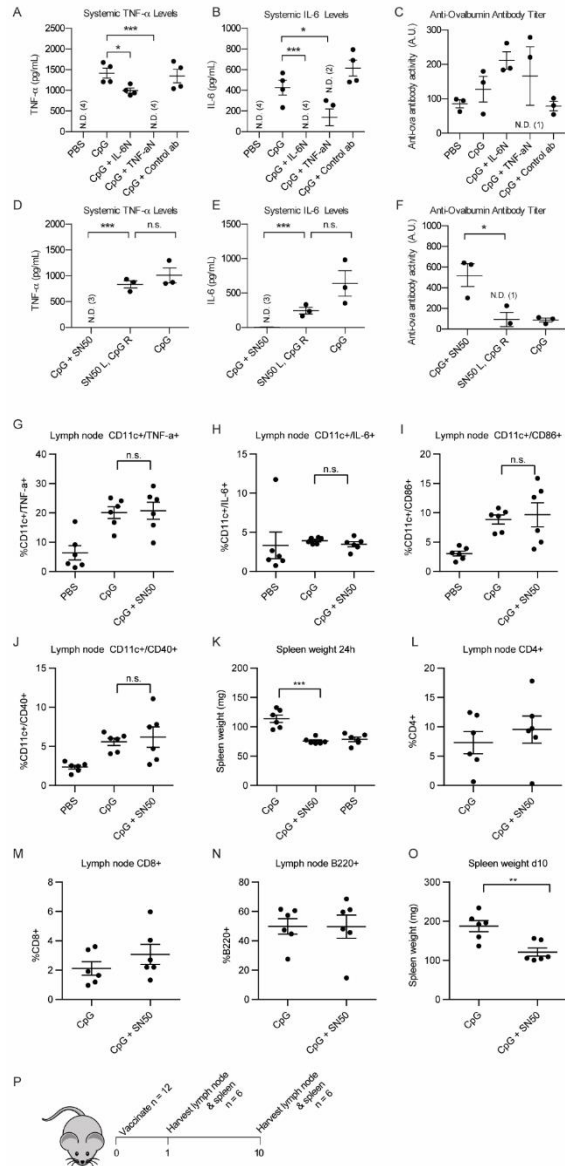


Figure 2.5. Exploration of SN50 mechanism of action. (A) Systemic TNF- α levels 1h post-vaccination with CpG, CpG + IL-6N, CpG + TNF- α N or CpG + Control ab, n = 4. (B) Systemic IL-6 levels 1h post-vaccination with CpG, CpG + IL-6N, CpG + TNF- α N or CpG + Control ab. (C) Anti-ovalbumin antibody level, day 28. (D) Systemic TNF- α levels in mice vaccinated with mixed CpG and SN50 (CpG + SN50), SN50 in left limb and CpG + OVA in right limb (SN50L, CpG R, or CpG alone, n=3). (E) Systemic IL-6 levels. (F) Anti-OVA antibody level, day 28. (G) CD11c+ TNF- α + cells in draining inguinal lymph node 24h after vaccination (H) CD11c+ IL-6+ cells in draining inguinal lymph node 24h after vaccination (I) CD11c+ CD86+ cells in draining inguinal lymph node 24h after vaccination (J) CD11c+ CD40+ cells in draining inguinal lymph node 24h after vaccination (K) Weight of spleen 24h after vaccination (L) CD4+ cells in draining inguinal lymph node 10 days post vaccination (M) CD8+ cells in draining inguinal lymph node 10 days post vaccination (N) B220+ cells in draining inguinal lymph node 10 days post vaccination (O) Weight of spleen 10 days after vaccination. (P) Experimental workflow for 24h and day 10 lymph node experiments.

Upon observing this in vivo modulation, we sought to determine whether SN50 acts locally or systemically. To examine this mechanism, we injected SN50 i.m. in the left hind limb and immediately injected CpG + OVA (SN50 L + CpG R) in the right hind limb. There was no significant difference in systemic cytokine levels tested between CpG and the SN50 L + CpG R group (**Fig. 2.5**), whereas SN50 + CpG + OVA (SN50 + CpG) injected simultaneously demonstrated reduction of TNF- α and IL-6. On day 28, we analyzed serum antibody concentrations, revealing a 5.5 fold difference between the SN50 + CpG and the SN50 L + CpG R group (**Fig. 2.5**). This demonstrates the importance of coadministration of the components and therefore indicates that SN50 is acting locally to both increase safety and protection.

We next wanted to examine how modulating systemic inflammation at early time points alters lymph node cytokine and cell surface expression and resulting cell populations. We injected mice with CpG + OVA, CpG + SN50 + OVA or PBS (**Fig. 2.5**). At 24 h we harvested the draining inguinal lymph node and analyzed the cells for dendritic cells (CD11c+) positive for TNF- α , IL-6, CD86 and CD40 (**Fig. 2.5, A11**). There was no significant difference in CD11c+ populations between CpG and CpG + SN50. On day 10, we examined the draining inguinal lymph node for CD4+, CD8+ and B220+ cells (**Fig. 2.5, A11**). There was no significant difference in cell populations between CpG and CpG + SN50. This demonstrates that the addition of SN50 does not detrimentally affect the recruitment of antigen presenting cells or their ability to secrete inflammatory cytokines or express CD86 and CD40 in the lymph node. Additionally, the addition of SN50 does not hamper the recruitment of adaptive immune cells. Interestingly, we noticed a distinct decrease in weight of the spleen at both time points when coadministering SN50 (**Fig. 2.5**).

From these experiments, we conclude that SN50 acts locally at the injection site to inhibit immediate cytokine production, containing inflammation before it is distributed systemically.

Based on our in vitro data, we believe CpG + SN50 enables TNF- α and IL-6 production locally at reduced levels. Our in vitro data suggests that immune cells exposed to CpG + SN50 express higher levels of cell surface receptors important for antigen presentation and effective T cell activation. However, in vivo, dendritic cells demonstrated no change in CD86 or CD40 expression with the addition of SN50. While our experiments confirm that SN50 reduces systemic inflammation and increases antibody levels in vivo, more in-depth exploration needs to be completed to fully understand the mechanism.

2.4 Conclusion

Using a broad range of TLR agonists, we show both in vitro and in vivo that a cell permeable inhibitor of the p50 subunit of NF- κ B, potentiates the immune response – reducing inflammation while increasing antibody responses. Co-administration of CpG with the immune potentiator results in significantly reduced levels of proinflammatory cytokines, often at undetectable levels. At the same time, this reduction in inflammation results in a 3-fold increase in the IgG levels of antibodies for the model antigen OVA. We examined how potentiation would enhance the capabilities of the adjuvants to improve the immune response. In our influenza model we directly examined side effects in response to the current commercial flu vaccine and Fz + CpG and determine that adding SN50 reduces side effects and systemic pro-inflammatory cytokine levels. We also demonstrate that the safety profile can be enhanced without negatively effecting the protective response. After vaccinated mice were challenged with influenza A, mice with SN50 added to the vaccine, lead to increased survival, less weight loss and less change in body temperature. To study the effects of potentiation on TLR agonists as vaccine adjuvants, we selected three diseases – influenza, dengue and HIV – all of which have had different challenges in vaccine development. In dengue vaccination, the goal is to increase antibody neutralization potential while

maintaining a safe profile. We demonstrate that there are no detrimental effects to dengue neutralization of antibodies with SN50, enabling us to mitigate side effects but maintain the protective response. In HIV, we vaccinated with HIV envelope protein gp120, CpG and SN50, increased both IgG and IgA levels. This method appears quite general as it works with many TLR agonists and antigens. Additionally, we demonstrate, for the first time, that directly inhibiting the inflammatory response at the injection site does not negatively affect the adaptive response. SN50 is one of hundreds of similar NF- κ B inhibitors. When used in combination with the appropriate TLR agonist, many may prove useful for eliciting specific and potentially tunable responses for distinct vaccines or immunotherapies. This methodology may find use in reducing the systemic side effects associated with inflammation seen in many adjuvanted vaccines.²¹ This method has the potential to enable a variety of PRR agonists to be used safely in vaccines, increasing the diversity of adaptive immune profiles and widening the scope of disease prevention and treatment.

In conclusion, we have demonstrated that using a specific NF- κ B inhibitor in combination with common immune adjuvants can decrease pro-inflammatory cytokine production while boosting cell-surface receptor expression for effective antigen presentation and T cell activation in mouse, human and NHP primary cells. The use of this inhibitor in vivo completely reduced systemic TNF- α and IL-6 to baseline levels while increasing the downstream adaptive humoral response from the vaccination. These phenomena were observed across a broad range of antigens for a variety of pathogens demonstrating that this may prove a general strategy for improving vaccination response while conforming to strict safety standards. There are hundreds of documented immune adjuvants that provide adequate protection against diseases but induce unsafe levels of inflammation to be approved for clinical use^{7,55,7,55} Additionally there are hundreds of NF- κ B inhibitors, some already with FDA approval, that could be multiplexed with different TLR

agonists to provide a broad range of responses.⁴⁴ We anticipate this framework will enable a variety of TLR agonists to be used safely in human vaccines, increasing the diversity of adaptive immune profiles and widening the scope of disease prevention and treatment.

2.5 Materials and Methods

Study Design: The overall objective of this study was to investigate the effect of SN50 on early innate immune responses and adaptive immune responses. Randomization was performed in the influenza challenge study. Otherwise, no randomization or blinding was performed. The experiments were designed to maximize data collection using fewer animals and to be able to include controls such as PBS injection and SN50 alone for comparison. The sample sizes were chosen based on preliminary experiments or literature precedent. Number of animals analyzed is stated in figure legends.

RAW Blue NF- κ B Assay: RAW-Blue™ NF- κ B cells (Invivogen) were passaged and plated in a 96 well plate at 100k cells/ well in 180 μ L DMEM containing 10% HIFBS. Cells were incubated at 37 °C and 5% CO₂ for 1 h. SN50 was added at indicated concentrations, cells were incubated 1 h. Immune agonists were added at their indicated concentrations. The volume of each well was brought to 200 μ L and incubated at 37 °C and 5% CO₂ for 18 h. After 18 h, 20 μ L of the cell supernatant was placed in 180 μ L freshly prepared QuantiBlue (Invivogen) solution and incubated at 37 °C and 5% CO₂ for up to 2 h. The plate was analyzed every hour using a Multiskan FC plate reader (Thermo Scientific) and absorbance was measured at 620 nm.

THP-1 Blue NF- κ B Assay: THP-Blue™ NF- κ B cells (Invivogen) were passaged and plated in a 96 well plate at 400k cells/ well in 180 μ L RPMI 1680 containing 10% HIFBS. Cells were

incubated at 37 °C and 5% CO₂ for 1 h. SN50 was added at indicated concentrations and cells were incubated for 1 h. Immune agonists were added at their indicated concentrations. The volume of each well was brought to 200 µL and incubated at 37 °C and 5% CO₂ for 18 h. After 18 h, the plate was spun down at 400 x g (Allegra X-30, Beckman Coulter) and 20 µL of the cell supernatant was placed in 180 µL freshly prepared QuantiBlue (Invivogen) solution and incubated at 37 °C and 5% CO₂ for up to 2 h. The plate was analyzed every hour using a Multiskan FC plate reader (Thermo Scientific) and absorbance was measured at 620 nm.

Gene expression: RAW 264.7 macrophages or THP-1 cells were passaged and plated in a cell culture treated 6- well plate at 4 x10⁶ cells/ well in 1.5 mL DMEM or RPMI (respectively) containing 10% HIFBS. SN50 (250 µg/mL) or PBS was added to wells and cells were incubated for 1 h at 37 °C and 5% CO₂ for 6 h. RNA was extracted using RNeasy Plus Mini kit (Qiagen). RT-PCR was performed using RT2 first strand kit (Qiagen) and BioRad thermocycler according to manufacturer's protocol. cDNA was stored at -20 °C. RT2 SYBR ROX qPCR Master mix (Qiagen) was used according to manufacturer's protocol. qPCR amplification was performed using a Stratagene Mx3005P thermocycler.

Flow Cytometry: All antibodies were purchased from Biolegend or ThermoFisher. Antibodies used in this study include: Mouse: APC TNF- α [MP6-XT22], FITC CD4 [RM4-5], APC IL-4 [11B11], FITC CD8a [53-6.7], PE IFN-γ [XMG1.2], FITC CD11c [N418], PE CD11c [N418], PE TNF- α [MP6-XT22],

APC IL-6 [MP5-20F3], FITC CD86 [PO3], APC CD40[3/23], PE CD8 [53-6.7], APC B220 [RA3-6B2], TNF- α neutralizing [TN3-19.12], IL-6 neutralizing [MP5-20F3]. Human: FITC CD86 [BU63], PE CD40 [HB14].

BMDC cell surface marker and cytokine staining: Monocytes were harvested from 6-week-old C57BL/6 mice. Monocytes were differentiated into dendritic cells (BMDCs) using supplemented culture medium: RPMI 1640 (Life Technologies), 10% HIFBS (Sigma), 20 ng/mL granulocyte-macrophage colony stimulating factor (produced using “66” cell line), 2 mM Lglutamine (Life Technologies), 1% antibiotic-antimycotic (Life Technologies), and 50 μ M beta-mercaptoethanol (Sigma). After 5 days of culture, BMDCs were incubated with 250 μ g/mL SN50. After 1 h CpG ODN 1826 (IDT) and 1 μ L/mL GolgiPlug (BD Biosciences) was added. Cells were incubated for 6 h at 37 °C in and 5% CO₂. Cells were stained for CD40, CD86 and intracellular IL- and TNF- α cytokine production and analyzed using BD Accuri C6 flow cytometer.

NHP cell surface marker and cytokine analysis: Blood samples were collected in EDTA coated collection tubes from Rhesus macaques. Whole blood was diluted to a final ratio of 1 parts blood to 1 part Phosphate buffered saline (PBS) and layered over Lympholyte®-Mammal Cell Separation Media (Cedarlane). Samples were centrifuged at 800 \times g for 20 min at room temperature and the buffy coat was collected and washed. Cells were counted and cryopreserved in 45% RPMI-1640 Media, 45% FBS, and 10% DMSO and stored in liquid nitrogen until tested. Samples were treated with SN50 (125 μ g/mL) and incubated 37 C and 5% CO₂ for 1h. After 1h LPS (1 μ g/mL) was added and cells were incubated for 12 h. Supernatant was tested for cytokine

secretion using BD Non-human Primate Th1/Th2 Cytokine Kit. Cells were pelleted and stained for CD86 expression using BD cytofix/cytoperm fixation /permeabilization solution kit according to manufacturer's protocol.

THP-1 cytokine and cell surface marker analysis: THP-1 cells (2×10^6 cells) were plated in a 12 well plate in 500 μ L RPMI containing 10% HIFBS. 100 μ g/mL SN50 was added and incubated at 37 C and 5% CO₂ for 1h. After 1h, LPS was added to wells (1 μ g/mL). After 6h cell supernatant was removed and analyzed for cytokines using Human Inflammatory Cytometric Bead array (BD). Cells were stained for CD86 and CD40 using BD cytofix/cytoperm fixation /permeabilization solution kit according to manufacturer's protocol.

SEM analysis: Sample suspensions obtained directly from injection mixtures were dried for 24 h, mounted on carbon tape, and sputter coated (South Bay Technologies) with approximately 2-4 nm of Au/Pd 60:40 or Ir. Scanning electron microscopy (SEM) of the sample suspensions was performed using an FEI Quanta 3D FEG dual beam (SEM/FIB) equipped with Inca EDS (Oxford Instruments).

In vivo studies: Animals: All animal procedures were performed under a protocol approved by the University of Chicago Institutional Animal Care and Use Committee (IACUC). 6-8 week-old C57/B6 female mice were purchased from Jackson Laboratory (JAX). All compounds were tested for endotoxin prior to use. All vaccinations were administered intramuscularly in the hind leg. Blood was collected from the saphenous vein at time points indicated.

Antigens were purchased from Sino Biological (HIV subgroup M, Influenza A H1N1 (A/California/04/2009) Hemagglutinin / HA Protein, Dengue virus DENV-2 (Strain New Guinea C) Capsid protein / DENV-C Protein (His Tag), Virogen (HIV-1 env (gp41) antigen) or Invitrogen (Vaccigrade Ovalbumin). Vaccigrade CpG ODN 1826 was purchased from Invivogen or Adipogen. SN50 was synthesized via solid phase peptide synthesis as previously described⁵⁷ and purified using Gilson preparatory HPLC.

Vaccinations: Mice were lightly anesthetized with isoflurane and injected intramuscularly in the hind leg with 50 μ L containing antigen, adjuvant and PBS. Antigen doses: ovalbumin (100 μ g), DENV2-C (5 μ g) and gp120 (3 μ g). CpG dose, 50 μ g. SN50, 500 μ g (unless otherwise stated). TNF- α N, 30 μ g. IL-6N, 30 μ g.

Plasma cytokine analysis: Blood was collected from mice at specified time points in 0.2 mL heparin coated collection tubes (VWR Scientific). Serum was isolated via centrifugation 2000 x g for 5 min. Supernatant was collected and stored at -80 °C until use. Serum was analyzed using BD Cytometric Bead Array Mouse Th1/Th2/Th17 cytokine kit or Mouse Inflammation cytokine kit according to manufacturer's protocol. Briefly, beads containing antibodies for desired cytokines were mixed with 50 μ L serum and 50 μ L PE detection reagent and incubated for 2 h. Beads were washed and analyzed using BD Accuri C6 flow cytometer. Data was analyzed using BD Accuri C6 software and Graphpad Prism.

Antibody quantification: Mice were vaccinated with indicated formulations. Blood was collected at time points indicated in 0.2 mL heparin coated collection tubes (VWR Scientific) for plasma or uncoated tubes for serum. Plasma was isolated via centrifugation (2000 x g, 5 min). Serum was isolated by allowing blood to clot for 15- 30 min RT and centrifuging (2000 x g for 10 min) at 4 °C. Serum was analyzed using a quantitative anti-ovalbumin total Ig's ELISA kit (Alpha Diagnostic International) according to the specified protocol. Total IgG and IgA was analyzed using total mouse IgG or IgA uncoated ELISA (Invitrogen) and was analyzed using Multiskan FC plate reader (Thermo Scientific) and absorbance was measured at 450 nm. Data was analyzed using Graphpad Prism.

Lymph node and spleen analysis: Mice were injected in both hind limbs with CpG + OVA, CpG + OVA + SN50 or PBS as indicated. After 24 h, mice were injected i.p. with 250 ug Brefeldin A (BFA). After 6h, mice were euthanized and the draining inguinal lymph nodes and spleen were harvested and placed in PBS containing BFA. Spleens were blotted dry and weighed. Cells were pushed through a 70 um filter with the back of syringe plunger. Both lymph nodes from a single mouse were pooled. The filter was washed with PBS containing BFA. Cells were pelleted 400 xg for 10 min and placed in Fc Block according to the manufacturer's instructions. Cells were fixed and stained using BD Cytfix/Cytoperm fixation and permeabilization kit (BD biosciences). On day 10 the same procedure was repeated without BFA. Cells were analyzed using NovoCyte flow cytometer (ACEA Biosciences, Inc.).

Influenza Challenge Model: Animals:

All animal procedures were performed under a protocol approved by the Illinois Institute of Technology Research Institute (IITRI) Animal Care and Use Committee (IACUC). 6-8 week-old C57/B6 female mice were purchased from Charles River. All compounds were tested for endotoxin prior to use. All vaccinations were administered intramuscularly in the hind leg.

Initial group assignments were assigned to using a computerized randomization procedure based on body weights that produce similar group mean values [ToxData® version 3.0 (PDS Pathology Data Systems, Inc., Basel, Switzerland)]. Mice were vaccinated by i.m. injection into the hind leg on Days 0 and 21. The vaccine material used in this study is Fluzone® quadrivalent influenza vaccine (Sanofi Pasteur). Each 0.5 mL dose of Fluzone® contains at least 15 µg of hemagglutinin (HA) from each of the following four influenza strains recommended for the 2017/2018 influenza season: A/Michigan/45/2015 X-275 (H1N1)pdm09-like strain, A/Hong Kong/4801/2014 X-263B (H3N2)-like strain, B/Phuket/3073/2013-like strain and B/Brisbane/60/2008-like strain. At least 1 µg of each strain was used in vaccination of the mice.

Body weights were collected 24 hr, 48 hr and 72 hr post-prime vaccination. Body temperatures were collected 1 hr, 3 hr, 24 hr, 48 hr and 72 hr post-prime vaccination. Blood samples were collected on days 0, 14, 28, 42, 56. Plasma was collected on day 0. Serum was collected on days 14, 28, 52 and 56. Five animals from each group were humanely euthanized on day 14 post-vaccination. Spleens were collected for T cell analysis. On day 43 post-vaccination, all mice were challenged via intranasal route with a lethal dose of A/Michigan/45/2015. The dose level of challenge virus used was an equivalent of 5 LD₅₀. For inoculation, mice were anesthetized with a ketamine (80 mg/kg) and xylazine (10 mg/kg) mixture. Once anesthetized, 0.025 mL of inoculum was delivered dropwise into the nares. The

mouse was held upright to allow the virus to be inhaled thoroughly then returned to its cage. After challenge, body weights and temperature readings were recorded daily through a transponder (BioMedic data systems, Seaford, DE) implanted subcutaneously in each mouse. Animals were monitored for morbidity/mortality for 14 days post-infection. Any animals meeting pre-determined moribund criteria (>20% weight loss) were humanely euthanized. Three animals from each group were humanely euthanized on day 3 post-challenge (Day 45) and lungs collected for viral quantitation by plaque assay/TCID₅₀. Tissues for viral titers were weighed then flash frozen in an ethanol/dry ice bath or liquid nitrogen and stored at $\leq -65^{\circ}\text{C}$. Frozen organs were thawed at 37°C for 5 min. Once thawed, organs were homogenized in MEM 10% w/v using a Bead Ruptor 12 (Omni International, Kennesaw, Georgia) in tubes containing 1.4 mm ceramic beads. Homogenized organs were centrifuged at $2,000 \times g$ for 5 min to remove cellular debris. The resulting supernatant was serially diluted 10-fold then transferred into respective wells of a 96-well plate containing a monolayer of Madin-Darby Canine Kidney Cells (MDCK) cells for titration. The TCID₅₀ assay will be performed. TCID₅₀ titers will be calculated using the method of Reed-Meunch. The remaining 5 mice in each group were monitored for the remaining days of the challenge.

Neutralization assays:

Serum samples were tested against a representative of each dengue serotype (DENV-1: strain Hawaii; DENV-2 strain New Guinea C; DENV-3 strain Philippines/H87/1956 and DENV-4 strain H241). Sera was serially diluted two-fold, (starting dilution 1:100) then incubated with standardized virus concentration of 50-120 PFU of each strain. The serum:virus mixture was transferred into respective wells of a 96-well plate which contained a monolayer of Vero

cells. The cells were incubated for 40 hours at 37 °C. After 40 hours of incubation, the cells were fixed with 1.0% PFA and stained by Anti-Flavivirus Group Antigen Antibody, clone D1-4G2-4-15 (Millipore Billerica, MA) followed by peroxidase-conjugated goat anti-mouse IgG (Kirkegaard and Perry Laboratories, Gaithersburg, MD). Spots were developed using TrueBlue Peroxidase Substrate (Kirkegaard and Perry Laboratories, Gaithersburg, MD). Plaques were visualized and counted using an ELISPOT instrument. Plaque reduction neutralization test titers (PRNT) were expressed in terms of conventional 50% PRNT end-point titers.

T cell analysis: Spleens were harvested from mice as described above at time point indicated. Splenocytes were isolated by pressing spleen fragments through a strainer attached to a 50-mL conical tube using a syringe plunger. Cells were washed through the strainer with PBS and centrifuged at 500 x g for 10 min. Supernatant was aspirated and the pellet was resuspended in 2 mL of pre-warmed lysing solution (BD Pharm Lyse™ lysing solution) and incubated at 37 °C for 2 minutes. 30 mL of PBS was added and cell suspension was centrifuged at 500 x g for 10 minutes. Supernatant was discarded and cells were resuspended in RPMI containing 10% HIFBS at 2×10^6 cells/ mL. 500 μ L was added to 24 well plate. Cells were incubated with 10 μ g/ mL Influenza A H1N1 (A/Michigan/45/2015) Hemagglutinin / HA1 Protein (His Tag) (SinoBiological). After 1h GolgiStop (BD Biosciences) was added and cells were incubated for 11 h at 37 °C and 5% CO₂. Cells were centrifuged 500 x g for 10 min and stained for CD4/ IL-4 (Biolegend o FITC anti-mouse CD4 [RM4-5], PerCP/Cy5.5 anti-mouse IL-4 [11B11]) or CD8/ IFN- γ (FITC anti-mouse CD8a [53-6.7], PE anti-mouse IFN- γ [XMG1.2]) using BD

Cytofix/Cytoperm Fixation/Permeabilization Solution Kit according to manufacturer's protocol and analyzed using a NovoCyte flow cytometer (ACEA Biosciences, Inc.).

Epitope analysis: Mouse serum was collected as described above and samples were analyzed using Multiwell RepliTope™ microarray for appropriate antigen (JPT Innovative Peptide Solutions) according to manufacturer's protocol. Briefly, serum samples were diluted in 3% BSA in 1x TBS-Buffer + 0.1% Tween20 (TBS-T) to a final concentration of 10 µg/mL. The microarray was fitted with an ArraySlide 24-4 chamber (JPT Innovative Peptide Solutions) to enable multi-sample analysis. 150 uL diluted serum was added to samples wells and incubated for 1h at 30 °C. Wells were washed 5x with TBS-T. 150 µL secondary antibody (1 µg/mL) was added to wells and incubated RT for 1h. Wells were washed 5x with TBS-T and 2x with nanopure water. Arrays were imaged using a Caliber I.D. RS-G4 confocal microscope and analyzed using ImageJ.

Safety and protection score: We assigned a safety score comprised of systemic TNF- α , IL-6 levels and weight loss post-vaccination. A score for each TNF- α , IL-6 and weight loss was assigned for each mouse. The safety score of a single mouse represents the summation of these individual scores. A protection score was assigned based on survival, change in body weight and change in body temperature post-challenge. Scores were determined by dividing values into quartiles, and assigned a number 0 to 4 based on the quartile. Higher values indicate an improved safety profile (lower TNF- α or IL-6, less weight loss after vaccination) or improved protection (survival, less weight loss, higher body temperature after challenge).

Statistics and replicates: Data is plotted and reported in the text as the mean \pm s.e.m. Sample size is as indicated in biological replicates in all in vivo and in vitro experiments. The sample sizes were chosen based on preliminary experiments or literature precedent indicating that the number would be sufficient to detect significant differences in mean values should they exist. P values were calculated using a one-way ANOVA and Tukey post hoc test or two-tailed unpaired heteroscedastic t-test where appropriate. All P values and test type for each figure are available in Table S1. All experiments have been repeated (sometimes with minor variations due to reagents and materials) and replication was successful.

2.6 References

1. Petrovsky, N. & Aguilar, J. C. Vaccine adjuvants: Current state and future trends. *Immunol. Cell Biol.* **82**, 488–496 (2004).
2. Coffman, R. L., Sher, A. & Seder, R. A. Vaccine Adjuvants: Putting Innate Immunity to Work. *Immunity* **33**, 492–503 (2010).
3. Pashine, A., Valiante, N. M. & Ulmer, J. B. Targeting the innate immune response with improved vaccine adjuvants. *Nat. Med.* **11**, S63–S68 (2005).
4. Hoebe, K., Janssen, E. & Beutler, B. The interface between innate and adaptive immunity. *Nature Immunology* (2004). doi:10.1038/ni1004-971
5. D'Agostino, P. M. *et al.* Viral-Induced Encephalitis Initiates Distinct and Functional CD103⁺ CD11b⁺ Brain Dendritic Cell Populations Within the Olfactory Bulb. *Proc. Natl. Acad. Sci.* **109**, 6175–6180 (2012).
6. Banchereau, J. & Steinman, R. M. Dendritic cells and the control of immunity. *Nature* **392**, 245–252 (1998).
7. van Duin, D., Medzhitov, R. & Shaw, A. C. Triggering TLR signaling in vaccination.

- Trends Immunol.* **27**, 49–55 (2006).
8. Dale, C. J. *et al.* Evaluation in macaques of HIV-1 DNA vaccines containing primate CpG motifs and fowlpoxvirus vaccines co-expressing IFN γ or IL-12. *Vaccine* **23**, 188–197 (2004).
 9. Weeratna, R., Comanita, L. & Davis, H. L. CPG ODN allows lower dose of antigen against hepatitis B surface antigen in BALB/c mice. *Immunol. Cell Biol.* **81**, 59–62
 10. Klinman, D. M., Xie, H. & Ivins, B. E. CpG oligonucleotides improve the protective immune response induced by the licensed anthrax vaccine. *Ann. N. Y. Acad. Sci.* **1082**, 137–150 (2006).
 11. Generation of antitumor immunity by cytotoxic T lymphocyte epitope peptide vaccination, CpG-oligodeoxynucleotide adjuvant, and CTLA-4 blockade. - Semantic Scholar. Available at: /paper/Generation-of-antitumor-immunity-by-cytotoxic-T-and-Davila-Kennedy/fab0d97dedfbc0c7326282191d11202abf19408d. (Accessed: 20th July 2018)
 12. Krieg, A. M. Toll-like receptor 9 (TLR9) agonists in the treatment of cancer. *Oncogene* **27**, 161–167 (2008).
 13. Ellis, R. D. *et al.* Phase 1 Study in Malaria Naïve Adults of BSAM2/Alhydrogel®+CPG 7909, a Blood Stage Vaccine against *P. falciparum* Malaria. *PLOS ONE* **7**, e46094 (2012).
 14. Cross, A. S. *et al.* Phase 1 testing of detoxified LPS/group B meningococcal outer membrane protein vaccine with and without synthetic CPG 7909 adjuvant for the prevention and treatment of sepsis. *Vaccine* **33**, 6719–6726 (2015).
 15. Bode, C., Zhao, G., Steinhagen, F., Kinjo, T. & Klinman, D. M. CpG DNA as a vaccine adjuvant. *Expert Rev. Vaccines* **10**, 499–511 (2011).
 16. CpG DNA as a vaccine adjuvant: Expert Review of Vaccines: Vol 2, No 2. Available at:

<https://www.tandfonline.com/doi/abs/10.1586/14760584.2.2.305>. (Accessed: 20th July 2018)

17. Kanzler, H., Barrat, F. J., Hessel, E. M. & Coffman, R. L. Therapeutic targeting of innate immunity with Toll-like receptor agonists and antagonists. *Nat. Med.* **13**, 552–559 (2007).
18. Mbow, M. L., De Gregorio, E., Valiante, N. M. & Rappuoli, R. New adjuvants for human vaccines. *Curr. Opin. Immunol.* **22**, 411–416 (2010).
19. Christian, L. M., Porter, K., Karlsson, E. & Schultz-Cherry, S. Proinflammatory cytokine responses correspond with subjective side effects after influenza virus vaccination. *Vaccine* **33**, 3360–3366 (2015).
20. Simon, W. L., Salk, H. M., Ovsyannikova, I. G., Kennedy, R. B. & Poland, G. A. Cytokine production associated with smallpox vaccine responses. *Immunotherapy* **6**, 1097–1112 (2014).
21. Pasquale, A. D., Preiss, S., Silva, F. T. D. & Garçon, N. Vaccine Adjuvants: from 1920 to 2015 and Beyond. *Vaccines* **3**, 320–343 (2015).
22. Barton, G. M. & Medzhitov, R. Toll-Like Receptor Signaling Pathways. *Science* **300**, 1524–1525 (2003).
23. Lawrence, T. The Nuclear Factor NF- κ B Pathway in Inflammation. *Cold Spring Harb. Perspect. Biol.* **1**, a001651–a001651 (2009).
24. Akira, S. & Takeda, K. Toll-like receptor signalling. *Nat. Rev. Immunol.* **4**, 499–511 (2004).
25. Hoffmann, A., Leung, T. H. & Baltimore, D. Genetic analysis of NF- κ B/Rel transcription factors defines functional specificities. *EMBO J.* **22**, 5530–5539 (2003).
26. Hoffmann, A. & Baltimore, D. Circuitry of nuclear factor kappaB signaling. *Immunol. Rev.*

- 210**, 171–186 (2006).
27. Baeuerle, P. A. & Henkel, T. Function and Activation of NF-kappaB in the Immune System. *Annu. Rev. Immunol.* **12**, 141–179 (1994).
 28. Dolcet, X., Llobet, D., Pallares, J. & Matias-Guiu, X. NF-kB in development and progression of human cancer. *Virchows Arch.* **446**, 475–482 (2005).
 29. Wang, C.-Y., Mayo, M. W. & Baldwin, A. S. TNF- and Cancer Therapy-Induced Apoptosis: Potentiation by Inhibition of NF-κB. *Science* **274**, 784–787 (1996).
 30. Xia, Y., Shen, S. & Verma, I. M. NF-κB, an active player in human cancers. *Cancer Immunol. Res.* **2**, 823–830 (2014).
 31. Erstad, D. J. & Cusack, J. C. Targeting the NF-κB pathway in cancer therapy. *Surg. Oncol. Clin. N. Am.* **22**, 705–746 (2013).
 32. Bacher, S. & Schmitz, M. L. The NF-kB Pathway as a Potential Target for Autoimmune Disease Therapy. (2004). doi:info:doi/10.2174/1381612043383584
 33. Palanki, M. s s. Inhibitors of AP-1 and NF-κB Mediated Transcriptional Activation: Therapeutic Potential in Autoimmune Diseases and Structural Diversity. (2002). doi:info:doi/10.2174/0929867023371265
 34. Letoha, T. *et al.* In Vitro and in Vivo Nuclear Factor-κB Inhibitory Effects of the Cell-Penetrating Penetratin Peptide. *Mol. Pharmacol.* **69**, 2027–2036 (2006).
 35. Liu, S. F., Ye, X. & Malik, A. B. In vivo inhibition of nuclear factor-kappa B activation prevents inducible nitric oxide synthase expression and systemic hypotension in a rat model of septic shock. *J. Immunol.* **159**, 3976–3983 (1997).
 36. Eigler, A., Sinha, B., Hartmann, G. & Endres, S. Taming TNF: strategies to restrain this proinflammatory cytokine. *Immunol. Today* **18**, 487–492 (1997).

37. Tak, P. P. & Firestein, G. S. NF- κ B: a key role in inflammatory diseases. *J. Clin. Invest.* **107**, 7–11 (2001).
38. Wang, J. *et al.* Distinct Roles of Different NF- κ B Subunits in Regulating Inflammatory and T Cell Stimulatory Gene Expression in Dendritic Cells. *J. Immunol.* **178**, 6777–6788 (2007).
39. Targeting Nuclear Import Shuttles, Importins/Karyopherins alpha by a Peptide Mimicking the NF κ B1/p50 Nuclear Localization Sequence.
40. Netea, M. G., Kullberg, B. J., Meer, V. der & M, J. W. Circulating Cytokines as Mediators of Fever. *Clin. Infect. Dis.* **31**, S178–S184 (2000).
41. Jung, H. *et al.* CpG incorporated DNA microparticles for elevated immune stimulation for antigen presenting cells. *RSC Adv.* **8**, 6608–6615 (2018).
42. Bouvier, N. M. & Lowen, A. C. Animal Models for Influenza Virus Pathogenesis and Transmission. *Viruses* **2**, 1530–1563 (2010).
43. Daniele, G. *et al.* The inflammatory status score including IL-6, TNF- α , osteopontin, fractalkine, MCP-1 and adiponectin underlies whole-body insulin resistance and hyperglycemia in type 2 diabetes mellitus. *Acta Diabetol.* **51**, 123–131 (2014).
44. Segev, G., Kass, P. H., Francey, T. & Cowgill, L. D. A Novel Clinical Scoring System for Outcome Prediction in Dogs with Acute Kidney Injury Managed by Hemodialysis. *J. Vet. Intern. Med.* **22**, 301–308 (2008).
45. Page, K. M. *et al.* The Cord Blood Apgar: a novel scoring system to optimize selection of banked cord blood grafts for transplantation (CME). *Transfusion (Paris)* **52**, 272–283 (2012).
46. Ramachandran, A. *et al.* Temporal changes in prevalence of diabetes and impaired glucose

- tolerance associated with lifestyle transition occurring in the rural population in India. *Diabetologia* **47**, 860–865 (2004).
47. Calabro, S., Tortoli, M., Baudner, B. C., Pacitto, A., Cortese, M., O’Hagan, D. T., ... & Wack, A. (2011). Vaccine adjuvants alum and MF59 induce rapid recruitment of neutrophils and monocytes that participate in antigen transport to draining lymph nodes. *Vaccine*, 29(9), 1812-1823.
 48. Schülke, S. *et al.* MPLA shows attenuated pro-inflammatory properties and diminished capacity to activate mast cells in comparison with LPS. *Allergy* **70**, 1259–1268 (2015).
 49. Fujita, Y. & Taguchi, H. Overview and outlook of Toll-like receptor ligand-antigen conjugate vaccines. *Ther. Deliv.* **3**, 749–760 (2012).
 50. Blander, J. M. & Medzhitov, R. Toll-dependent selection of microbial antigens for presentation by dendritic cells. *Nature* **440**, 808–812 (2006).
 51. Lynn, G. M. *et al.* In vivo characterization of the physicochemical properties of polymer-linked TLR agonists that enhance vaccine immunogenicity. *Nat. Biotechnol.* **33**, 1201–1210 (2015).
 52. Chan, M. *et al.* Synthesis and characterization of PEGylated toll like receptor 7 ligands. *Bioconjug. Chem.* **22**, 445–454 (2011).
 53. Ignacio, B. J., Albin, T. J., Esser-Kahn, A. P. & Verdoes, M. Toll-like Receptor Agonist Conjugation: A Chemical Perspective. *Bioconjug. Chem.* **29**, 587–603 (2018).
 54. Ebrahimian, M. *et al.* Co-delivery of Dual Toll-Like Receptor Agonists and Antigen in Poly(Lactic-Co-Glycolic) Acid/Polyethylenimine Cationic Hybrid Nanoparticles Promote Efficient In Vivo Immune Responses. *Front. Immunol.* **8**, (2017).
 55. Bhardwaj, N., Gnjjatic, S. & Sawhney, N. B. TLR AGONISTS: Are They Good Adjuvants?

Cancer J. Sudbury Mass **16**, 382–391 (2010).

56. Inhibitors of NF-kappaB signaling: 785 and counting. doi:10.1038/sj.onc.1209982

57. Liu, X. Y. *et al.* Peptide-directed Suppression of a Pro-inflammatory Cytokine Response. *J. Biol. Chem.* **275**, 16774–16778 (2000).

3 Small molecule NF- κ B inhibitors as immune potentiators for enhancement of vaccine adjuvants

3.1 Summary

Adjuvants are added to vaccines to enhance the immune response and provide increased protection. In the last decade, hundreds of synthetic immune adjuvants have been created, but very few are safe enough to be included in clinical vaccines. Here we present that small molecule NF- κ B inhibitors can be used to both increase the safety and improve the protective response of vaccination. Additionally, we synthesize a library of derivatives identifying several promising candidates for use in vaccine formulations. We further demonstrate that the anti-inflammatory action of the NF- κ B is not coupled to the immune-boosting potential.

3.2 Introduction

Vaccines remain one of the most effective ways of preventing disease. Despite their immense success in preventing diseases such as polio, tetanus, and small pox, diseases such as HIV and dengue present challenges that current clinical vaccine technology cannot provide. To solve this problem, one strategy that has been explored is to include adjuvants, components of a vaccine that enhance the immune response.¹ Although adjuvanted vaccines often lead to a higher level and quality of immune response that cannot be achieved with current approved adjuvants, to date very few have been approved for use in human vaccines due to the side effects they incur.²⁻⁴ We recently reported that vaccines could be improved through the use of a peptide NF- κ B inhibitor, SN50.⁵ The addition of SN50 to adjuvanted vaccines led to increased safety and decreased side effects while enhancing protection against disease. Although this method proved

both general across a wide range of adjuvants and effective against antigens of a variety of diseases, large amount of the peptide was required to enable optimal safety and protection. Scale-up of peptides present synthetic challenges and can result in expensive production costs, limiting their use in a clinical setting.^{6,7} Peptides can also induce an immune response against themselves leading to decreased enhancement in subsequent vaccinations. We chose to explore other small molecule NF- κ B inhibitors as immune potentiators to overcome these challenges.

Here we demonstrate that some small molecule NF- κ B inhibitors are effective at reducing adjuvant-induced inflammation while also increasing the adaptive immune response. We demonstrate that not all NF- κ B inhibitors are effective immune potentiators. We found honokiol and capsaicin to be effective at both limiting inflammation and potentiating the adaptive response. Through knockout studies, we demonstrate that the increase in antigen specific antibodies is independent from the anti-inflammatory activity. We explored derivatives of honokiol and found several promising candidates.

3.3 Results and discussion

3.3.1 Exploration of small molecule NF- κ B inhibitors in vitro

To begin exploring alternative NF- κ B inhibitors we examined the literature for promising candidates. Due to the strong correlation between NF- κ B activation and sepsis⁸, cancer^{9,10} and autoimmune disorders¹¹, a large library of NF- κ B inhibitors have been identified.¹² We first wanted to analyze the potential of a variety small molecule NF- κ B inhibitors to inhibit inflammation in vitro in combination with lipopolysaccharide (LPS), a TLR4 agonist. We chose several common commercially available NF- κ B inhibitors and tested them in RAW macrophages alongside the most commonly used FDA approved anti-inflammatory drugs

acetaminophen and ibuprofen.^{13,14} We treated RAW macrophages with inhibitors and LPS and assayed the supernatant for IL-6 secretion (**Fig 3.1**).

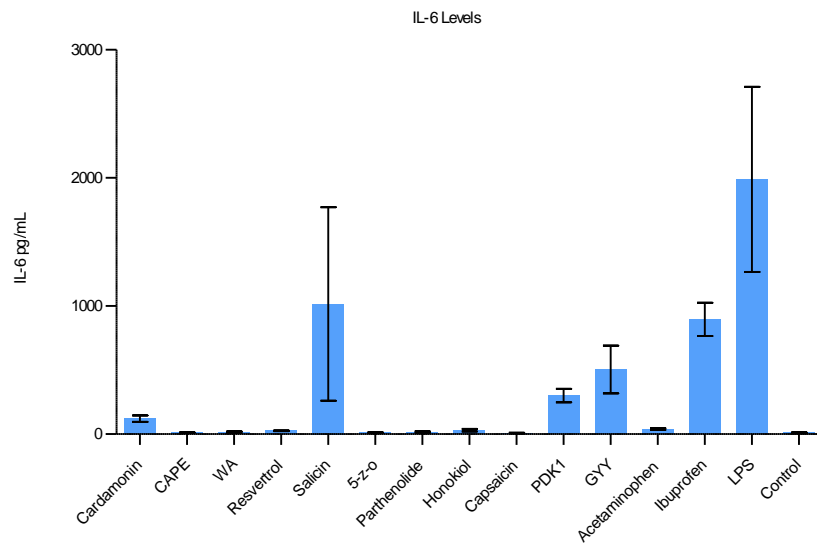


Figure 3.1 Small molecule inhibitor screen in vitro.

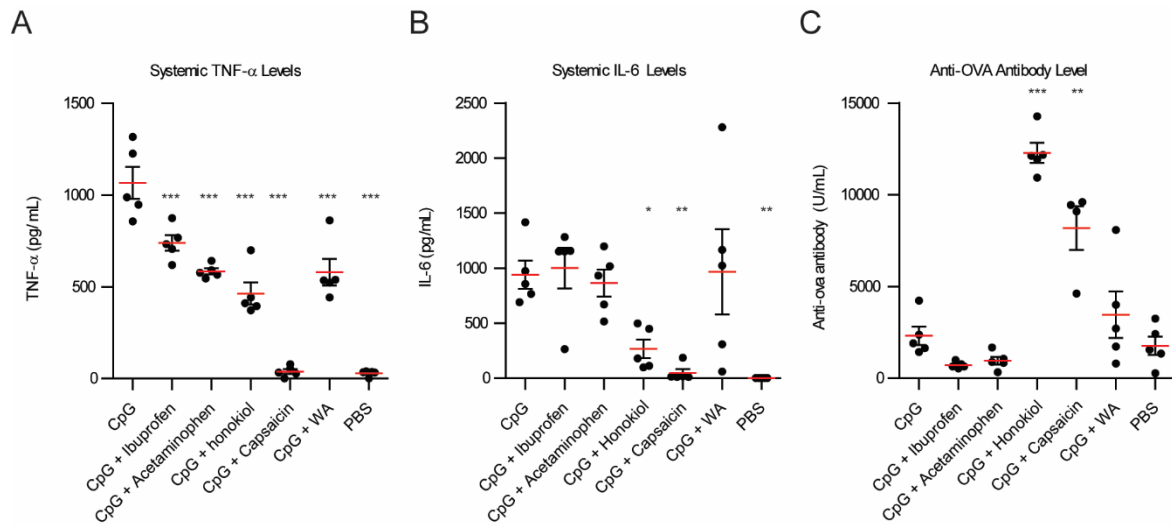


Figure 3.2. Small molecule inhibitor screen in vivo. (A) Systemic TNF- α expression 1h post vaccination. (B) Systemic IL-6 expression 1h post-vaccination. (C) Anti-OVA antibody titer 21 days post-vaccination.

3.3.2 Exploration of small molecule NF- κ B inhibitors in vivo

We next wanted to examine how these inhibitors would alter safety and protection in vivo. To test this in vivo, we tested the small molecule inhibitors that were the most effective at inhibiting IL-6 expression in vitro, capsaicin, honokiol and withaferin A and ran them alongside acetaminophen and ibuprofen. For our in vivo vaccination, we used ovalbumin (OVA) as a model antigen to examine the changes in humoral response. We vaccinated mice with 100 μ g OVA, 50 μ g CpG, and inhibitor. Inhibitors: 800 μ g ibuprofen, 2 mg acetaminophen, 400 μ g honokiol, 20 μ g capsaicin or 600 μ g WA. Due to the difficulty in solubility, all inhibitors were suspended in addavax, a squalene-based oil-in-water nano-emulsion, to enable effective vaccine suspensions. We chose to analyze systemic levels of TNF- α and IL-6 because high levels of these cytokines are pyrogenic, unsafe and have been correlated with vaccine-related side effects.

¹⁵⁻¹⁷ Mice vaccinated with CpG demonstrated high levels of TNF- α (1067 pg/mL) (**Fig. 3.2a**).

Addition of an NF- κ B inhibitor decreased the level of TNF- α . Ibuprofen decreased to 738 pg/mL (1.4 fold), Acetaminophen (1.8 fold), honokiol (2.3 fold), capsaicin (28 fold to background levels), and WA by 1.8 fold. The systemic levels of IL-6 were also high with CpG vaccination (941 pg/mL). The groups that included an NF- κ B inhibitor did not always decrease the level of IL-6 (**Fig. 3.2b**). Ibuprofen, acetaminophen and WA did not decrease IL-6 expression significantly. However, honokiol and capsaicin dramatically reduced the systemic levels of IL-6 to 266 pg/mL (3.5 fold) and 47.4 pg/mL (20 fold), respectively.

On day 21, we analyzed the anti-OVA antibody levels (**Fig. 3.2c**). CpG was 1.3 fold more than PBS. Ibuprofen and acetaminophen were 3.2 and 2.4 fold lower than CpG alone. CpG + honokiol was 5.3 fold more than CpG alone. CpG + capsaicin was 3.5 fold higher than CpG alone. CpG + WA was 1.5 fold lower than CpG alone.

3.3.3. Dose-dependence of capsaicin and honokiol

Capsaicin and honokiol demonstrated exceptional promise in these studies so we wanted to examine them further. We wanted to understand how changing the dose would alter innate and adaptive immune responses. For honokiol, we tested a concentration 2-fold higher (800 μ g) and 2-fold lower (200 μ g). High concentrations of capsaicin can induce side effects from systemic activation of TRPV1. We wanted to examine if we could lower the dose, but maintain adequate anti-inflammatory activity and antibody boosting potential. We chose to test a dose 4-fold lower (5 μ g) and 20-fold lower (1 μ g). All doses of honokiol demonstrated a significant decrease in TNF- α expression compared to CpG alone, however there was no significant difference between the different doses. Capsaicin decreased TNF- α levels significantly across all doses compared to CpG alone and 5 μ g and 20 μ g decreased levels of TNF- α significantly more than 1 μ g (**Fig.**

3.3a). The level of IL-6 was only decreased with 400 μ g and 800 μ g honokiol and 20 μ g capsaicin (**Fig. 3.3b**). Twenty-one days later, we analyzed differences in anti-OVA antibody titer and found that all doses of honokiol increased levels of anti-OVA antibodies compared to CpG alone and the highest level was found with 400 μ g honokiol (**Fig. 3.3c**). 1 μ g and 5 μ g of capsaicin did not change level of anti-OVA antibodies in the serum compared to CpG alone, however 20 μ g significantly increased serum levels.

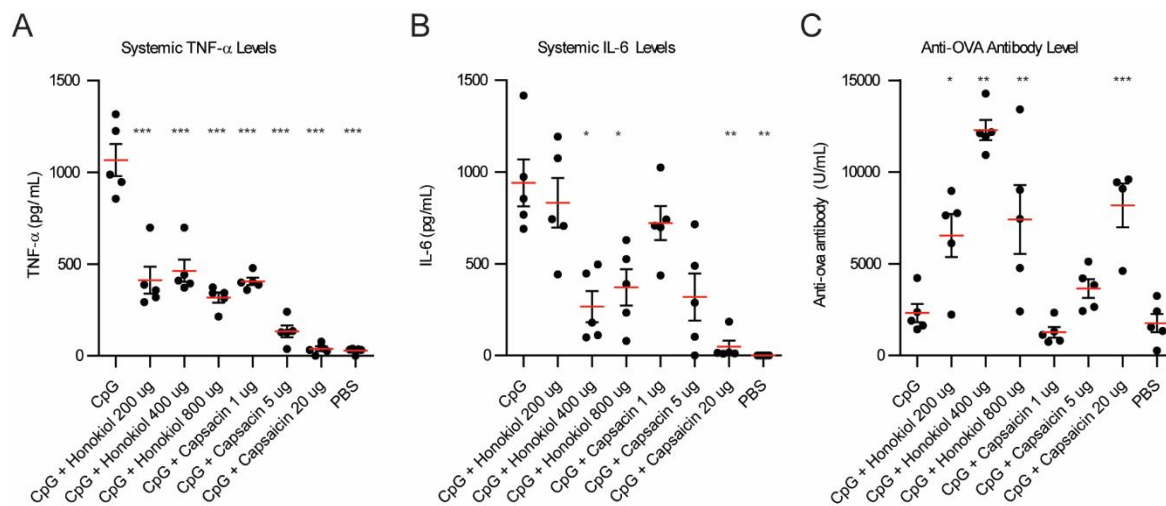


Figure 3.3. Dose effects of honokiol and capsaicin. (A) Systemic TNF- α levels 1h post vaccination. (B) Systemic IL-6 levels 1h post-vaccination. (C) Anti-OVA antibody levels 21 days post-vaccination.

3.3.4 Determining the TRPV1-mediated effects of capsaicin

The main *in vivo* target for capsaicin is the transient receptor potential cation channel subfamily V member 1 (TRPV1). TRPV1 is known to modulate the immune response in a variety of ways, and importantly, has been implicated in dampening systemic inflammation associated with sepsis.^{18–22} However, it has never been explored in a vaccine setting. To understand how activation of TRPV1 may be modulating the effects of the adjuvant, we compared the immediate inflammatory response of the vaccination in wild type mice (WT) and

TRPV1 knockout mice. We vaccinated WT and TRPV1 KO mice with 100 μ g OVA and: 50 μ g CpG, 50 μ g CpG + 20 μ g capsaicin or PBS. We analyzed systemic levels of TNF- α and IL-6 1h after vaccination. We found that CpG induced high levels of TNF- α and IL-6 in both WT and TRPV1 KO mice. Addition of capsaicin dramatically and significantly reduced both TNF- α levels and IL-6 levels in the WT mice (**Fig. 3.4a, 3.4b**). Although the mean was slightly lower for both TNF- α and IL-6 in the TRPV1 KO mice, these differences were not statistically significant. This demonstrates that TRPV1 activation is responsible for the capsaicin-induced decrease in systemic cytokine levels. To examine if the increased antibody titer was due to TRPV1 activation on day 21, we analyzed levels of anti-OVA antibodies in the serum (**Fig. 3.4c**). Interestingly, we found that anti-OVA antibody titers were increased in groups with Capsaicin + CpG in both WT and KO mice. This implies that the antibody-boosting activity of capsaicin is separate from TRPV1-dependent decrease in inflammatory cytokines. This result demonstrates both that the decrease in inflammation is not responsible for the antibody-boosting activity of the NF-kB inhibitor a result that we demonstrated previously,⁵ and also that the enhancement of the adaptive response is TRPV1 independent.

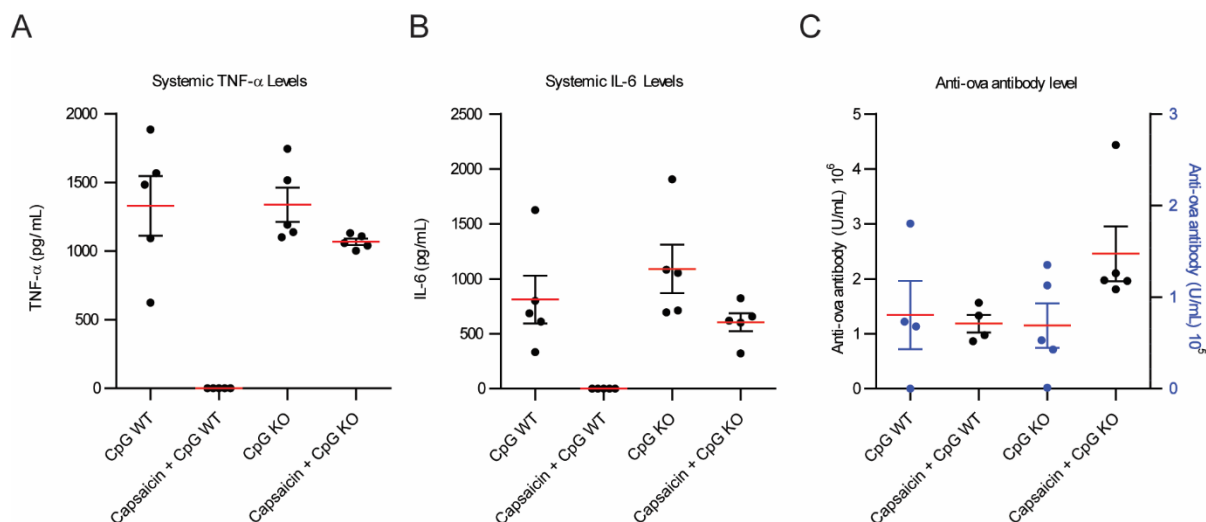
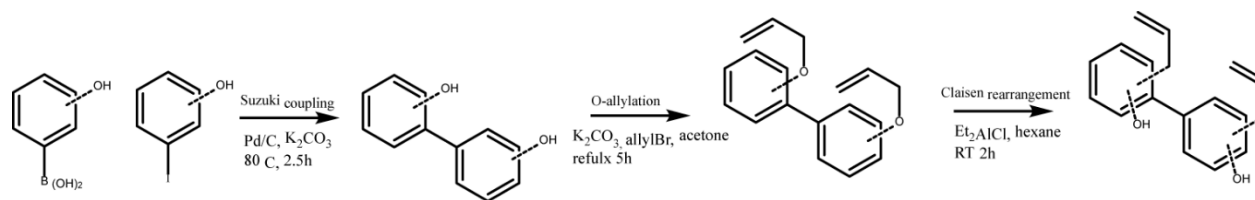


Figure 3.4. Role of TRPV1 of capsaicin induced anti-inflammatory and immune potentiation. (A) Systemic TNF- α levels 1h post vaccination in wild type (WT) mice and TRPV1 KO (KO). (B) Systemic IL-6 levels 1h post-vaccination. (C) Anti-OVA antibody level 21 days post-vaccination. Left axis, black. Right axis, blue.

3.3.5 Synthesis of honokiol derivative library

To further explore honokiol, we synthesized a library of derivatives. Honokiol derivative libraries have been synthesized previously and examined for their effects on neuroprotection²³, antimicrobial agents²⁴ and anti-cancer²⁵ among others.^{26,27} However, to date no such study has examined the effects of honokiol analogs on vaccines or anti-inflammatory activity and antigen presenting ability. Phenylphenols and biphenols were prepared using Pd-catalyzed Suzuki coupling using corresponding iodophenols and hydroxyphenylboronic acids as starting materials. These compounds were *O*-allylated using allylBr. Resulting compounds were subjected to Claisen rearrangement using diethyl aluminum chloride to yield a variety of ring substitutions (**Scheme 1**).



Scheme 1. Honokiol derivative synthesis.

We analyzed how the honokiol derivatives altered IL-6 production in RAW macrophages. We chose to analyze the hydroxybiphenyls and *O*-allylated derivatives in addition to the product from the Claisen rearrangement to understand how these functional groups play a role in the anti-inflammatory action or increase in adaptive immune response (**Fig. 3.5a**). We treated RAW macrophages with honokiol derivatives and LPS and analyzed IL-6 expression. The addition of LPS alone without a honokiol derivative gave high levels of IL-6 expression (5200 pg/mL). The addition of honokiol, made the IL-6 levels non-detectable. Several derivatives including: 9, 11, 20, 29b, 58a and 58d also demonstrated non-detectable levels of IL-6 expression. We are currently assessing the impact of the derivatives on CD86 and CD40 cell surface receptor expression and plan to test the most promising candidates *in vivo*.

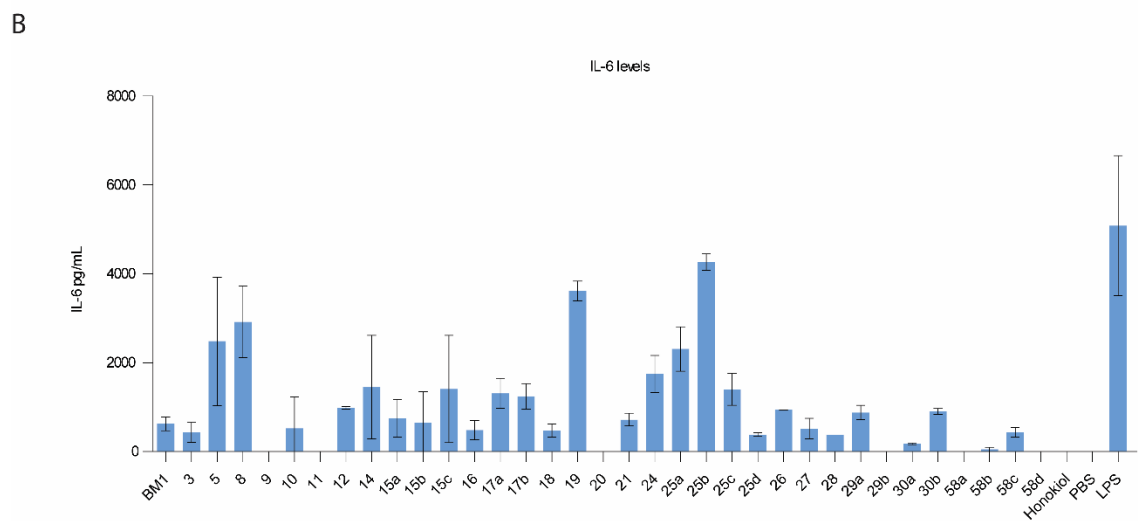
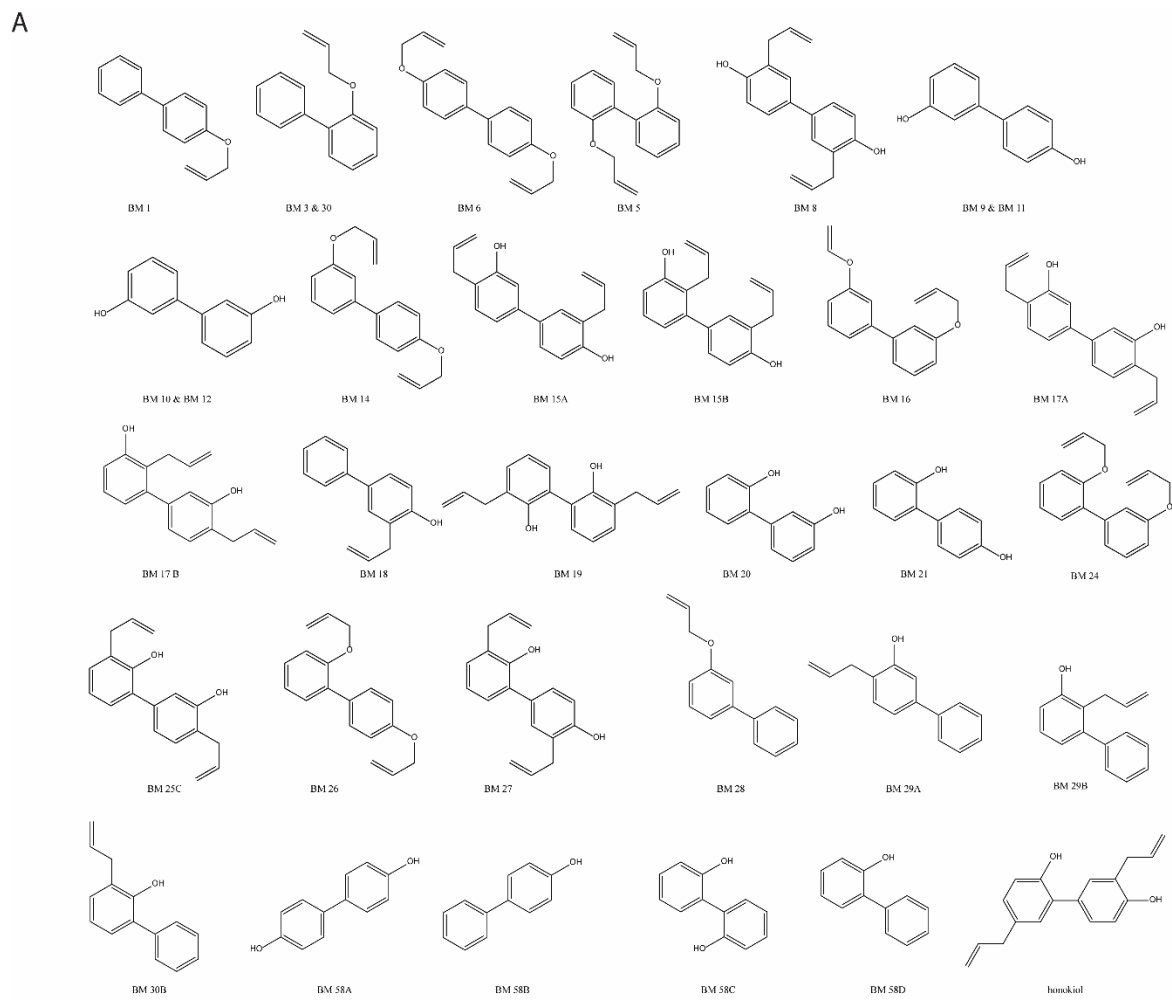


Figure 3.5 Honokiol derivatives and their inhibitory activity on IL-6 expression. (A) Structures of honokiol derivatives. **(B)** IL-6 expression of RAW macrophages treated with honokiol derivatives and LPS.

3.4 Conclusion

In summary, we present that some small molecule inhibitors of NF- κ B can be used to decrease the inflammatory effects of adjuvanted vaccination potentially enabling safer vaccination while also acting as immune potentiators and increasing the antibody titer. We identified two such immune potentiators, honokiol and capsaicin that effectively decrease inflammation while increasing the adaptive response. We additionally provide evidence that implies that the decrease in inflammation is separate from the increase in antibody response, potentially enabling distinct tunability of either response. This study also identifies that not just any NF- κ B inhibitor can be used to the same effect enabling further modulation of the immune response. We further examined a library of honokiol derivatives and found that several honokiol derivatives are promising candidates to test in vivo. In conclusion, we have demonstrated that using small molecule NF- κ B inhibitors in combination with common immune adjuvants can decrease pro-inflammatory cytokine production while boosting antibody titers.

3.5 Materials and methods

In vitro assays

RAW macrophage cytokine analysis: RAW 264.7 macrophages were passaged and plated in a cell culture treated 12- well plate at 0.5×10^6 cells/ well in 1 mL DMEM containing 10% FBS. Cells were grown for 2 days. Media was exchanged for 1 mL DMEM containing 10% HIFBS. Inhibitors were added at indicated concentrations and incubated for 45 min. After 45 min, LPS was added at 100 ng/mL and incubated at 37 °C and 5% CO₂ for 24 h. Cell supernatant was removed and analyzed using BD Cytometric Bead Array Mouse Inflammation Kit.

In vivo assays: All animal procedures were performed under a protocol approved by the University of Chicago Institutional Animal Care and Use Committee (IACUC). 6-8 week-old C57/B6 female mice were purchased from Jackson Laboratory (JAX). 6-8 week-old C57/B6 female *Trpv1*^{tm1Ju} mice were purchased from JAX for TRPV1 KO experiment. All compounds were tested for endotoxin prior to use. All vaccinations were administered intramuscularly in the hind leg. Blood was collected from the saphenous vein at time points indicated.

Antigens were purchased from Invitrogen (Vaccigrade Ovalbumin). Vaccigrade R848 was purchased from Invitrogen and vaccigrade CpG ODN 1826 was purchased from Invivogen or Adipogen.

Vaccination: Mice were lightly anesthetized with isoflurane and injected intramuscularly in the hind leg with 50 μ L containing ovalbumin (100 μ g), adjuvant, inhibitor and PBS. Adjuvant doses: CpG, 50 μ g; R848, 50 μ g. Inhibitor concentrations: Honokiol (400 μ g), Capsaicin (20 μ g), Withaferin A (600 μ g), acetaminophen (2 mg), ibuprofen (800 μ g).

Plasma cytokine analysis: Blood was collected from mice at 1h post-vaccination in 0.2 mL heparin coated collection tubes (VWR Scientific). Serum was isolated via centrifugation 2000 x g for 5 min. Supernatant was collected and stored at -80 °C until use. Serum was analyzed using BD Cytometric Bead Array Mouse Inflammation cytokine kit according to manufacturer's protocol. Briefly, beads containing antibodies for desired cytokines were mixed with 50 μ L serum and 50 μ L PE detection reagent and incubated for 2 h. Beads were washed and analyzed using Novocyte flow cytometer. Data was analyzed using Graphpad Prism.

Antibody quantification: Mice were vaccinated with indicated formulations. Blood was collected at time points indicated in 0.2 mL heparin coated collection tubes (VWR Scientific) for plasma or

uncoated tubes for serum. Plasma was isolated via centrifugation (2000 x g, 5 min). Serum was isolated by allowing blood to clot for 15- 30 min RT and centrifuging (2000 x g for 10 min) at 4 °C. Serum was analyzed using a quantitative anti-ovalbumin total Ig's ELISA kit (Alpha Diagnostic International) according to the specified protocol. Data was analyzed using Graphpad Prism.

Chemistry

Conditions for Suzuki Coupling: Hydroxyphenol boronic acid (20 mmol) was dissolved in 100 mL water. Appropriate iodophenol (10 mmol) and K_2CO_3 (40 mmol) was added followed by Pd/C (2 mol %). Solution heated to 80 C for 3h. Solution was acidified with 1M HCl and extracted with EtoAc and washed with brine. Solvent evaporated in vacuo. Compound was purified by column chromatography.

Conditions for O-allylations: Phenol (1 mmol) (Derivative 1-?) was dissolved in dry acetone (5 mL) and K_2CO_3 (2 mmol) added. AllylBr was added dropwise and refluxed. Reaction was monitored by TLC until completion (5-12h). Reaction mixture was cooled and volatiles were removed in vacuo. 10% NaOH was added to the mixture and extraction was performed using ethyl acetate, washed with brine and organic layers dried using $MgSO_4$. Solvent was removed in vacuo affording an oily material that was purified by column chromatography to yield the O-allylated derivative.

Conditions for Claisen rearrangement: O-allylated derivatives (1 mmol) were dissolved in dry hexane (10 mL). Et_2AlCl in dry hexane (4 mL) was added dropwise under argon. Mixture was stirred at room temperature for 2h. The mixture was cooled on an ice bath and quenched using 2M HCl (20 mL). Extraction was performed with EtOAc, washed with brine and dried over

MgSO₄. Solvent was removed in vacuo affording an oily material that was purified by column chromatography to yield the C-allyl derivative.

3.6 References

1. Roush, S. W., Murphy, T. V. & Group, and the V.-P. D. T. W. Historical Comparisons of Morbidity and Mortality for Vaccine-Preventable Diseases in the United States. *JAMA* **298**, 2155–2163 (2007).
2. Coffman, R. L., Sher, A. & Seder, R. A. Vaccine adjuvants: putting innate immunity to work. *Immunity* **33**, 492–503 (2010).
3. Audibert, F. M. & Lise, L. D. Adjuvants: current status, clinical perspectives and future prospects. *Trends in Pharmacological Sciences* **14**, 174–178 (1993).
4. Bhardwaj, N., Gnjjatic, S. & Sawhney, N. B. TLR AGONISTS: Are They Good Adjuvants? *Cancer J* **16**, 382–391 (2010).
5. Tom, J. K. *et al.* Applications of Immunomodulatory Immune Synergies to Adjuvant Discovery and Vaccine Development. *Trends in Biotechnology* **37**, 373–388 (2019).
6. Immune potentiator for increased safety and improved protection of vaccines by NF-κB modulation | bioRxiv. Available at: <https://www.biorxiv.org/content/10.1101/489732v1>.
7. Lau, J. L. & Dunn, M. K. Therapeutic peptides: Historical perspectives, current development trends, and future directions. *Bioorganic & Medicinal Chemistry* **26**, 2700–2707 (2018).
8. Otvos, L. & Wade, J. D. Current challenges in peptide-based drug discovery. *Front Chem* **2**, (2014).
9. Shimaoka, M., & Park, E. J. (2008). Advances in understanding sepsis. *European Journal of Anaesthesiology*, 25(S42), 146-153.
10. Dolcet, X., Llobet, D., Pallares, J. & Matias-

- Guiu, X. NF- κ B in development and progression of human cancer. *Virchows Arch* **446**, 475–482 (2005).
11. Xia, Y., Shen, S. & Verma, I. M. NF- κ B, an active player in human cancers. *Cancer Immunol Res* **2**, 823–830 (2014).
 12. Bacher, S., & Schmitz, M. L. (2004). The NF- κ B pathway as a potential target for autoimmune disease therapy. *Current pharmaceutical design*, 10(23), 2827-2837.
 13. Gilmore, T. D., & Herscovitch, M. (2006). Inhibitors of NF- κ B signaling: 785 and counting. *Oncogene*, 25(51), 6887.
 14. Scheuren, N., Bang, H., Münster, T., Brune, K. & Pahl, A. Modulation of transcription factor NF- κ B by enantiomers of the nonsteroidal drug ibuprofen. *British Journal of Pharmacology* **123**, 645–652 (1998).
 15. Boulares, A. H., Giardina, C., Inan, M. S., Khairallah, E. A. & Cohen, S. D. Acetaminophen inhibits NF- κ B activation by interfering with the oxidant signal in murine Hepa 1-6 cells. *Toxicol. Sci.* **55**, 370–375 (2000).
 16. Christian, L. M., Porter, K., Karlsson, E. & Schultz-Cherry, S. Proinflammatory cytokine responses correspond with subjective side effects after influenza virus vaccination. *Vaccine* **33**, 3360–3366 (2015).
 17. Simon, W. L., Salk, H. M., Ovsyannikova, I. G., Kennedy, R. B. & Poland, G. A. Cytokine production associated with smallpox vaccine responses. *Immunotherapy* **6**, 1097–1112 (2014).
 18. Netea, M. G., Kullberg, B. J., Meer, V. der & M, J. W. Circulating Cytokines as Mediators of Fever. *Clin Infect Dis* **31**, S178–S184 (2000).
 19. Brito, R., Sheth, S., Mukherjea, D., Rybak, L. P. & Ramkumar, V. TRPV1: A Potential

- Drug Target for Treating Various Diseases. *Cells* **3**, 517–545 (2014).
20. Wang, Y. & Wang, D. H. TRPV1 Ablation Aggravates Inflammatory Responses and Organ Damage during Endotoxic Shock. *Clin. Vaccine Immunol.* **20**, 1008–1015 (2013).
 21. Toledo-Mauriño, J. J. *et al.* The Transient Receptor Potential Vanilloid 1 Is Associated with Active Inflammation in Ulcerative Colitis. *Mediators of Inflammation* (2018).
doi:10.1155/2018/6570371
 22. Bodkin, J. V. & Fernandes, E. S. TRPV1 and SP: key elements for sepsis outcome? *Br J Pharmacol* **170**, 1279–1292 (2013).
 23. Fernandes, E. S. *et al.* TRPV1 deletion enhances local inflammation and accelerates the onset of systemic inflammatory response syndrome. *J. Immunol.* **188**, 5741–5751 (2012).
 24. Elokely, K. *et al.* Understanding TRPV1 activation by ligands: Insights from the binding modes of capsaicin and resiniferatoxin. *PNAS* **113**, E137–E145 (2016).
 25. Tripathi, S., Chan, M.-H. & Chen, C. An expedient synthesis of honokiol and its analogues as potential neuropreventive agents. *Bioorganic & Medicinal Chemistry Letters* **22**, 216–221 (2012).
 26. Kim, Y.-S. *et al.* Synthesis and microbiological evaluation of honokiol derivatives as new antimicrobial agents. *Arch. Pharm. Res.* **33**, 61–65 (2010).
 27. Sánchez-Peris, M., Murga, J., Falomir, E., Carda, M. & Marco, J. A. Synthesis of honokiol analogues and evaluation of their modulating action on VEGF protein secretion and telomerase-related gene expressions. *Chem Biol Drug Des* **89**, 577–584 (2017).
 28. Shen, J.-L. *et al.* Honokiol and magnolol as multifunctional antioxidative molecules for dermatologic disorders. *Molecules* **15**, 6452–6465 (2010).
 29. Lee, Y.-J. *et al.* Therapeutic applications of compounds in the Magnolia family. *Pharmacol.*

Ther. **130**, 157–176 (2011).

4 Surface Coating of Nanoparticles Reduces Background Inflammatory Activity while Increasing Particle Uptake and Delivery

*This chapter has been published in ACS Biomater. Sci. Eng., 3 (2), 206–213, 2017

4.1 Summary

In the study of host-pathogen interactions, vaccines and drug delivery, particulate delivery system are widely used to mimic pathogen size, pattern recognition receptor agonist presentation, and target cells or organs. However, some of the polymeric systems used in particulate delivery have inherent inflammatory properties that are variable and non-specific. These properties enhance their adjuvant activity, but confound the analysis of signaling mechanisms. Here, we present a method for particle coating with minimal background immune activation *via* passivation of the surface with silica-silane. We show herein that a silica-silane shell passivates polymer particles rendering them inert to activation of innate immune cells. The method is broadly applicable and can be used to coat polymeric particles of many different compositions. This method of silica-silane coating also allows conjugation of amine-bearing agonists and provides for controlled variation of agonist loading. Finally, we demonstrate our particles maintain and enhance qualities of known pathogens making this a potentially general method for improving immune agonist activity.

4.2 Introduction

To better understand vaccines and immunotherapies, many researchers are elucidating the mechanisms by which the innate immune system responds to bacterial pathogens.^{1a-c} Our group, and many others, are interested in how micron-sized pathogens stimulate multiple innate immune

receptors to elicit protective responses.^{2a-p} In our own work, we employed the current methods used in many studies to conjugate pattern recognition receptor agonists to commercial polystyrene particles to study these processes.^{2a-p} However, as others have reported, naked polystyrene has an inherent, non-specific background activation of innate immune cells, convoluting the results.^{3a-i} Indeed, innate immune activation has been a recurring problem for many nanoscale materials, highlighting the need for inert particles and coatings.^{3a-i} For us, it was difficult to differentiate the signal of the polystyrene particle from its conjugated agonists. Here we present a coating method for polymeric particles that reduces the background inflammatory response caused by nanoparticles while providing a chemical handle for conjugation of immune agonists. In addition, this coating is more “cell-like”, overcoming the intrinsic hydrophobicity of polystyrene, allowing the particles to be more uniformly dispersed in aqueous solutions without surfactant stabilization. This method provides a general route for researchers attempting to reduce non-specific nanoparticle inflammatory properties and will find use in studies of the innate immune system. Particles with this coating will allow researchers to analyze responses solely from the agonists while mimicking the size and agonist presentation of a pathogen.

4.3 Design of polymeric delivery system

In designing an improved polymeric delivery system, we sought a general design strategy that would apply to different polymeric particles for both cellular and in vivo applications. Our design was guided by three main principles: low immunogenicity, ease of functionalization and pathogen mimicry. We further showed that this shell formation technique is generalizable to multiple polymeric cores (**Fig. 4.1**).

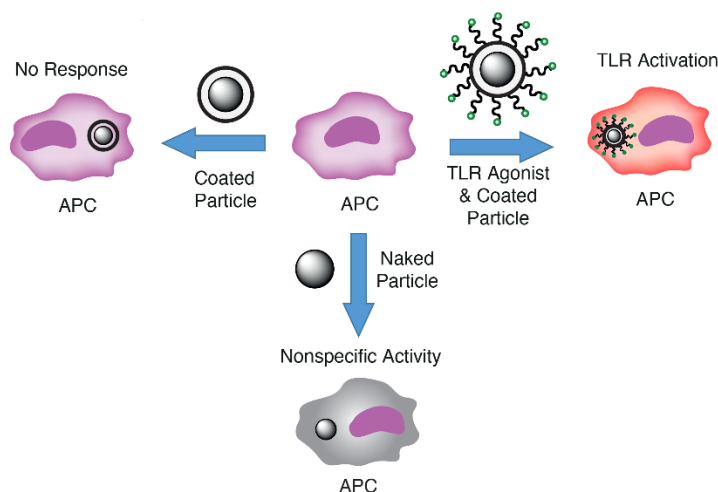


Figure 4.1. Schematic of cellular outcomes of particle exposure. Coated polystyrene particles alone do not elicit an immune response (top left). Agonist-functionalized coated polystyrene particles activate the cell’s immune response based on the agonists loaded on the surface (top right), whereas polystyrene particles cause nonspecific activation of immune cells (bottom). APC: Antigen-presenting cell.

4.4 Results and Discussion

4.4.1 Synthesis of coated polystyrene particles

We hypothesized that if the particles had a more biologically-relevant surface potential it would reduce immunogenicity. To create a test particle, we synthesized monodisperse polystyrene (PS) particles.⁴ This synthesis was accomplished by first dissolving purified styrene monomer and poly(vinylpyrrolidone) MW 40,000 in ethanol and purging with dry nitrogen for 1 h. The addition of the poly(vinylpyrrolidone) increased the viscosity of the monomer solution. The stir rate was adjusted to 200 rpm to promote the formation of micron-sized particles. Polymerization was initiated by the addition of 1 wt% AIBN, and the mixture was stirred at 70 °C for 24 h. To remove unreacted material, we centrifuged the reaction mixture and washed the

pellet three times with ethanol. We next screened conditions to synthesize a uniform tetraethyl orthosilicate (TEOS)-mercaptopilane copolymer shell. This judicious choice of silane allowed us to graft a heterobifunctional crosslinker, maleimide-PEG₆-succinimidyl ester (maleimide-PEG₆-NHS) through the maleimide to the surface of the particles. The succinimidyl ester moiety on the crosslinker allowed us to attach agonists containing an amine handle. We found that optimal coatings were achieved using an emulsion polymerization approach.⁵ In a representative coating procedure used for all core particle types, a flask was charged with cyclohexane, *n*-hexanol, water, Triton X-114, and sonicated for 20 min. To this emulsion, uncoated particles were added, and the resulting mixture was sonicated for an additional 40 min to increase particle suspension. TEOS was added dropwise followed by 14 M ammonia solution and the mixture stirred for 30 min. 3-Mercaptopilane was then added, and the reaction mixture stirred for 6 h. The mixture was centrifuged and then washed three times with ethanol to provide silica-silane coated microparticles. The particles were characterized by a combination of light microscopy, dynamic light scattering (DLS), zeta potential, scanning electron microscopy (SEM) and energy-dispersive X-ray spectroscopy (EDS). SEM analysis confirmed the coated particles retained relative size dispersities (**Fig. 4.2a and Fig. C1-C24**). High-resolution SEM analysis of the particle surface suggested that the coating was established by a Pickering-type emulsion process.⁶

4.4.2 Physical properties of coated microparticles

Before testing the immune activity of the particles, we assayed the physical properties of the coated particles. Using light microscopy, we examined particle morphology and bulk solution behavior (**Fig. 4.2 and Fig. 4.3**). The particles were dispersed in ethanol to provide similar suspension and sedimentation rates across different particle types (**Fig. 4.2b**).

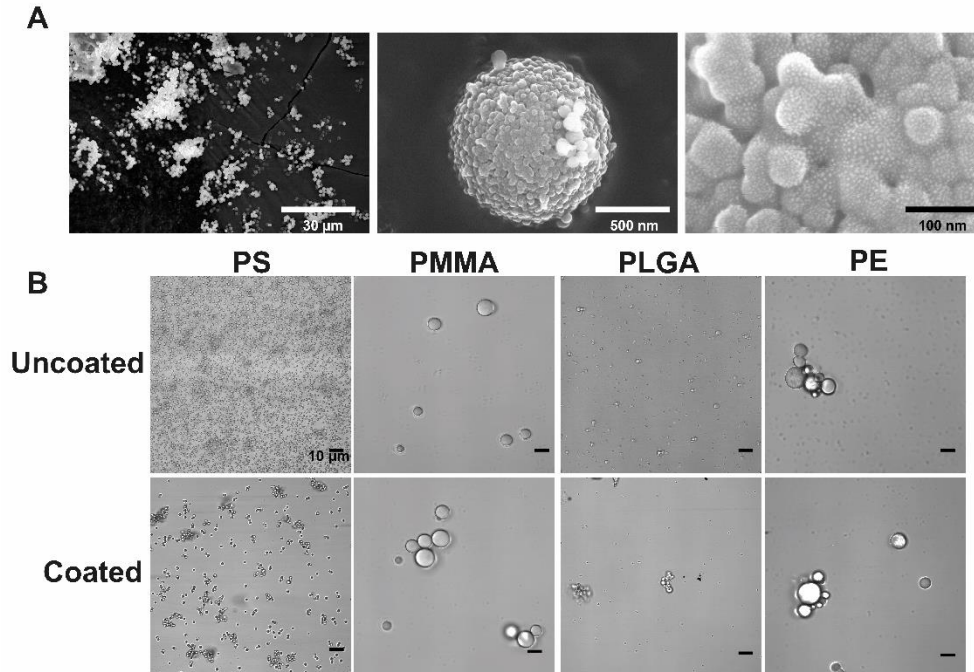


Figure 4.2. Microscopy of particles. A) Scanning electron microscopy of PS coat particle at 1,677x; 80,000x; and 500,000x magnification (left to right). B) Brightfield microscopy of dispersions of uncoated and coated particles in ethanol to give accurate representations of particle size and features. Aggregation in ethanol does not reflect aggregation in aqueous solutions.

We also examined dispersions of PS and coated PS particles (PS coat) in an aqueous medium, which is more relevant for biological studies. We determined that coated PS was more uniformly dispersed in aqueous solution (cell culture media) than PS (**Fig. 4.3**).

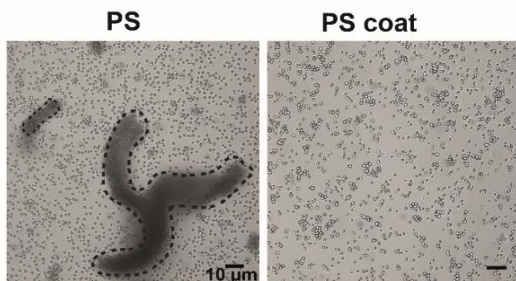


Figure 4.3. Light microscopy of particles in media. Microscopy of dispersions of PS and PS coat particles in cell culture media, demonstrating the clumping behavior of the PS particles. Clumps are denoted by dotted outlines.

4.4.3 Immune response to core-shell constructs

After validating uniform coating of the particles in the TEOS-mercaptopilane copolymer, we tested the immunogenicity of the particles coated with only the copolymer (before treatment with crosslinker or agonist) and compared it to their uncoated equivalents. To determine activity, we employed the transgenic RAW macrophage RAW-Blue™ NF-κB reporter cell line that provides a colorimetric readout of NF-κB activity.^{7a-d} This cell line is commonly used as an assay for immunogenicity due to the central role of the transcription factor NF-κB in immune activation and cytokine production. NF-κB is a central transcription factor in immune response specifically the inflammatory response associated with innate immunity. We observed a dramatic and significant difference between PS and coated PS particles. To demonstrate generality, we also tested coated poly(methyl methacrylate) (PMMA), poly(lactic-co-glycolic acid) (PLGA) and polyethylene (PE) particles (**Fig. 4.4**). All TEOS-mercaptopilane coated particles showed a significant reduction in NF-κB activity compared to their uncoated equivalents in all polymers except PE. Both coated PLGA and PMMA particles showed no significant difference in NF-κB

activity compared to cells with no particles added (PBS) demonstrating that the coating passivates immune activation.

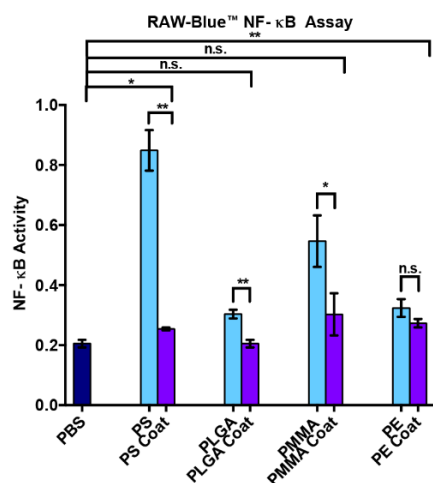


Figure 4.4. NF-κB activity of coated and uncoated particles. Blue bars: uncoated particles.

Purple bars: particles with TEOS-mercaptopilane coating. RAW macrophages were stimulated for 18 h with coated or uncoated particles at 1:1 stoichiometry of particles to cells and then assayed for NF-κB activity. PBS: phosphate-buffered saline solution; PS: polystyrene particles; PS coat: TEOS-mercaptopilane coated PS particles; PLGA: poly(lactic co-glycolic acid) particles; PLGA coat: TEOS-mercaptopilane coated PLGA particles; PMMA: poly(methylmethacrylate) particles; PMMA coat: TEOS-mercaptopilane coated PMMA particles; PE: polyethylene particles; PE coat: TEOS-mercaptopilane coated PE particles.*p < 0.05, **p < 0.01.

To further test the ability of the coating to passivate the immunogenicity of the polymer surface, we also tested immunogenicity in THP-1 cells (human APCs) by observing IL-1β secretion (**Fig. 4.5**). IL-1β is a common inflammatory cytokine observed with nanoparticles.^{12a-c} We found that the coating decreased IL-1β expression in all cases except PE which we believe is due to the low

immunogenicity of uncoated PE. Further we found a statistically significant difference between PS and PS coat and PMMA and PMMA coat this reinforces our findings from the NF- κ B activity assay.

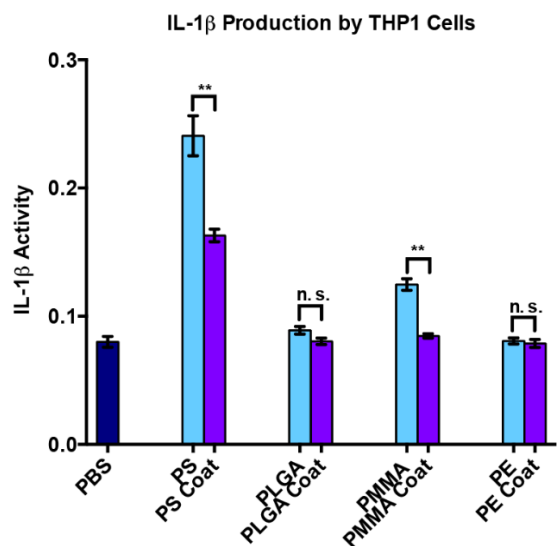


Figure 4.5. IL-1 β expression in THP-1 cells. Blue bars: uncoated particles. Purple bars: particles with TEOS-mercaptopilane coating. THP-1 cells were stimulated for 18 h with coated or uncoated particles at 1:1 stoichiometry of particles to cells and then assayed for IL-1 β activity. PBS: phosphate-buffered saline solution; PS: polystyrene particles; PS coat: TEOS-mercaptopilane coated PS particles; PLGA: poly(lactic co-glycolic acid) particles; PLGA coat: TEOS-mercaptopilane coated PLGA particles; PMMA: poly(methylmethacrylate) particles; PMMA coat: TEOS-mercaptopilane coated PMMA particles; PE: polyethylene particles; PE coat: TEOS-mercaptopilane coated PE particles. * $p < 0.05$, ** $p < 0.01$.

For further studies we focused on polystyrene particles because they are extremely uniform in size and we intend to use them in future applications. To explore how the coating affects immune

signaling and downstream effects, we performed a quantitative PCR analysis of key immune genes. This assay allowed us to monitor the expression levels of inflammatory markers and cell surface receptors involved in the innate immune response. We included TLR2 and TLR9 in our assay, as these are the target receptors for our model agonists. Changes in expression levels of these receptors from the particle itself would confound results in future experiments. We found that important immune players: CD4, TLR9, MyD88, TLR2 and TNF- α were upregulated in response to stimulation from PS particles. The coated particles did not demonstrate this degree of immunogenicity (**Table 4.1**).

	PS	PS coat
Cd4 (***)	1.132 $\sigma \pm 0.18$	0.6169 $\sigma \pm 0.15$
IL-10 (n. s.)	1 $\sigma \pm 0.17$	0.9265 $\sigma \pm 0.11$
TLR9 (*)	1.561 $\sigma \pm 0.18$	1 $\sigma \pm 0.18$
MyD88 (***)	1.569 $\sigma \pm 0.12$	1 $\sigma \pm 0.13$
TLR2 (***)	1.757 $\sigma \pm 0.15$	0.9908 $\sigma \pm 0.18$
TNF-a (**)	1.635 $\sigma \pm 0.19$	1.089 $\sigma \pm 0.19$

Table 4.1. qPCR panel of immune genes. RAW macrophages were stimulated for 4 h with PS or PS coat particles at 1:1 stoichiometry of particles to cells and then assayed. Values shown are fold change over unstimulated cells. Red, grey, and green signify upregulation, no change, and down regulation, respectively. Statistical significance between PS and PS coat values: CD4 (***) ; IL-10 (n.s.); TLR9 (*); MyD88 (***) ; TLR2 (***) ; TNF- α (**). *p < 0.05, **p < 0.01, ***p < 0.001.

4.4.4 Agonist loading

After demonstrating the improved immune compatibility of our TEOS-mercaptopilane copolymer coating, we wanted to ascertain if the particles could be loaded with agonists. The TLR9 agonist CpG-1826 was used as a model because an amine-bearing, highly fluorescent version is available that retains robust bioactivity.⁷

Uniform labeling of the core-shell particles was accomplished *via* treatment with a heterobifunctional crosslinker and subsequent conjugation with a fluorophore-labeled immune agonist. Due to the wide availability of amine-functionalized immune agonists, we selected a cross-linker with a succinimidyl group, maleimide-PEG₆-NHS. We included a poly(ethylene glycol) spacer arm to optimize agonist presentation. Additionally, the maleimide was used to link the crosslinker to the free thiols derived from the mercaptopilane functionalization on the particle.

To control agonist loading we varied the concentration of the crosslinked particles in a solution of FAM-CpG-NH₂ (**Fig. 4.6a**). Flow cytometry indicated a shift in median fluorescence corresponding to an increase in the amount of FAM-CpG per particle (**Fig. 4.6b**) demonstrating the ability to dose the particle with varying amounts of agonist. Using a colorimetric readout of NF- κ B, we determined that NF- κ B activity increased with increasing agonist loading on the particles (**Fig. 4.6c**). Similarly, we increased the stoichiometry of particles to cells and observed an increase in the overall NF- κ B activity. To demonstrate the generality of this method, we loaded the particles with lipoteichoic acid (LTA), a TLR2 agonist.⁸ Our results indicated that the increased LTA loading corresponded with increased NF- κ B activation. Confocal microscopy of the particle bearing cells confirmed that they were internalized (**Fig. 4.7b and c**).

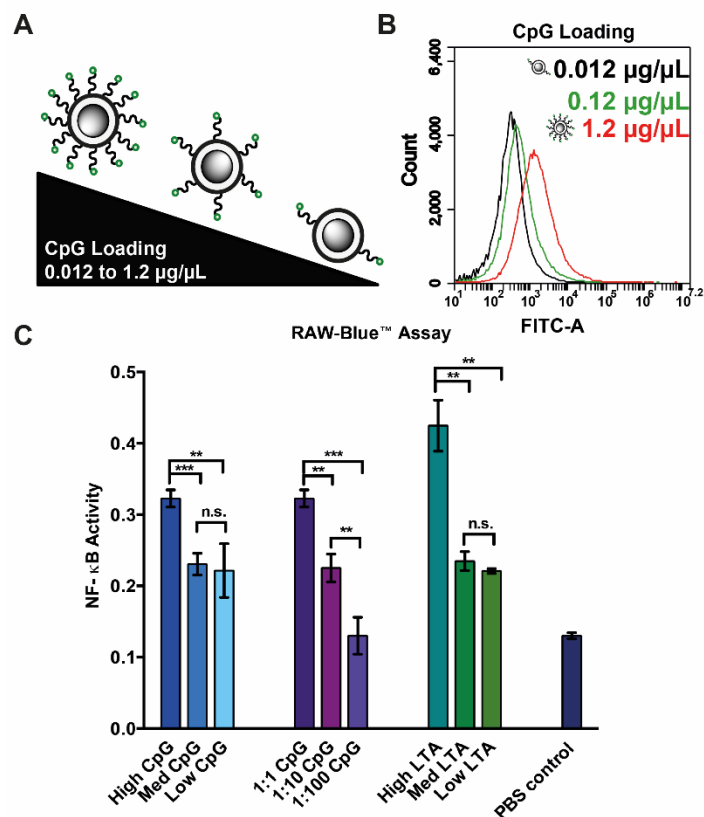


Figure 4.6. Cell activation and endocytosis of coated and uncoated particles. A) Flow cytometry analysis of PS coat particles loaded with increasing amounts of FAM-CpG from 0.012 $\mu\text{g}/\mu\text{L}$ to 1.2 $\mu\text{g}/\mu\text{L}$. B) Agonist titration analysis using RAW macrophage RAW-Blue™ NF- κB activity assay. High, med and low refer to the concentration of free agonist in the PS coat particle loading reaction (1.2, 0.12 and 0.012 $\mu\text{g}/\mu\text{L}$ CpG, respectively and 20, 2 and 0.2 $\mu\text{g}/\text{mL}$ LTA, respectively). Ratios refer to stoichiometry of particles to cells.

Differences in uptake were observed between PS particle and coated PS particles. Macrophages exposed to coated PS particles display internalization, while PS particles remain un-internalized (**Fig. 4.7a**). Further differences were observed in the aggregation of the two particle types. PS particles tend to form large, aggregated clumps while the coated PS particles

are more evenly suspended throughout the medium (**Fig. 4.7b and c**). The aggregates in the PS-CpG varied in size, including some extremely large aggregates approximately 70 μm in diameter (**Fig. C25**), lowering the effective concentration of the particles. These results indicate that the coated particles provide a more uniform bioavailability providing better control of agonist dosing.

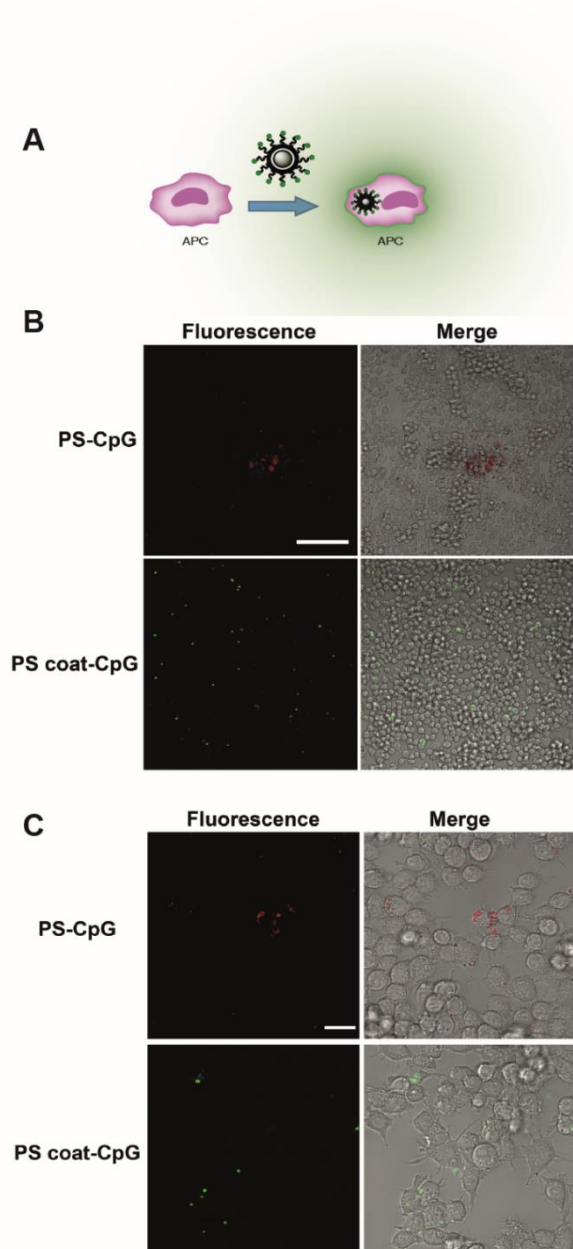


Figure 4.7. Cell internalization of particles. A) Schematic of particle internalization. B) Confocal microscopy (63x magnification) of RAW macrophages incubated with PS-CpG (top) or PS coat-CpG (bottom) for 4 h. Stoichiometry of particles to cells was 1:1. PS-CpG and PS coat-CpG samples were imaged using 561 nm or 488 nm laser excitation, respectively. Scale bar: 20 μm . C) Confocal microscopy of samples in B at 20x magnification. Scale bar: 100 μm .

4.4.5 Biomimimetic Nature of Core-Shell Particles

To study the biomimetic nature of our particles, we first examined the zeta potential of coated and uncoated particles. We found that coating the particles decreased the zeta potential by -1.2 to -20.8 mV compared to their uncoated precursors (**Table C1**). This negative zeta potential confers several benefits to the coated particle including: (1) reduced clumping, which increases particle dosing consistency, and (2) surface potential similar to both mammalian cells (-19.4 mV) and bacteria (-21.9 mV).^{9,10} We hypothesized that these advantages would increase the immune cell uptake of the particles.

To test this hypothesis, we devised a cellular uptake experiment. We incubated RAW 264.7 macrophages with fluorescein-labeled PS, coated fluorescein-labeled PS, or commercially available Alexa Fluor® 488-labeled, heat-inactivated E.coli at 1:1 stoichiometry of particles to cells. After 4 h, we examined the fluorescence of the RAW cells using flow cytometry (**Fig. 4.8**). We found that 1.8% of cells treated with labeled PS particles took up the particles. In contrast, 44.0% of cells showed uptake of the coated fluorescein-labeled PS particles. Further, 98.5% of cells displayed uptake of the labeled E. coli. These results showed that the uptake profile of the coated PS particles is increased compared to that of the PS particle, and therefore, closer to that of the pathogenic E. coli or a mammalian cell. We hypothesize that the reason for the lowered uptake of the coated PS particles in contrast to E. coli is due to the presence of TLR agonists on the surface of the E. coli that induce endocytosis in immune cells.^{11a-d}

In order to assay the ability of our particles to recreate a pathogenic insult, we incubated RAW 264.7 cells with CpG-loaded particles. We compared coated PS particles functionalized with FAM-CpG, commercially available amine-modified PS particles that we functionalized

with CpG, and Alexa Fluor® 488-labeled, heat-inactivated E.coli (**Fig. 4.8**). Cells were incubated with particles or E. coli for 4 h at a ratio of one particle or E. coli to one cell. We found that 3.7% of cells incubated with PS-CpG particles successfully internalized the particles. In contrast, 52.1% of cells incubated with coated PS-CpG particles displayed fluorescence, indicating successful uptake of the particles. This compares favorably with the fluorescent E.coli which had uptake by 98.5% of the cells. We hypothesize that the coated polymer had more uptake because the zeta potential is closer to that of E. coli or a mammalian cell. Additionally, PS particles are hydrophobic and prone to clumping, lowering the effective concentration. E.coli have an additional advantage over the coated PS-CpG particles in that they display many different TLR agonists which activate the cells – potentially increasing uptake.^{11a-d}

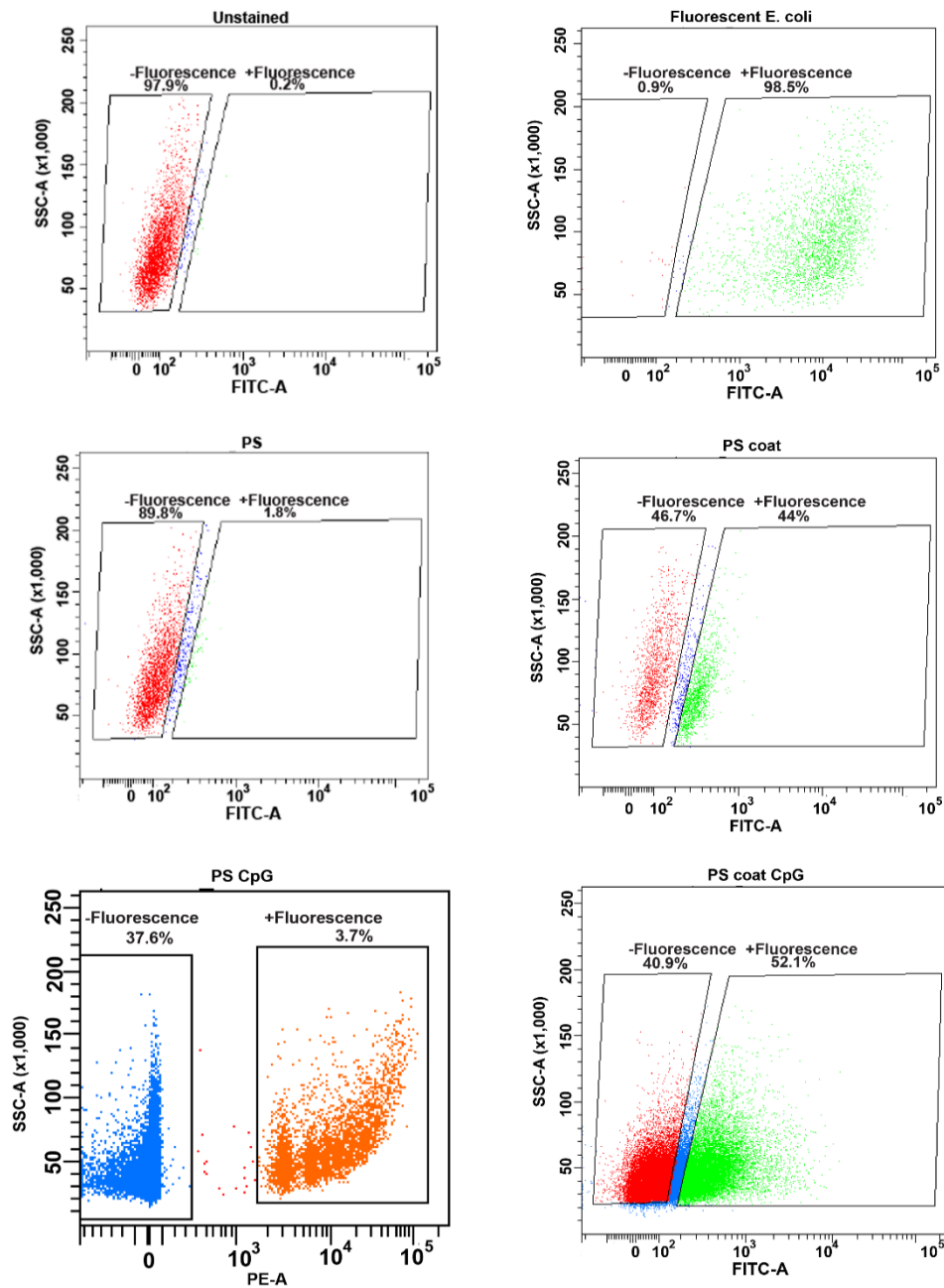


Figure 4.8. Cell uptake of particles. Flow cytometry plots of unstained cells, PS particle, PS coat particle and fluorescent bacteria (top to bottom).

After sorting, the cells were analyzed by fluorescence microscopy (**Fig. 4.9**). The microscopy of the cells sorted for the FITC or AlexaFluor488 marker showed punctate green fluorescence on

the interior of the cells indicating uptake of the particles or bacteria. Enough cells for microscopy was only obtained for cells incubated with PS coat, PS coat- CpG and fluorescent E.coli. This is due to the low percentage of cells positive for uptake of PS or PS-CpG particles.

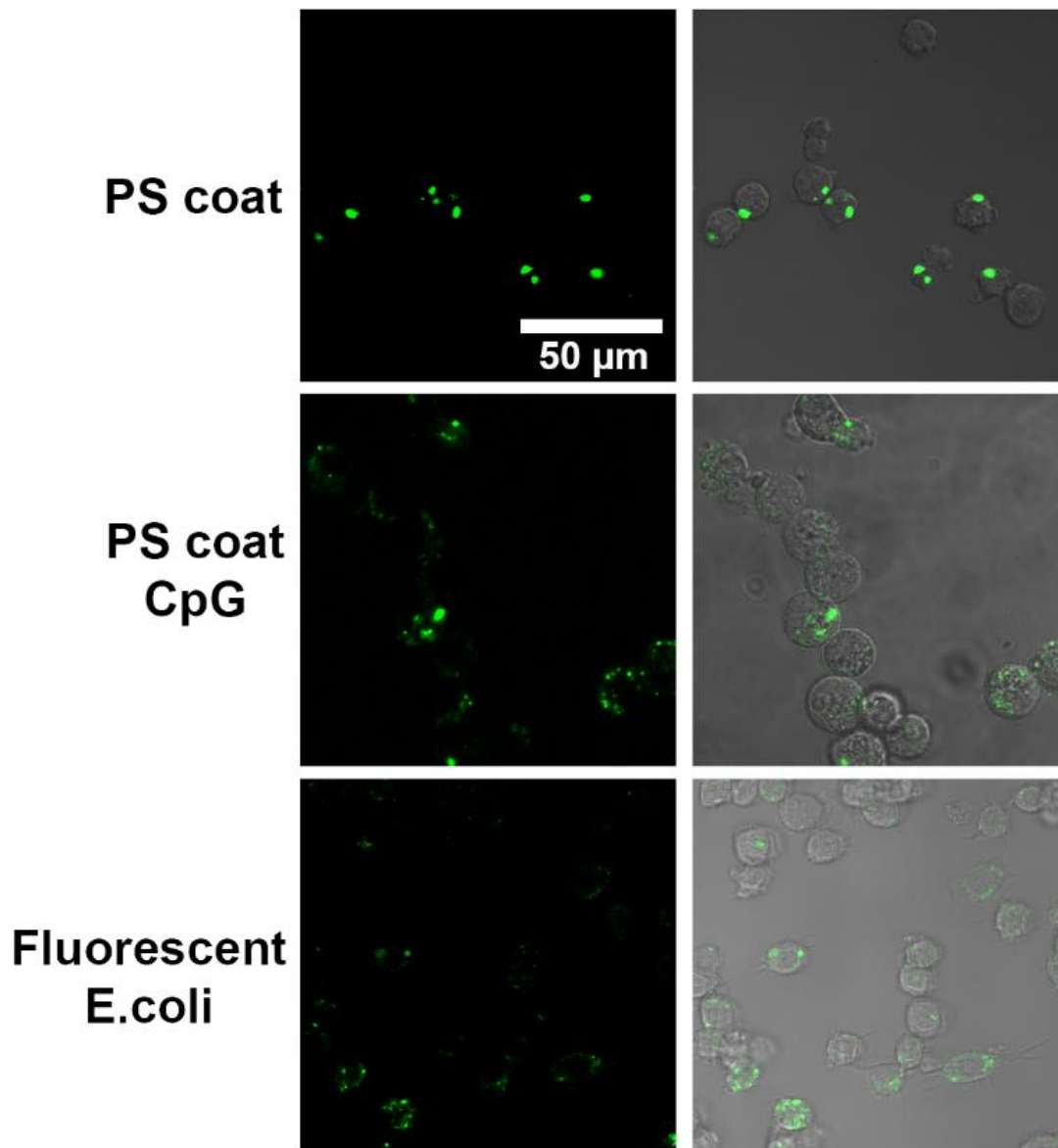


Figure 4.9. Fluorescence microscopy of sorted cells. Cells FACS sorted for green fluorescence demonstrate the presence of particle puncta.

4.5 Conclusion

Particulate forms of polystyrene and other common delivery polymers non-specifically activate the immune system to varying degrees, while limiting the amount of particulate matter that is internalized. To incorporate these useful polymers into tools to study the immune system, we developed a method to passivate their surface. This technique provides a significant decrease in the immunogenicity of common polymer particles. We further showed that this easy and scalable coating technique can be applied to many polymeric particles conferring them with the same useful qualities, including ease of crosslinking and agonist loading, uniform dispersion in aqueous solutions, and increased cellular uptake. The coated particles display surface properties closely resembling that of a pathogen, opening new avenues for study of the innate immune system and adjuvant development.

4.6 Materials and Methods

5'-FAM-TCCATGACGTTCCCTGACGTT-3'-NH₂ (FAM-CpG-amino) was purchased from IDT. All cell culture reagents were obtained from Life Technologies unless otherwise specified. Chemicals were from Sigma Aldrich unless otherwise specified. PMMA (3-10 μm) and PE (3-16 μm) particles were purchased from Cospheric. PLGA (2 μm) particles were purchased from Sigma Aldrich. Rhodamine-NH₂ (1 μm) functionalized polystyrene particles were purchased from Fisher Scientific. AlexaFluor® 488 functionalized heat inactivated E.coli were purchased from ThermoFisher Pierce.

Synthesis of 1 μm polystyrene particles: Uniform, spherical polystyrene particles were synthesized via controlled styrene polymerization. Polyvinylpyrrolidone, MW 40,000 (2.0 g) and styrene (20 g), washed with NaOH and dried with MgSO₄, was dissolved in EtOH (250 mL)

and purged with nitrogen for 1 h. AIBN (0.2 g) was added and the mixture stirred at 70 °C and 200 rpm (IKA) for 24 h. Mixture was pelleted by centrifugation at 3400 rpm (Baxter Varifuge 3.0R) for 30 minutes and washed 3x in 30 mL EtOH to remove residual monomer, initiator and stabilizer. PS particles were stored in EtOH at 4 °C.

Synthesis of functionalized silica shell on polymer particles: Cyclohexane (45 mL), *n*-hexanol (10.8 mL), endotoxin-free water (2 mL) and Triton X-114 (10.8 mL) were placed in a round bottom flask and sonicated for 20 min. Particles (0.2 g) were added and the suspension was sonicated for 40 min. TEOS (400 µL) was added dropwise followed by 14 M aqueous ammonia (1.2 mL). Solution was stirred for 30 min RT. 3-Mercaptosilane (200 µL) was added dropwise and stirred for 6 h. TEOS-mercaptopilane copolymer coated particles were pelleted at 3400 rpm for 30 min and washed 3x with EtOH. Particles were dried at 70 °C overnight.

Agonist attachment to functionalized particles: TEOS-mercaptopilane copolymer coated particles or NH₂-functionalized polystyrene particles (0.4 g) and maleimide-PEG₆-NHS (0.4 g) were suspended in 5 mL DMSO and 5 mL dPBS, sonicated for 1 h and incubated at 37 °C overnight. Resulting particles were pelleted and washed 3x in DMSO. FAM-CpG-NH₂ (0.5-5 eq.) was added in 50 mM Tris-HCl, 150 mM NaCl (pH 8) and sonicated for 1 h in the dark and incubated at 37 °C for 0.5-4 h. Particles were pelleted and removed and resulting supernatant was measured using NanoDrop 2000 (ThermoScientific) to gauge DNA loading by measuring the DNA remaining in solution. Resulting particles were pelleted and washed 3x with DMSO and 3x with dPBS and stored at 4 °C.

Flow cytometry of agonist labeled particles: Particles were placed in dPBS and sonicated for 1 h. Particles were aliquoted and diluted 1:50 in a 1.5 mL microcentrifuge tube in dPBS. Particles

were analyzed using Accuri C6 flow cytometer. Gating parameters were selected for size of a single particle.

SEM and EDS of particles: Scanning electron microscopy (SEM) and energy-dispersive spectroscopy (EDS) of the particles was performed using an FEI Quanta 3D FEG dual beam (SEM/FIB) equipped with Inca EDS (Oxford Instruments). High-resolution images were taken with an FEI Magellan 400 XHR SEM. particle samples were dried under vacuum for 24 h, mounted on carbon tape, and sputter coated (South Bay Technologies) with approximately 2-4 nm of Au/Pd 60:40 or Ir.

Zeta potential: Zeta potential was performed using a Zetasizer ZS Nano DLS (Malvern). Particles were suspended at a concentration of approximately 1 mg/mL in a solution of 10 mM NaCl in nanopure water. The mixture was then sonicated (Bransonic) for 8 minutes, and vortexed immediately before measurement.

Dynamic Light Scattering: Dynamic light scattering (DLS) was performed using a Zetasizer ZS Nano DLS (Malvern). The particles were placed in a solution of 10 mM NaCl in nanopure water at 1 mg/mL.

Light microscopy of particles: 1×10^5 particles were placed in 200 μ L phosphate-buffered saline (PBS) or EtOH in an 8-well coverslip bottom plate (ThermoScientific). Particles were imaged using Zeiss LSM780 confocal microscope and Zeiss Plan-Apochromat 63x/1.40 Oil objective.

Microscopy of particle internalization: RAW 264.7 macrophages were plated at 1×10^5 cells/well in an 8-well coverslip bottom plate in 200 μ L Dulbecco's modified eagle medium (DMEM) containing 10% heat-inactivated fetal bovine serum (HIFBS) and incubated at 37 °C, 5% CO₂ for 24 h. Media was changed to DMEM, 10% HIFBS and cells were incubated for 1 h. Particles were added at a 1:1 ratio of cells to particles and incubated for 4 h. Cells were imaged using a

Zeiss LSM780 confocal microscope and Zeiss Plan-Apochromat 63x/1.40 Oil objective and 488 nm laser.

RAW-Blue™ NF-κB Assay: RAW-Blue™ NF-κB cells (Invivogen) were passaged and plated in a 96 well plate at 100k cells/ well in 180 μL DMEM containing 10% HIFBS. Cells were incubated at 37 °C and 5% CO₂ for 1 h. Particles were counted using flow cytometer. 100k particles were added to each well (1 particle:1 cell). The volume of each well was brought to 200 μL and incubated at 37 °C and 5% CO₂ for 18 h. After 18 h, 20 μL of the cell supernatant was placed in 180 μL freshly prepared QuantiBlue (Invivogen) solution and incubated at 37 °C/ 5% CO₂ for up to 2 h. The plate was analyzed every hour using a Multiskan FC plate reader (Thermo Scientific) and absorbance was measured at 620 nm.

THP-1 IL-1β: THP-1 cells were cultured in Roswell Park Memorial Institute medium (RPMI) 1640 medium supplemented with 10% HIFBS. 3.6×10^5 cells were plated in each well of a 96 well plate in 180 μL DMEM supplemented with 10 % HIFBS. Cells were incubated with 20 μL of LPS at 10 μg/mL was for 3 h at 37 °C/5% CO₂. Supernatant was removed and 180 μL supplemented RPMI added to the cells. 20 μL of particle suspension (1.8×10^7 particles/mL) was added to the cells. Cells were incubated overnight at 37 °C/5% CO₂. Detection of IL-1β was accomplished using HEK-Blue IL-1β cells (Invivogen). HEK-Blue IL-1β cells were washed twice with pre-warmed dPBS and detached using a cell scraper. Cells were resuspended in fresh pre-warmed DMEM supplemented with 10% HIFBS. 5×10^5 cells were placed in each well in 150 μL supplemented DMEM. 50 μL THP-1 cell supernatant was added to each well. Cells were incubated overnight 37 °C in 5% CO₂. IL-1β production was determined by adding 150 μL QuantiBlue (Invivogen) solution and incubated at 37 °C/ 5% CO₂ for up to 2 h. to 50 μL HEK-

Blue IL-1 β cell supernatant. The plate was analyzed every hour using a Multiskan FC plate reader (Thermo Scientific) and absorbance was measured at 620 nm.

Particle vs. E. coli Uptake Analysis: RAW 264.7 macrophages were passaged and 1×10^7 cells were placed in 15 mL conical tube. Particles or heat inactivated fluorescent bacteria were added at a ratio of 1:1. Cells were incubated at 37 °C 5% CO₂ for 4 h. Cells were pelleted and washed 3x with dPBS and placed in 5 mL FACS tubes. Cells were sorted using FACSAria Fusion flow cytometer (BD).

qPCR Analysis: RAW 264.7 (2×10^6 cells) were plated in a 6 well plate in 2 mL DMEM/10% HIFBS. 2×10^6 particles were added to each well. Cells were incubated for 4 h and RNA was extracted using RNeasy Plus Mini kit (Qiagen). RT-PCR was performed using RT² first strand kit (Qiagen) and BioRad thermocycler according to manufacturer's protocol. cDNA was stored at -20 °C. RT² SYBR ROX qPCR Master mix (Qiagen) was used according to manufacturer's protocol. qPCR amplification was performed using a Stratagene Mx3005P thermocycler.

4.7 References

1.
 - a. Hubbell, J.; Thomas, S.; Swartz, M. Materials engineering for immunomodulation *Nature* **2009**, *462*(7272), 499–460.
 - b. Moyer, T.; Zmolek, A.; Irvine, D. Beyond antigens and adjuvants: formulating future vaccines. *Eur. J. Clin. Invest.* **2016**, *126*(3), 799–808.
 - c. Irvine, D.; Swartz, M.; Szeto, G. Engineering synthetic vaccines using cues from natural immunity. *Nat. Mater.* **2013**, *12*, 978–990.
 - d. Pradhan, P.; Qin, H.; Leleux, J.; Gwak, D.; Sakamaki, I.; Kwak, L.; Roy, K. The effect of combined IL10 siRNA and CpG ODN as pathogen-mimicking microparticles on Th1/Th2

cytokine balance in dendritic cells and protective immunity against B cell lymphoma.

Biomaterials **2014**, *35*(21), 5491–5504.

e. Kasturi, S.; Skountzou, I.; Albrecht, R.; Koutsouanos, D.; Hua, T.; Nakaya, H.; Ravindran, R.; Stewart, S.; Alam, M.; Kwissa, M.; Villinger, F.; Murthy, N.; Steel, J.; Jacob, J.; Hogan, R.; Garcia-Sastre, A.; Compans, R.; Pulendran, B. Programming the magnitude and persistence of antibody responses with innate immunity. *Nature*, **2011**, *470*, 543–547.

2.

a. Peterson, L.; Ramer-Tait, A.; Broderick, S.; Kong, C.; Ulery, B.; Rajan, K.; Wannamuelher, M.; Narasimhan, B. Activation of innate immune responses in a pathogen-mimicking manner by amphiphilic polyanhydride nanoparticle adjuvants. *Biomaterials* **2011**, *32*(28), 6822.

b. Stutts, L.; Esser-Kahn, A. A Light-Controlled TLR4 Agonist and Selectable Activation of Cell Subpopulations. *ChemBioChem* **2015**, *16*(12), 1744–1748.

c. Mancini, R.; Tom, J.; Esser-Kahn, A. Covalently Coupled Immunostimulant Heterodimers. *Angew. Chem. Int. Ed.* **2014**, *53*(1), 189–192.

d. Mancini, R.; Stutts, L.; Moore, T.; Esser-Kahn, A. Controlling the Origins of Inflammation with a Photoactive Lipopeptide Immunopotentiator. *Angew. Chem. Int. Ed.* **2015**, *54*(20), 5962–5965.

e. Fyatiyanos, K.; Rodriguez- Lorenzo, L.; Clift, M.; Blank, F.; Vanhecke, D.; Von Garnier, C.; Petri-Fink, A.; Rothen-Rutishauser, B. Uptake efficiency of surface modified gold nanoparticles does not correlate with functional changes and cytokine secretion in human dendritic cells in vitro. *Nanomedicine* **2015**, *11*(3), 633–644.

- f. Toy, R.; Roy, K. Engineering nanoparticles to overcome barriers to immunotherapy. *Bioeng. Transl. Med.* **2016**, *1*(1), 47–62.
- g. Leleux, J.; Atalis, A.; Roy, K. Engineering immunity: Modulating dendritic cell subsets and lymph node response to direct immune-polarization and vaccine efficacy. *J. Controlled Release* **2015**, *219*, 610–621.
- h. Siefert, A.; Caplan, M.; Fahmy, T. Artificial bacterial biomimetic nanoparticles synergize pathogen-associated molecular patterns for vaccine efficacy. *Biomaterials* **2016**, *97*, 85–96.
- i. Moon, J.; Suh, H.; Li, A.; Ockenhouse, C.; Yadava, A.; Irvine, D. Enhancing humoral responses to a malaria antigen with nanoparticle vaccines that expand Tfh cells and promote germinal center induction. *Proc. Natl. Acad. Sci. U.S.A.* **2012**, *109*(4), 1080–1085.
- j. Nuhn, L.; Vanparijs, N.; Beuckelaer, A.; Lybaert, L.; Verstraete, G.; Deswarte, K.; Lieneklaus, S.; Shukla, N.; Salyer, A.; Lambrecht, B.; Grooten, J.; David, S.; Koker, S.; De Geest, B. pH-degradable imidazoquinoline-ligated nanogels for lymph node-focused immune activation. *Proc. Natl. Acad. Sci. U.S.A.* **2016**, *113*(29), 8098–8103.
- k. Andorko, J.; Gammon, J.; Tostanoski, L.; Zeng, Q.; Jewell, C. Targeted Programming of the Lymph Node Environment Causes Evolution of Local and Systemic Immunity. *Cell. Mol. Bioeng.* **2016**, *9*(3), 418–432.
- l. Irvine, D.; Hanson, M.; Rakhra, K.; Tokatlian, T. Synthetic Nanoparticles for Vaccines and Immunotherapy. *Chem. Rev.* **2015**, *115* (19), pp 11109–11146.
- m. Koshy, S.; Mooney, D. Biomaterials for enhancing anti-cancer immunity. *Curr. Opin. Biotech.* **2016**, *40*, 1–8.
- n. Dowling, D.; Levy, O. Pediatric vaccine adjuvants: Components of the modern vaccinologist's toolbox. *Pediatr. Infect. Dis. J.* **2015**, *34*(12), 1395–1398.

- o. Meyer, R.; Sunshin, J.; Green, J. Biomimetic particles as therapeutics. *Trends Biotechnol.* **2015**, *33*(9), 514–524.
- p. Lynn, G.; Laga, R.; Darrah, P.; Ishizuka, A.; Balaci, A.; Dulcey, A.; Pechar, M.; Pola, R.; Gerner, M.; Yamamoto, A.; Buechler, C.; Quinn, K.; Smelkinson, M.; Vanek, O.; Cawood, R.; Hills, Y.; Vasalatiy, O.; Kastenmüller, K.; Francica, J.; Stutts, L.; Tom, J.; Ryu, K.; Esser-Kahn, A.; Etrych T.; Fisher, K.; Seymour, L.; Seder, R. In vivo characterization of the physiochemical properties of polymer-linked TLR agonists that enhance vaccine immunogenicity. *Nat. Biotechnol.* **2015**, *33*(11), 1201–1210.
- 3.
- a. Seong, S.; Matzinger, P. Hydrophobicity: an ancient damage-associated molecular pattern that initiates innate immune responses. *Nat. Rev. Immunol.* **2004**, *4*(6), 469–478.
- b. Farrera, C.; Fadel, B. It takes two to tango: Understanding the interactions between engineered nanomaterials and the immune system. *Eur. J. Pharm. Biopharm.* **2015**, *95*, 3–12.
- c. Gustafson, H.; Holt-Casper, D.; Grainger, D.; Ghandehari, H. Nanoparticle uptake: The phagocyte problem. *Nano Today* **2015**, *10*(4), 487–510.
- d. Fadeel, B. Clear and present danger? Engineered nanoparticles and the immune system. *Swiss Med. Wkly.* 2012, *142*, w13609. Lunov, O.; Syrovets, T.; Loos, C.; Nienhaus, G.; Mailander, V.; Landfester, K.; Rouis, M.; Simmet, T. Amino-Functionalized Polystyrene Nanoparticles Activate the NLRP3 Inflammasome in Human Macrophages. *ACS Nano* **2011**, *5*(12), 9648–9657.
- e. Lundqvist, M.; Stigler, J.; Elia, G.; Lynch, I.; Cedervall, T.; Dawson, K. Nanoparticle size and surface properties determine the protein corona with possible implications for biological impacts. *Proc. Natl. Acad. Sci. U.S.A.* **2008**, *105*(38), 14265–14270.

- f. Ekdahl, K.; Lambris, J.; Elwing, H.; Ricklin, D.; Nilsson, P.; Teramura, Y.; Nicholls, I.; Nilsson, B. Innate immunity activation on biomaterial surfaces: A mechanistic model and coping strategies. *Adv. Drug Deliv. Rev.* **2012**, *63*(12), 1042–1050.
- g. Lunov, O.; Syrovets, T.; Loos, C.; Nienhaus, G.; Mailander, V.; Landfester, K.; Rouis, M.; Simmet, T. Amino-Functionalized Polystyrene Nanoparticles Activate the NLRP3 Inflammasome in Human Macrophages. *ACS Nano* **2011**, *5*(12), 9648–9657.
- h. Lundqvist, M.; Stigler, J.; Elia, G.; Lynch, I.; Cedervall, T.; Dawson, K. Nanoparticle size and surface properties determine the protein corona with possible implications for biological impacts. *Proc. Natl. Acad. Sci. U.S.A.* **2008**, *105*(38), 14265–14270.
- i. Many of the most effective materials, many cited in 2, avoid this inherent inflammation through molecular design, but this may not be a viable option for those lacking synthetic approaches and require more steps to achieve basic understanding.
4. Hong, J.; Han, H.; Hong, C.; Shim, S. A direct preparation of silica shell on polystyrene microspheres prepared by dispersion polymerization with polyvinylpyrrolidone *J. Polym. Sci. A. Polym. Chem.* **2008**, *46*(8), 2884–2890.
5. Thickett, S.; Gilbert, R. Emulsion polymerization: State of the art in kinetics and mechanisms. *Polymer* **2007**, *48*(24), 6965–6991.
6. Pickering, S. CXCVI.—Emulsions. *J. Chem. Soc., Trans.* **1907**, 2001–2021.
- 7.
- a. Ballas, Z.; Krieg, A.; Warren, T.; Rasmussen, W.; Davis, H.; Waldschmidt, M.; Weiner, G. Divergent Therapeutic and Immunologic Effects of Oligodeoxynucleotides with Distinct CpG Motifs. *J. Immunol.* **2001**, *167*(9), 4878–4886.

- b. Hayden, M.; West, A.; Ghosh, S. NF- κ B and the immune response. *Oncogene*. **2006**, *25*, 6758-6780.
- c. Silverman N, Maniatis T. NF- κ B signaling pathways in mammalian and insect innate immunity. *Genes Dev*. **2001**, *15*, 2321–2342.
- d. Libermann, T.; Baltimore, D. Activation of interleukin-6 gene expression through the NF- κ B transcription factor. *Mol. Cell. Biol*. **1990**, *10*(5), 2327-2334.
8. Schwandner, R.; Dziarski, R.; Wesche, H.; Rothe, M. Peptidoglycan- and Lipoteichoic acid-induced cell activation is mediated by Toll-like receptor 2. *J. Biol. Chem*. **1999**, *274*, 17406–17409.
9. Alves, C.; Melo, M.; Franquelim, H.; Ferre, H.; Planas, M.; Feliu, L.; Bardaji, E.; Kowalczyk, W.; Andreu, D.; Santos, N.; Fernandes, M.; Castanho, M. Escherichia coli Cell Surface Perturbation and Disruption Induced by Antimicrobial Peptides BP100 and pepR. *J. Biol. Chem*. **2010**, *286*(36), 27536–27544.
10. Bondar, O. V.; Saifullina, D. V.; Shakhmaeva, I. I.; Mavlyutova, I. I.; Abdullin, T. I. Monitoring of the Zeta Potential of Human Cells upon Reduction in Their Viability and Interaction with Polymers. *Acta Naturae* **2012**, *4*(1), 78–81.
- 11.
- a. Takeuchi, T.; Hoshino, K.; Kawai, T.; Sanjo, H.; Takada, H.; Ogawa, T.; Takeda, K.; Akira, S. Differential roles of TLR2 and TLR4 in recognition of gram-negative and gram-positive bacterial cell wall components. *Immunity*, **1999**, *11*(4), 443–451.
- b. Platt, C.; Ma, J.; Chalouni, C.; Ebersold, M.; Bou-Reslan, H.; Carano, R.; Mellman, I.; Delamarre, L. Mature dendritic cells use endocytic receptors to capture and present antigens. *Proc. Natl. Acad. Sci. U.S.A.*, **2009**, *107*(9), 4287-4292.

- c. Sorkin, A.; von Zastrow, M.; Endocytosis and signalling: intertwining molecular networks. *Nat. Rev. Mol. Cell Biol.* **2009**, 10, 609-622.
- d. Blander, J.; Medzhitov, R. Regulation of Phagosome Maturation by Signals from Toll-Like Receptors. *Science* **2004**, 304(5673), 1014-1018.
- 12.
- a. Demento, S.; Eisenbarth, S.; Foellmer, H.; Platt, C.; Caplan, M.; Saltzman, W.; Mellman, I.; Ledizet, M.; Fikrig, E.; Flavell, R.; Fahmy, T. Inflammasome-activating nanoparticles as modular systems for optimizing vaccine efficacy. *Vaccine*, **2009**, 3013-3021.
- b. Baron, L.; Gombault, A.; Fammy, M.; Villeret, B.; Savigy, F.; Guillou, N.; Panek, C.; Le Bert, C.; Lagente, V.; Rassendren, F.; Riteau, N.; Couillin, I. The NLRP3 inflammasome is activated by nanoparticles through ATP, ADP and adenosine. *Cell Death and Disease*, **2015**, 6, e1629.
- c. Hari, A.; Zhang, Y.; Tu, Z.; Detampel, P.; Stenner, M.; Ganguly, A.; Shi, Y. Activation of NLRP3 inflammasome by crystalline structures via cell surface contact. *Scientific Reports*, **2014**, 4, 7281.

5 A Photoactivatable Innate Immune Receptor for Optogenetic Inflammation

*This chapter has been published in ACS Chem. Biol. 12(2), 347-350, 2017

5.1 Summary

Few tools exist to directly examine spatial and temporal elements of immune activation. To elucidate the spatiotemporal aspects of innate immune responses, we designed an optogenetic pattern recognition receptor that activates in response to blue light. We demonstrate direct receptor activation, leading to control of downstream signaling pathways in a variety of relevant cell types and labeling of activated cells via a split fluorescent reporter.

5.2 Introduction

There is a common element in both preventing disease through vaccination and the chronic inflammation of autoimmune diseases- activation of the innate immune system by Pattern Recognition Receptors (PRRs).¹ These recognition events are position and time-dependent, leading to robust protection from disease in some cases and autoimmune disorders in others. The spatiotemporal sequence of activation and its cellular context determines the type and magnitude of the immune response.^{2,3} Despite the importance of understanding the pattern of receptor signaling, few spatial or temporal techniques exist to control PRR activation. In the field of neurobiology, light with its exquisite spatiotemporal precision, has helped determine how complex networks of cells enact unique signaling mechanisms.⁴ Recently, we reported the use of photoactivated Toll-like receptor agonists to control temporal activation of innate immune receptors.⁵⁻⁷ However, spatial control using such technologies is limited by the available

synthetic tools and the challenge of receptor activity and diverse location of immune cells within an organism. Here we show a genetically encoded, photoactivated PRR that allows light-mediated control of innate immune signaling. The engineered receptor is a fusion of the light-activated cryptochrome system, CRY2/CIB1, and the cytosolic pattern recognition receptor DAI (DNA-dependent activator of IFN-regulatory factors). This genetic fusion renders the DAI receptor inducible via dimerization by blue light. Genetic encoding allows the receptor to be expressed selectively within a designated cell type and to originate the signal only from selected cells. We show that the receptor activates cellular markers of innate immunity within 2 hours of blue light exposure. Additionally, the system reports which cells have been activated using dimerization via a split-fluorescence reporter assay. The light-activated receptor was inserted into multiple cell types including RAW macrophages and HEK293. A genetically encoded, light-activated innate immune receptor will enable unprecedented control and analysis of complex innate immune interactions potentially including wound healing and paracrine signaling effects.

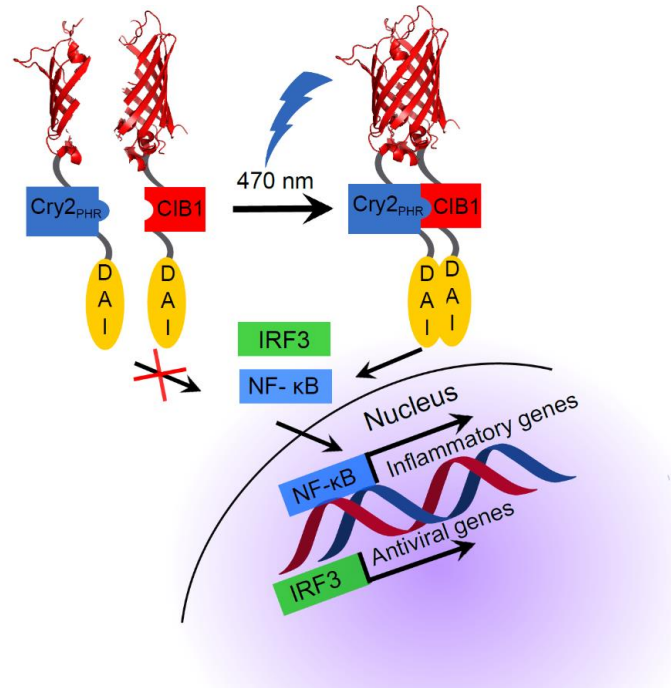


Figure 5.1. Schematic of photo-DAI activation. To achieve photoactivation, the CRY2/CIB1 domains are fused to one of two split domains of mCherry and identical copies of the DNA-dependent activator of IFN-regulatory factors (DAI) receptor. Activation with blue light (470 nm) induces dimerization of CRY2/CIB1, DAI, and subsequent fluorescence from the coupled mCherry. The photo-DAI enacts the transcription of interferons activating the innate immune system.

5.3 Results and Discussion

5.3.1 Design of Photoactivated receptor

In designing a photoactivated receptor, we sought to apply a general design strategy that would work for many different innate immune receptors. As most PRRs use dimerization to control signaling, light-induced dimerization would yield a general method to gain light-mediated control of innate immune receptors.^{2,7,8} We chose the DAI receptor as a proof-of-

concept effector module due to its convenient properties for protein engineering as well as a precedent for genetic manipulation and controlled dimerization resulting in controlled activation.⁹ DAI is a cytosolic PRR that homodimerizes upon binding dsDNA, activating the NF- κ B and IRF3 pathways.⁹ Engineered DAI activated IFN pathways in response to chemical dimerization by a rapamycin derivative, making this receptor a promising candidate for light-induced dimerization.⁹ CRY2 (cryptochrome 2) and its binding partner CIB1 (cryptochrome interacting basic helix-loop-helix 1) are a robust blue light-induced dimerization system used in many mammalian cells.¹⁰⁻¹² To minimize the increased molecular weight, we used the CRY2_{PHR} subconstruct, which is sufficient to induce dimerization. Lacking nuclear import capability, it would maintain the CRY2-DAI fusion protein in the desired cytoplasmic compartment.¹⁰ The C-

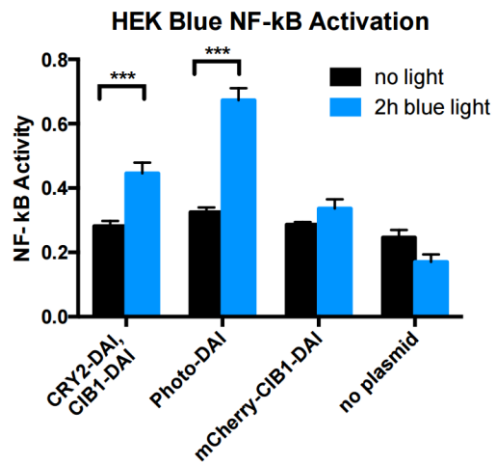


Figure 5.2. Photo-DAI activity in HEK Blue cells. Black bars: cells incubated in the dark. Blue bars: Cells exposed to light for 2 h. Error bars denote standard deviation. n=3 replicates. ***p < 0.001.

terminus of DAI is used for downstream signaling, and we hypothesized that an N-terminal fusion would not inhibit DAI activity.^{9,13} We therefore generated a photo-inducible DAI system via co-expression of DAI variants as C-terminal fusions to either CRY2_{PHR} or CIB1 (**Fig. 5.1**).

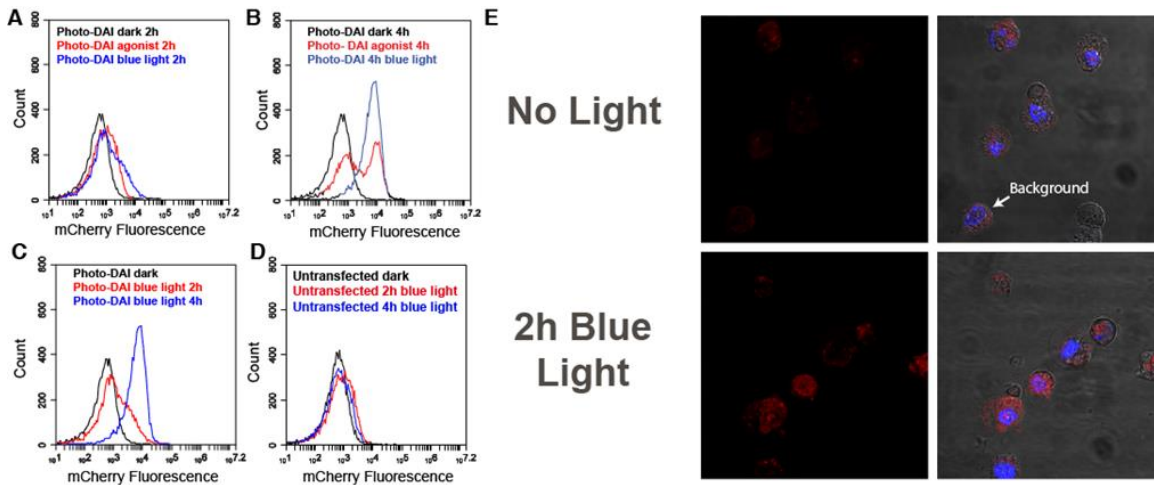


Figure 5.3. Fluorescent reporting of dimerization from cells expressing photo-DAI. A: Flow cytometry of HEK cells expressing photo-DAI after 2 h of exposure to either blue light or the native DAI agonist (100 ng/mL Poly(dA:dT)). Cells incubated for 2 h in the dark (black), with Poly(dA:dT)(red), or with blue light (blue). B: Cells expressing photo-DAI exposed to either blue light or Poly(dA:dT) for 4h. Cells incubated for 4h in the dark (black), with Poly(dA:dT) (red), or with blue light (blue). C: Cells transfected with photo-DAI exposed to blue light for 0h, 2h or 4h. Cells incubated in the dark, 4h (black), cells exposed to 2h blue light (red), or 4h (blue). D: Untransfected cells exposed to blue light for 0h, 2h or 4h. Cells incubated in the dark, 4h (black), cells exposed to blue light 2h (red) or 4h (blue). E: Microscope images of HEK cells expressing photo-DAI Left: mCherry channel Right: merge channel of mCherry and DAPI. Top: incubated in the dark. Bottom: 2h blue light exposure.

5.3.2 Blue light-induced Photo-DAI activation

After completing the design of the light-activated DAI, we tested light-induced dimerization. We transfected HEK-Blue TLR4 cells with photo-DAI constructs (**Fig. 5.1**). Cells were subjected to 470-490 nm light for 2 hours (1.5 W/m²) and activation was measured using a colorimetric assay detecting NF- κ B activity. NF- κ B is an important transcription factor in immune activation and results in an upregulation of cytokines, chemokines and cell surface receptors- alerting the immune system of potential pathogen invasion.¹⁹ Cells containing photo-DAI showed higher NF- κ B activation than untransfected cells (**Fig. 5.2, Fig. D1**). Constructs

fused to split-mCherry (Photo-DAI), a common label for BiFC¹⁴, showed a larger fold-change between illuminated and dark states, demonstrating light-mediated control of activation.

To validate that dimerization was occurring in response to blue light and that the BiFC would mark immune activation, we examined the fluorescence from the photo-DAI system using flow cytometry and confocal microscopy (**Fig. 5.3, Fig. D2**). After 2 h of either blue light exposure or exposure to the native DAI agonist, 100 ng/mL Poly(dA:dT), cells began to show a shift in red fluorescence (**Fig. 5.3a**). After 4 h of exposure to either blue light or native agonist, cells began to show a dramatic shift in fluorescence (**Fig. 5.3b**). In addition to activation and

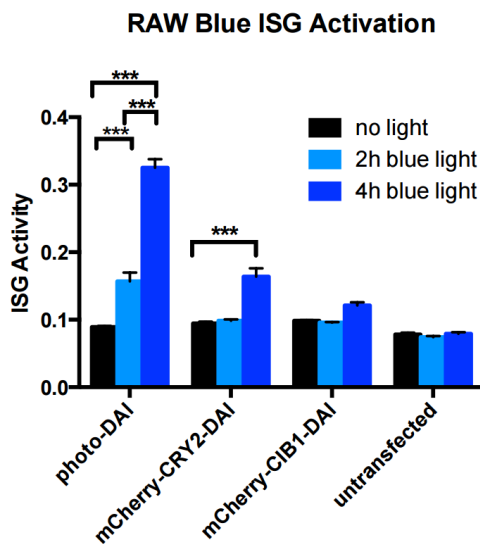


Figure 5.4. Biological activity of RAW Blue ISG cells transduced with photo-DAI system. Black bars: cells incubated in the dark. Light blue bars: Cells exposed to blue light for 2 h. Blue bars: Cells exposed to light for 4 h. Error bars denote standard deviation, n= 3 replicates. ***p < 0.001.

fluorescence of mCherry, we observed a light-mediated temporal element to the dimerization of the receptor (**Fig. 5.3c**).

Blue light stimulation for 2 h elicited red fluorescence in 25% of transfected cells.

Within 4 h of stimulation, 84% of cells expressing photo-DAI displayed mCherry fluorescence. In contrast, the native ligand

for DAI, 100 ng/mL Poly(dA:dT), stimulated only 42% of transfected cells

with two distinct populations of cells

remaining after 4 h of agonist exposure (**Fig. 5.3a-c**). In addition, untransfected cells exposed to blue light for 2 h or 4 h demonstrated no significant change in fluorescence (**Fig. 5.3d**).

To determine whether activated cells could be tracked, we imaged cells transfected with photo-DAI after 2 h blue light exposure. Cells incubated in the dark demonstrated a low level of

mCherry fluorescence, while cells exposed to blue light for 2 h elicited robust fluorescence (**Fig. 5.3e**).

For reporting on the broad set of different immune cells, we tested if this receptor would function in other cell types. Beyond the initial HEK cells, we also examined the ability of photo-DAI to activate IRF3 signaling in RAW macrophages (**Fig. 5.4**). IRF3 is an important transcription factor activated in response to viruses and upregulates cytokines and chemokines involved in an antiviral immune response.¹⁸ Accordingly, RAW cells were transduced with either the full photo-DAI system or the CRY2_{PHR} or CIB1 half of the photo-DAI system using a lentiviral vector. Transduced cells were irradiated with blue light for 2 h or 4 h, alongside a control plate that remained in the dark. The activity of cells expressing photo-DAI corresponded to the exposure time of blue light. Cells expressing mCherry-CRY2-DAI also showed a modest light-mediated response due to the propensity for light-activated CRY2 to self-oligomerize¹⁰, although the activation was less than that of the full photo-DAI system – indicating that both dimerization partners are necessary for maximum DAI activity.

5.4 Conclusion

We have created an optogenetic DAI receptor via genetic fusion to a protein pair capable of undergoing photo-induced dimerization. Our engineered receptor activates NF- κ B and IRF3 nuclear translocation in response to blue light stimulation. By fusing a split fluorescent reporter to this complex, cells containing the dimerized receptor can be identified. This method can be widely applied to a variety of innate immune receptors and their downstream pathways. This method could be applied in vivo to examine the effects of spatial and temporal induction of

inflammation, providing useful information for understanding its effects on vaccination, diabetes, arthritis, and development.

5.5 Materials and Methods

Plasmid Construction: Linearized DNA was obtained by a standard Q5 HotStart PCR protocol and the following PCR conditions: initial denaturation (98 °C, 30 sec), 27 cycles (98 °C, 10 sec; appropriate T_m , 30 sec; 72 °C 30 sec kb^{-1}), final extension (72 °C, 2 min) in a BioRad C1000 thermocycler. Linearized DNA fragments (1:1 molar ratios of 100 ng vector:insert) were added to 10 μ L Gibson Master Mix (NEB) and incubated for 1 h at 50 °C and transformed into chemically competent Top10 *E.coli* (Life Technologies). All plasmids were sequenced, Retrogen (San Diego, CA).



Plasmid Isolation: All plasmids were transformed into Mach1 T1R or Top10 chemically competent *E.coli* (Life Technologies). A single colony was placed in 3 mL 2xYT media with appropriate antibiotic and allowed to grow overnight in a 37 °C shaking incubator. Plasmids were minipreped using QIAprep Spin Miniprep Kit (Qiagen) according to manufacturer protocol. Plasmid was eluted using 30 μ L HyClone™ purified endotoxin- free distilled water (GE healthcare). Concentration was determined using NanoDrop2000 (Thermo Scientific).

HEK-Blue TLR4 Assay: Cells were grown in a 6-well plate to 60% confluency and transfected using Lipofectamine 3000 (Life Technologies). Cells were incubated for 3 days to ensure cytoplasmic plasmid was destroyed and would not interfere with the assay. Cells were passaged and plated in a 96 well plate at 2.5×10^5 cells per well in 200 μ L DMEM supplemented with 10% (v/v) HIFBS. Cells were exposed to blue light for 2 h using a UVP Chromato-Vue UV transilluminator (115V 60Hz 1.8 Amp) and UVP UV/Blue converter plate (1.2 W/m^2) and incubated at 37 °C and 5% CO₂ for 20 h. After 20 h, 20 μ L of the cell supernatant was placed in 180 μ L freshly prepared QuantiBlue (Invivogen) solution and incubated at 37 °C and 5% CO₂ for up to 6 h. The plate was analyzed every hour using a Multiskan FC plate reader (Thermo Scientific) and absorbance was measured at 620 nm.

RAW Macrophage Plasmid Transduction: HEK293T cells were plated in a 10 cm plate at 1×10^6 cells and grown for two days to 90% confluency. Cells were split 1:3 in 10 cm plates and grown for 24 h to 70% confluency. Plasmid was obtained as previously described. Cells were transfected with: transfer plasmid containing gene of interest, packing plasmids, envelope plasmid at a 5:2:2:1 ratio respectively via Lipofectamine 3000 transfection (pMDLg/pRRE, Addgene:12251; pRSV-Rev, Addgene:12253; pMD2.G, Addgene:12259). Cells were washed after 15 h and media was replaced with DMEM supplemented with 20 mM HEPES, 4 mM sodium butyrate and 10% (v/v) FBS. Viral supernatant was collected after 48 h and replaced with growth media. A second batch of viral supernatant was collected 48 h later. Viral stocks were pooled and centrifuged at 500 xg to rid of cellular debris. Virus was concentrated using Lenti-X Concentrator (Clontech) and resuspended at 1:100 original volume. Virus was immediately titrated at 1 μ L, 10 μ L, and 100 μ L and the remainder stored at -80 °C. Raw macrophages were

spininfected in a tabletop centrifuge for 90 min, 30 °C, 2500 RPM and incubated at 37 °C and 5% CO₂ for 2 days.

RAW-Blue ISG Assay: Cells were grown in a 6-well plate to 60% confluency and transduced at a MOI of 1. Cells were incubated for 3 days to ensure cytoplasmic plasmid was destroyed and would not interfere with the assay. Infected cells were selected by sorting for mTurquoise (FACS AriaFusion). Cells were passaged and plated in a 96 well plate at 2.5×10^5 cells per well in 200 μ L DMEM supplemented with 10% (v/v) HIFBS. Cells were exposed to blue light for 2 h using a UVP Chromato-Vue UV transilluminator (115V 60Hz 1.8 Amp) and UVP UV/Blue converter plate (1.2 W/m^2) and incubated at 37 °C and 5% CO₂ for 20 h. After 20 h, 20 μ L of the cell supernatant was placed in 180 μ L freshly prepared QuantiBlue (Invivogen) solution and incubated at 37 °C and 5% CO₂ for up to 6 h. The plate was analyzed every hour using a Multiskan FC plate reader (Thermo Scientific) and absorbance was measured at 620 nm.

Flow Cytometry of Transduced RAW Macrophages: Cells plated for continued growth were passaged and resuspended in DMEM supplemented with 10% FBS. 1.5 μ L (3×10^5 cells) was placed in 1.5 mL microcentrifuge tubes and washed twice with PBS supplemented with 5% (v/v) FBS and placed in a final volume of 300 μ L PBS supplemented with 5% (v/v) FBS. Cells were analyzed using Accuri C6 flow cytometer. Gating parameters were selected for size of a single cell.

5.6 References

1. Mogensen, T. (2009) Pathogen recognition and inflammatory signaling in innate immune defenses. *Clin. Microbiol. Rev.* 22(2), 240-273.
2. Honda, K., Ohba, Y., Yanai, H., Negishi, H., Mizutani, T., Takaoka, A., Taya, C., Taniguchi, T. (2005) Spatiotemporal regulation of MyD88-IRF-7 signalling for robust type-I interferon induction. *Nature* 434, 1035–1040.
3. Xue, Q., Lu, Y., Eisele, M., Sulistijio, E., Khan, N., Fan, R., Miller-Jensen, K. (2015) Analysis of single-cell cytokine secretion reveals a role for paracrine signaling in coordinating macrophage responses to TLR4 stimulation. *Sci. Signal.* 8(381), ra59.
4. Lima, S., Miesenböck, G. (2005) Remote control of behavior through genetically targeted photostimulation of neurons. *Cell* 121, 141-152.
5. Mancini, R., Stutts, L., Moore, T., Esser-Kahn, A. (2015) Controlling the origins of inflammation with a photoactive lipopeptide immunopotentiator. *Angew.Chem. Int. Ed.* 54, 5962 –5965.
6. Stutts, L., Esser-Kahn, A.P. (2015) Directing the Immune System with Chemical Compounds. *ChemBiochem.* 16 (20), 1744–1748.
7. Ryu, K., Stutts, L., Tom, J., Mancini, R., Esser-Kahn, A. (2014) Stimulation of Innate Immune Cells by Light-Activated TLR7/8 Agonists. *J. Am. Chem.Soc.* 136, 10823–10825.
8. Mancini, R., Tom, J., Esser-Kahn, A. (2014) A Light-Controlled TLR4 Agonist and Selectable Activation of Cell Subpopulations *Angew. Chem. Int. Ed.* 53,189 –192.

9. Takano, A., Wang, Z., Choi, M., Yanai, H., Negishi, H., Ban, T., Taniguchi, T. (2007) DAI (DLM-1/ZBP1) is a cytosolic DNA sensor and an activator of innate immune response. *Nature* **2007** 448, 501–505.
10. Kennedy, M., Hughes, R., Peteya, L., Schwartz, J., Ehlers, M., Tucker, C. (2010) Rapid blue-light-mediated induction of protein interactions in living cells *Nat. Methods* 7, 973–975.
11. Konermann, S., Brigham, M., Trevino, A., Hsu, P., Heidenreich, M., Cong, L., Platt, R., Schott, D., Church, G., Zhang, F. (2013) Optical control of mammalian endogenous transcription and epigenetic states. *Nature* 500, 472–476.
12. Polstein, L., Gersbach, C. (2015) A light-inducible CRISPR/Cas9 system for control of endogenous gene activation. *Nat. Chem. Biol.* 11, 198–200.
13. Rebsamen, M., Heinz, L., Meylan, E., Michallet, M., Schroder, K., Hofmann, K., Vazquez, J., Benedict, C., Tschopp, J. (2009) DAI/ZBP1 recruits RIP1 and RIP3 through RIP homotypic interaction motifs to activate NF- κ B. *EMBO Rep.* 10(8), 916-922.
14. Fan, J., Cui, Z., Wei, H., Zhang, Z., Zhou, Y., Wang, Y. (2008) Split mCherry as a new red bimolecular fluorescence complementation system for visualizing protein-protein interactions in living cells. *Biochem. Biophys. Res. Commun* 367(1), 47-53.
15. Dull, T., Zufferey R., Kelly, M., Mandel, R.J., Nguyen, M., Trono, D., Naldini, L. (1998) A third-generation lentivirus vector with a conditional packaging system. *J. Virol.* 72(11), 8463–71.
16. Kennedy, M. J., Hughes, R.M., Peteya, L.A., Schwartz, J.W., Ehlers, M.D., Tucker, C.L. (2010) Rapid blue-light-mediated induction of protein interactions in living cells. *Nat. Methods* 7, 973–975.

17. Ai, H., Olenych, S., Wong, P., Davidson, M., Campbell, R. (2008) Hue-shifted monomeric variants of Clavulariacyan fluorescent protein: identification of the molecular determinants of color and applications in fluorescence imaging *BMC Biol.* 6(13), 1–13.
18. Chow, J., Franz, K., Kagan, J. (2015) PRRs are watching you: Localization of innate sensing and signaling regulators *J. Virology* 104-109.
19. Hoffmann, A., Baltimore, D. (2006) Circuitry of nuclear factor κ B signaling. *Immunological reviews* 171-186.

Appendix A: Chapter 2

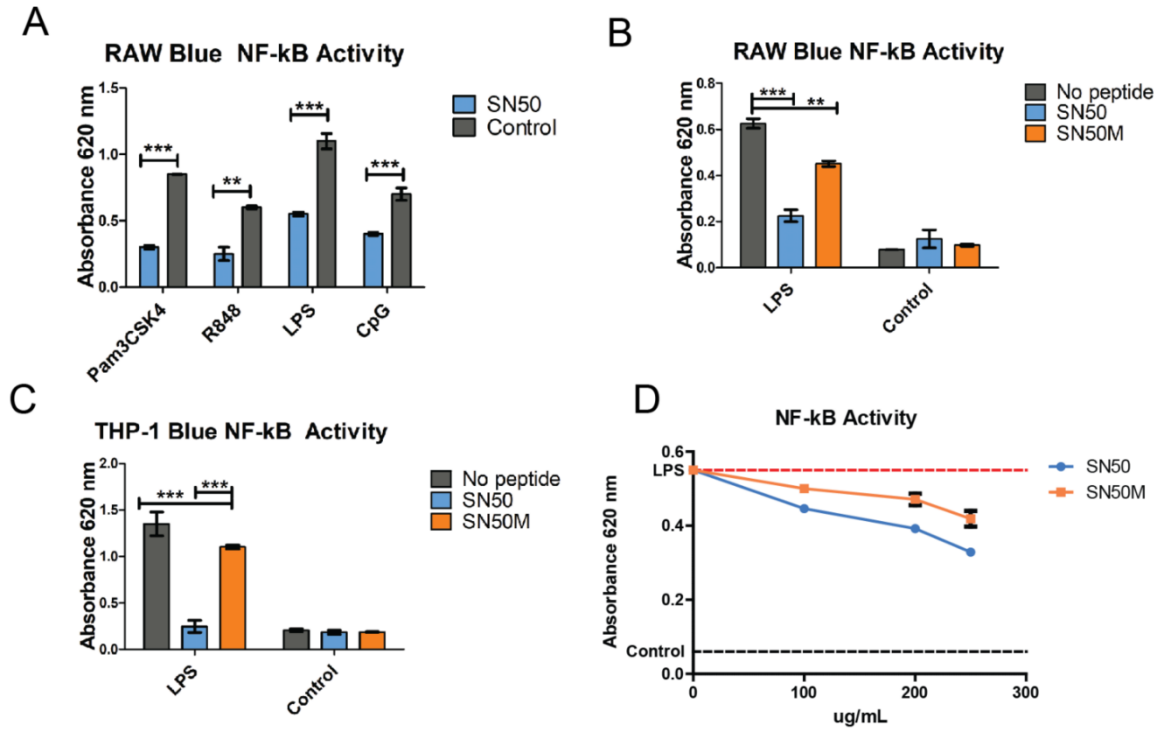


Figure A1. NF- κ B activity in mouse and human cells. (A) NF- κ B activity in RAW blue macrophages stimulated with various TLR agonists and SN50 (blue bars), TLR agonists alone (grey bars). (B) RAW blue NF- κ B activity of cells stimulated with SN50 (blue bars) and the control peptide SN50M (grey bars). (C) THP-1 NF- κ B activity of cells stimulated with no peptide (grey bars), SN50 (blue bars) or SN50M (orange bars). (D) Concentration screen of 100 ng/mL LPS and various concentrations of SN50 (blue line) and SN50M (orange line).

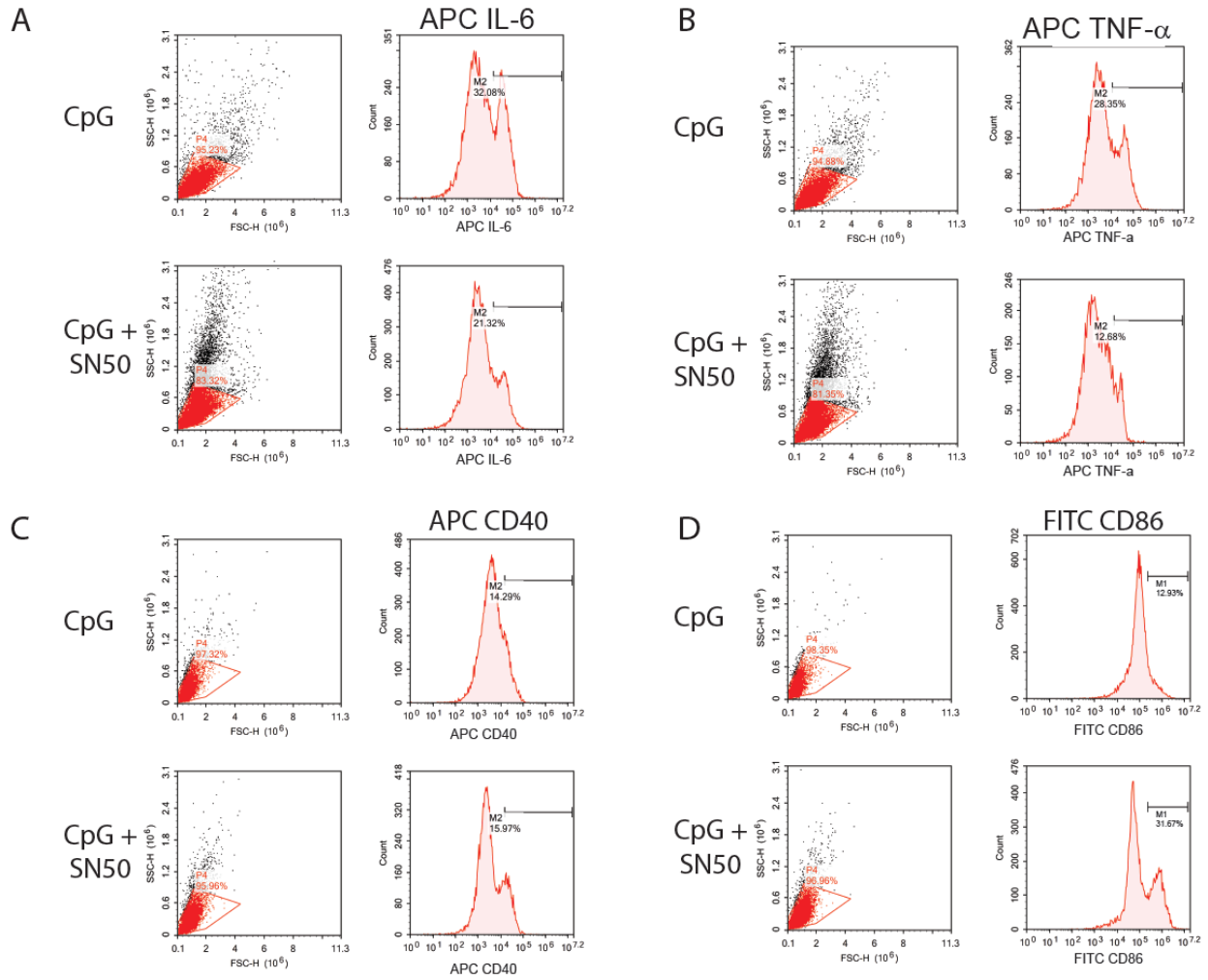


Figure A2. Gating strategy for BMDC flow cytometry. TNF- α (APC), IL-6 (APC), CD86 (FITC) and CD40 (PE).

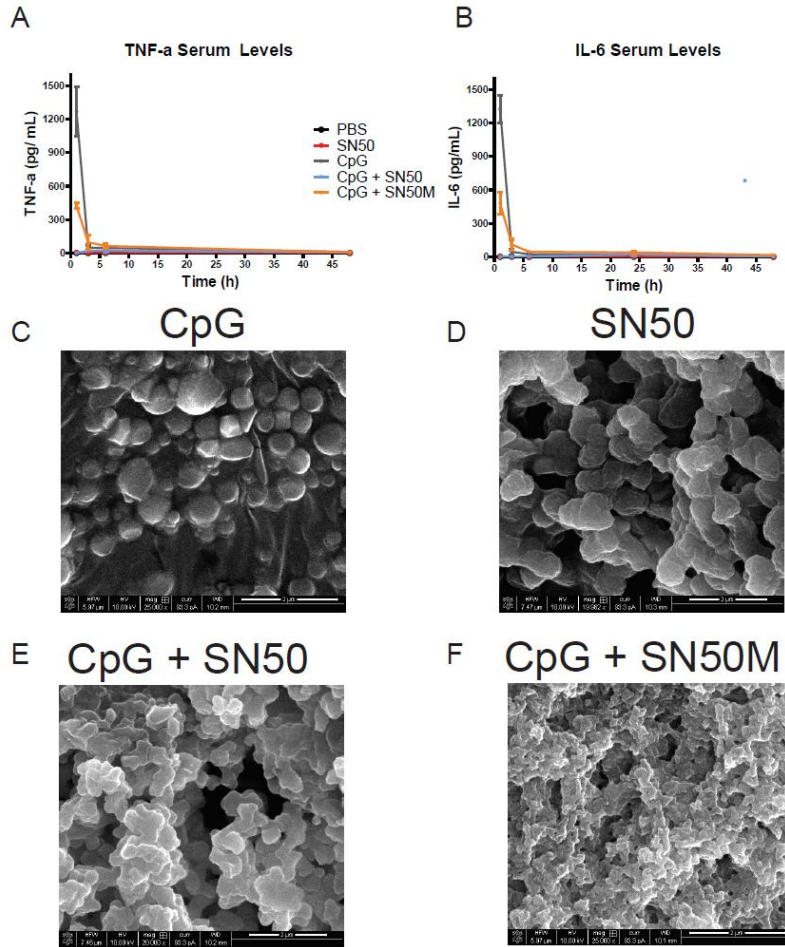


Figure A3. Proinflammatory Cytokine Analysis Time Course (A) Systemic TNF- α levels measured at 1h, 3h, 6h, 24, 48 h post vaccination. (B) Systemic IL-6 levels. (C-F) SEM image of OVA vaccinations. (C) CpG + OVA (D) SN50 + OVA (E) CpG + SN50 + OVA (F) CpG + SN50M + OVA. Scale bar 2 μ m.

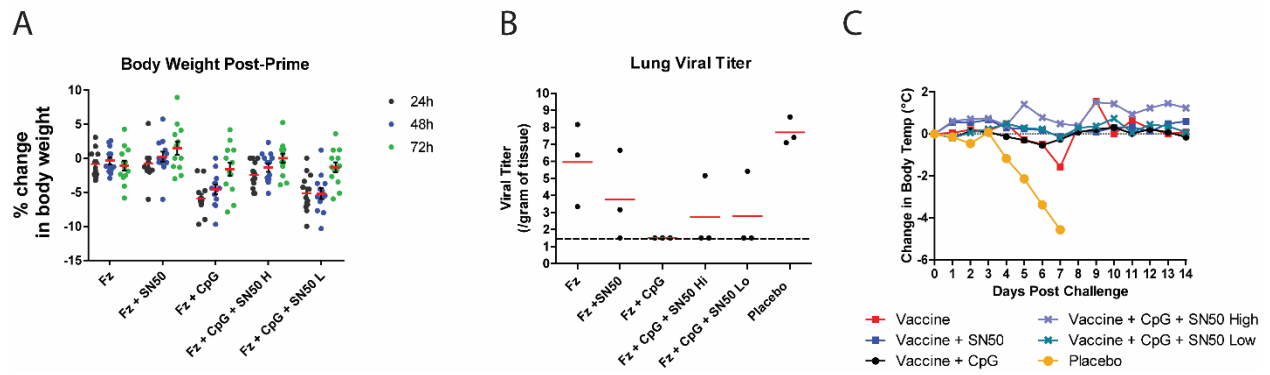
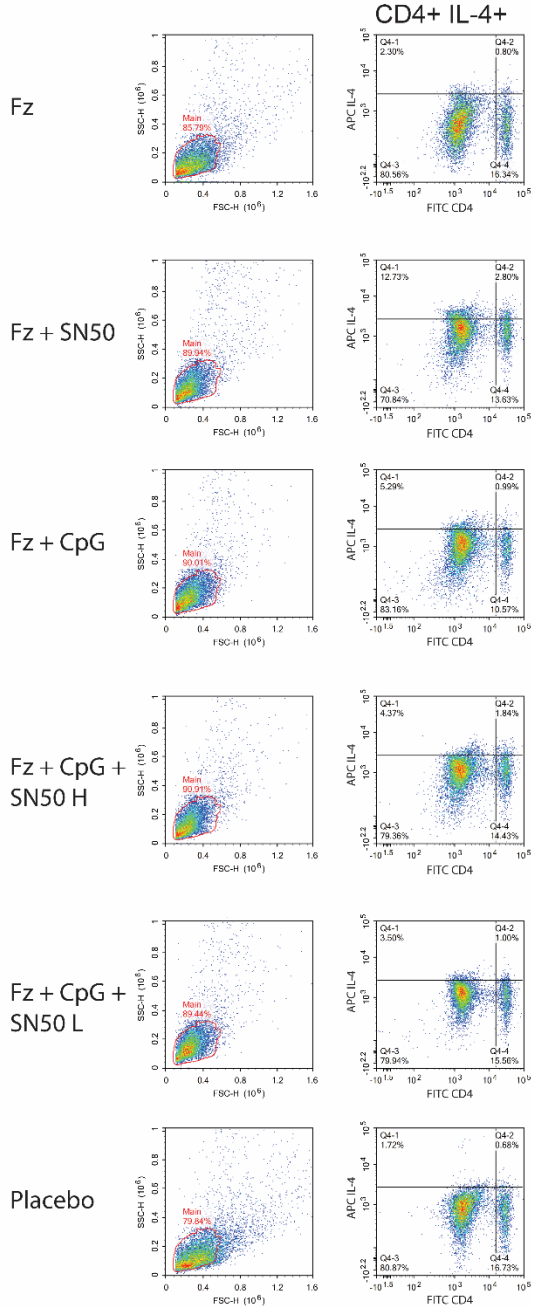


Figure A4. Weight Loss Post-Vaccination. (A) Weight loss 24h (black dot), 48h (blue dot) and 72h (green dot) post prime. Fz = Fluzone 2017-2018 flu vaccine. (B) Lung viral titer d3 post-infection. (C) Full temperature curve for 14 days post-challenge. Fz (black line), Fz + SN50 (blue line), Fz + CpG (grey line), Fz + CpG + SN50 Hi (red line), Fz + CpG + SN50 Lo (purple line), Placebo (yellow line).

A



B

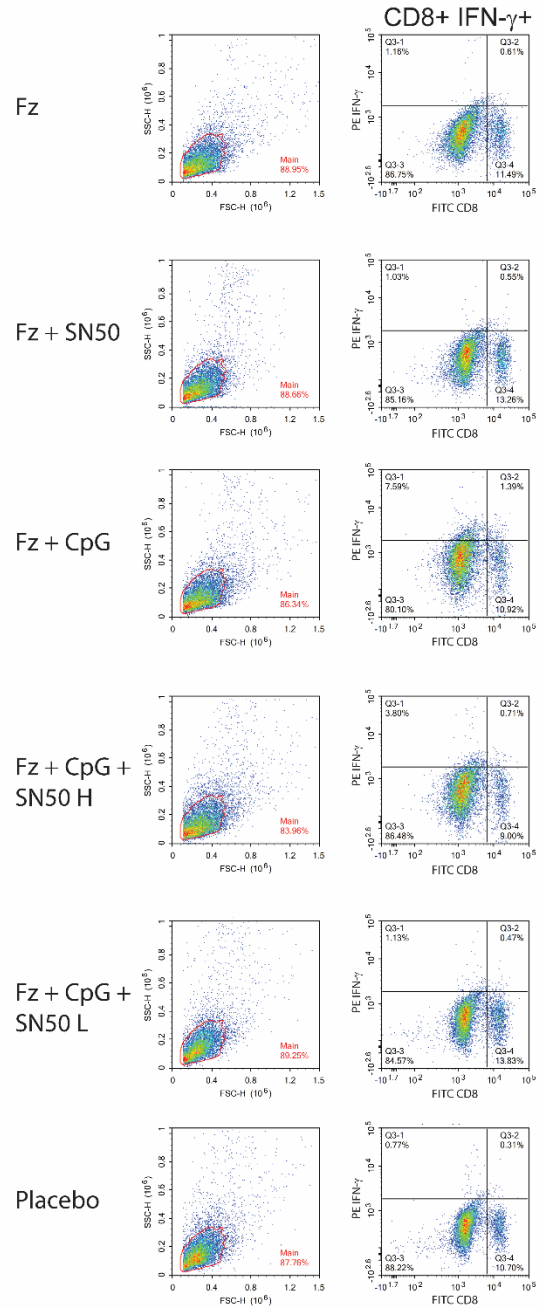


Figure A5. Gating strategy for antigen specific splenocyte assay. (A) CD4+ IL-4+ cells (B) CD8+ IFN- γ + cells.

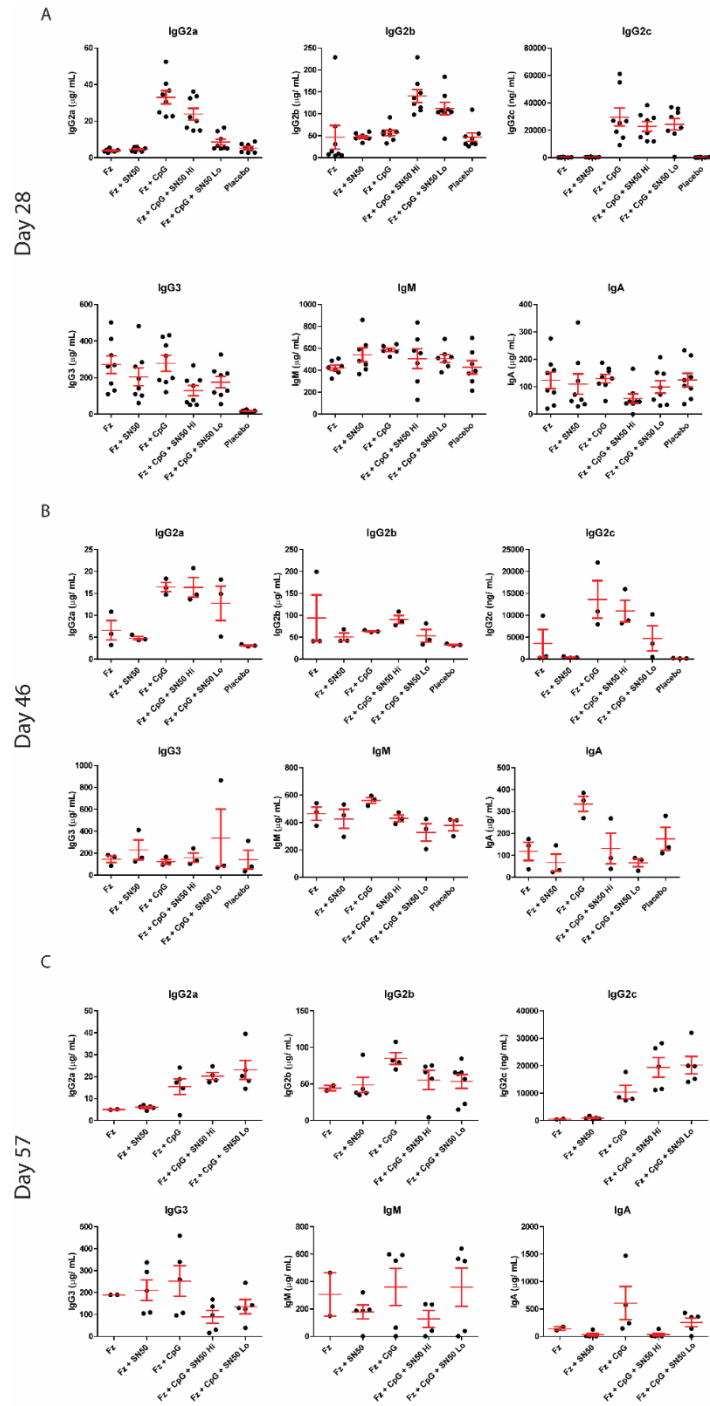


Figure A6. Serum IgG2a, IgG2b, IgG3, IgM, IgA Antibody concentrations at (A) day 28 post-vaccination, n=8. (B) Day 46 (d3 post infection) n=3. (C) Day 57 (d14 post infection) Fz (n= 2), Fz + SN50 (n=5), Fz + CpG (n=5), Fz + CpG + SN50 Hi (n=5), Fz + CpG + SN50 Lo (n=5). Fz = Fluzone 2017-2018 flu vaccine.

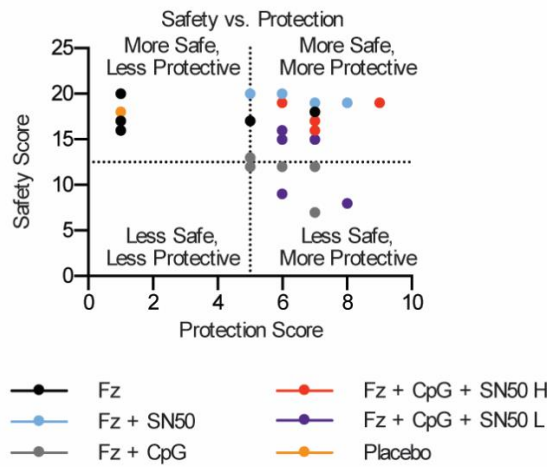


Figure A7. Safety vs. Protection score

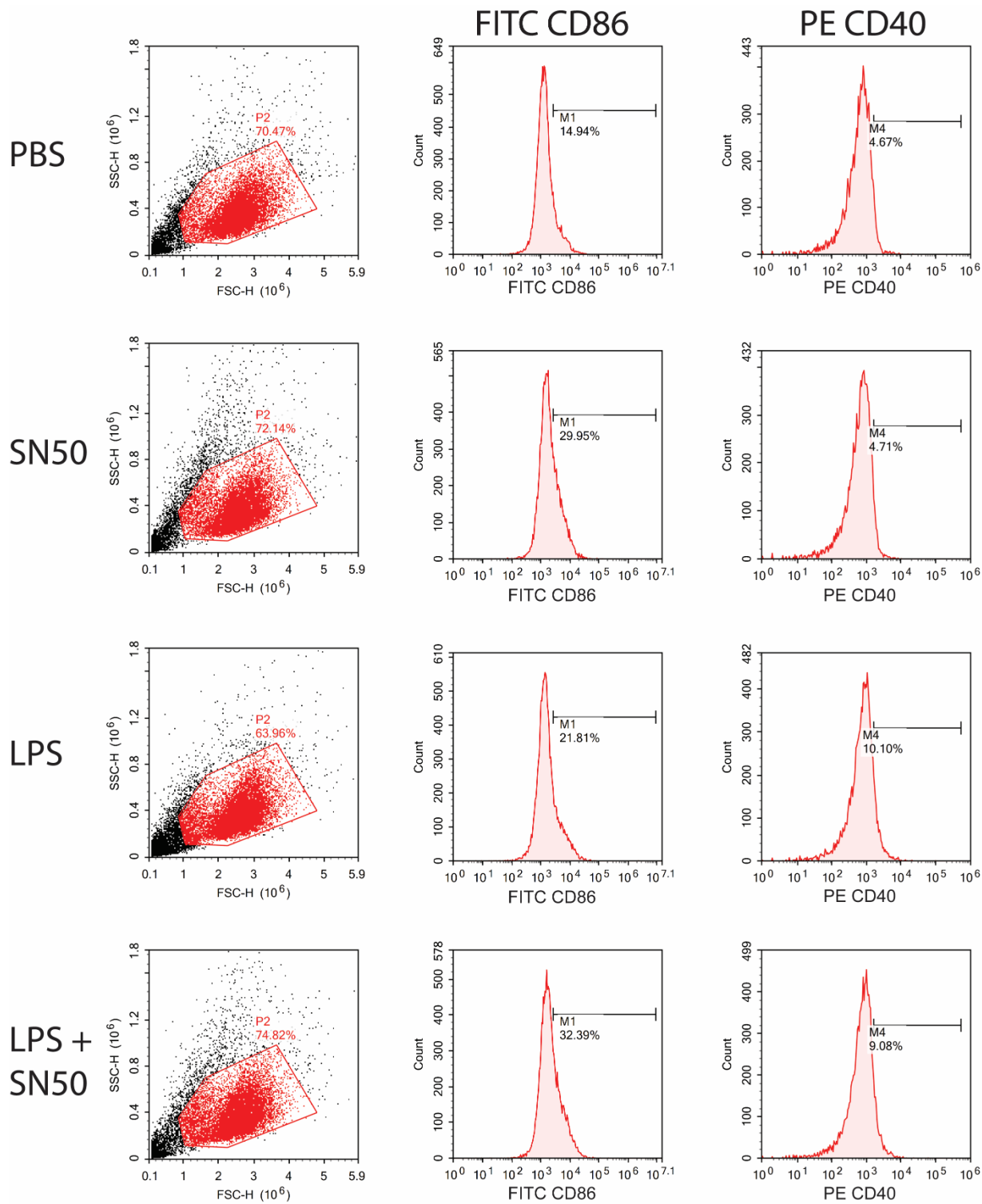


Figure A8. Gating strategy for THP-1 cell surface staining CD86 (FITC), CD40 (PE).

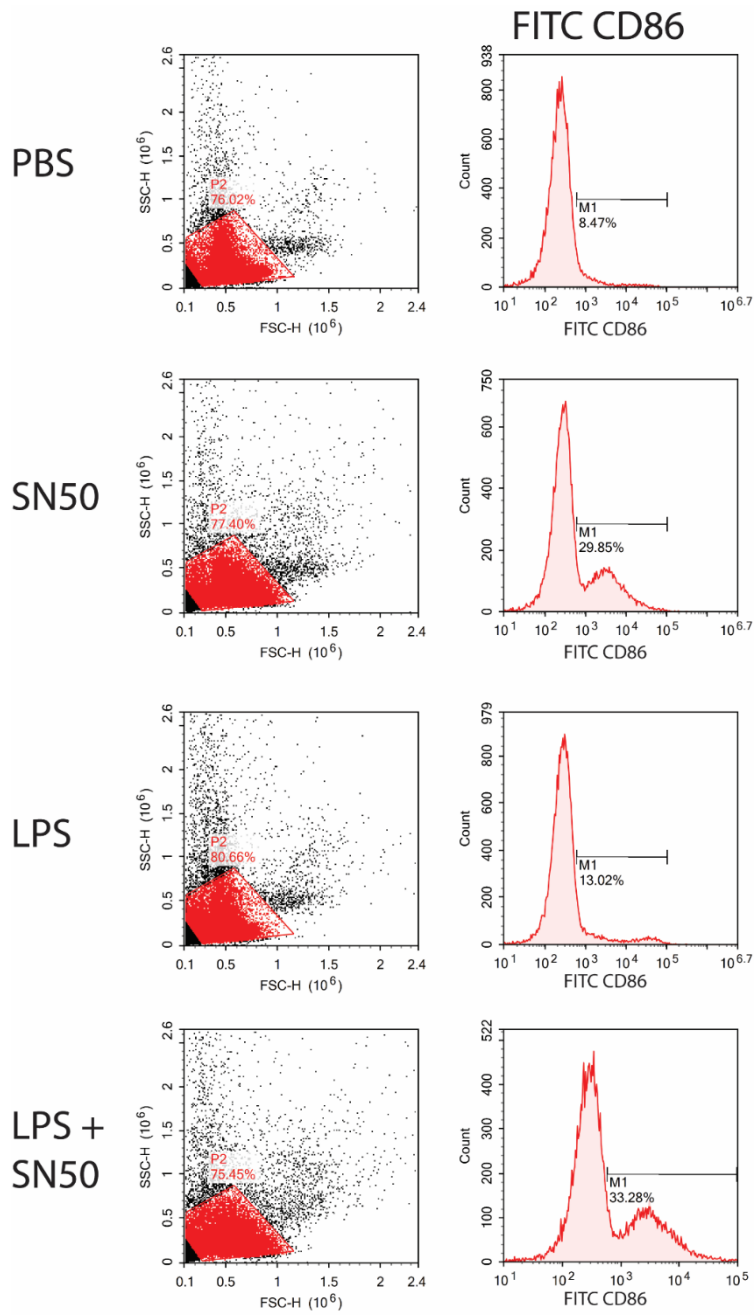


Figure A9. Gating strategy for NHP PBMC cell surface staining, CD86 (FITC).

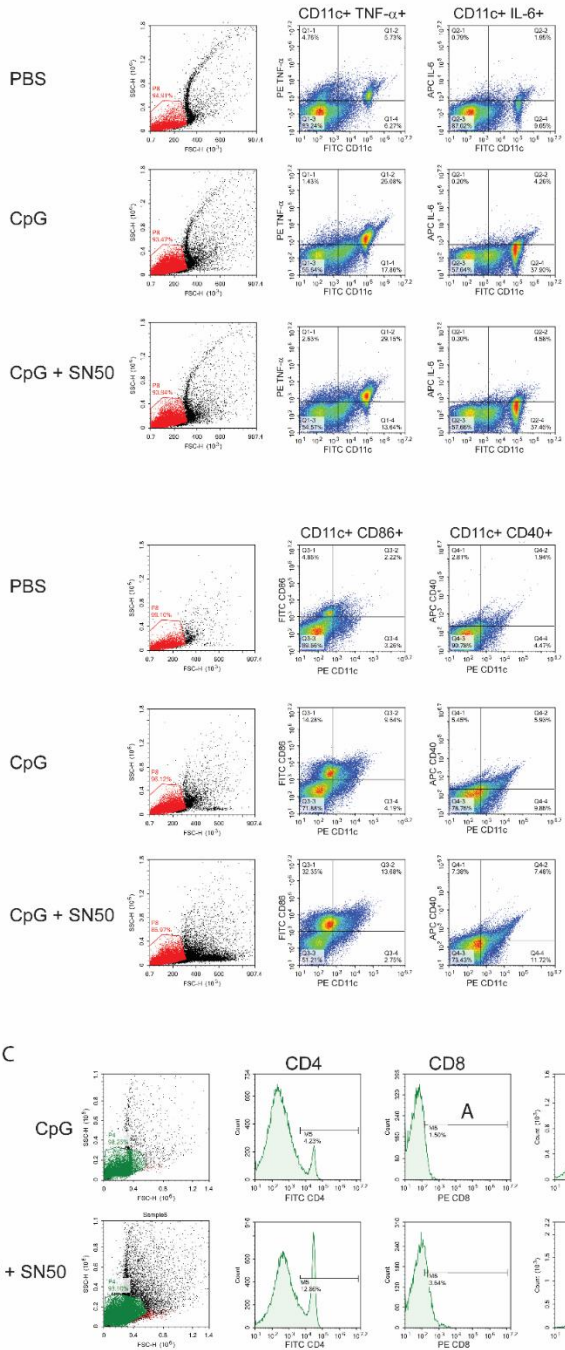


Figure A10. Lymph node flow cytometry gating strategy. (A) Lymph node 24h CD11c+ TNF- α + and CD11c+ IL-6+ gating strategy. (B) Lymph node 24h CD11c+ CD86+ and CD11c+ CD40+ gating strategy. (C) Lymph node d10 CD4+, CD8+ and B220+ gating strategy.

Appendix B: Chapter 3

BM5

^1H NMR (400 MHz, CDCl_3) δ 7.29 (dtd, $J = 8.2, 7.2, 3.8$ Hz, 4H), 7.09 – 6.99 (m, 2H), 6.95 (d, $J = 8.2$ Hz, 2H), 5.92 (ddt, $J = 17.3, 10.6, 4.8$ Hz, 2H), 5.22 (ddd, $J = 17.3, 3.5, 1.8$ Hz, 4H), 5.13 (ddd, $J = 10.6, 3.2, 1.6$ Hz, 4H), 4.51 (dt, $J = 4.6, 1.7$ Hz, 4H).

BM8

^1H NMR (400 MHz, CDCl_3) δ 7.38 – 7.22 (m, 4H), 6.87 (t, $J = 10.0$ Hz, 2H), 6.06 (ddt, $J = 16.5, 10.1, 6.3$ Hz, 2H), 5.28 – 5.12 (m, 4H), 3.47 (d, $J = 6.3$ Hz, 4H).

BM1

^1H NMR (400 MHz, CDCl_3) δ 7.54 (ddt, $J = 11.8, 5.2, 2.2$ Hz, 4H), 7.46 – 7.37 (m, 2H), 7.34 – 7.28 (m, 1H), 7.04 – 6.96 (m, 2H), 6.09 (ddt, $J = 17.2, 10.5, 5.3$ Hz, 1H), 5.45 (dq, $J = 17.3, 1.6$ Hz, 1H), 5.31 (dq, $J = 10.5, 1.4$ Hz, 1H), 4.59 (dt, $J = 5.3, 1.5$ Hz, 2H).

BM3

^1H NMR (400 MHz, CDCl_3) δ 7.58 (dq, $J = 2.6, 1.7$ Hz, 2H), 7.48 – 7.38 (m, 2H), 7.38 – 7.27 (m, 3H), 7.09 – 7.02 (m, 1H), 6.99 (dd, $J = 8.2, 0.8$ Hz, 1H), 6.00 (ddt, $J = 17.3, 10.6, 4.8$ Hz, 1H), 5.34 (dq, $J = 17.3, 1.7$ Hz, 1H), 5.21 (dq, $J = 10.6, 1.6$ Hz, 1H), 4.55 (dt, $J = 4.8, 1.7$ Hz, 2H).

BM6

^1H NMR (400 MHz, CDCl_3) δ 7.49 – 7.44 (m, 4H), 7.03 – 6.90 (m, 4H), 6.08 (ddt, $J = 17.2, 10.6, 5.3$ Hz, 2H), 5.44 (dq, $J = 17.3, 1.6$ Hz, 2H), 5.30 (dq, $J = 10.5, 1.4$ Hz, 2H), 4.57 (dt, $J = 5.3, 1.5$ Hz, 4H).

BM14

^1H NMR (400 MHz, CDCl_3) δ 7.56 – 7.48 (m, 2H), 7.32 (t, $J = 7.9$ Hz, 1H), 7.14 (ddd, $J = 7.7, 1.6, 0.9$ Hz, 1H), 7.12 – 7.09 (m, 1H), 7.02 – 6.94 (m, 2H), 6.86 (ddd, $J = 8.2, 2.6, 0.9$ Hz, 1H), 6.21 – 6.02 (m, 2H), 5.44 (ddd, $J = 17.3, 3.1, 1.5$ Hz, 2H), 5.34 – 5.26 (m, 2H), 4.64 – 4.55 (m, 4H).

BM30A

^1H NMR (400 MHz, CDCl_3) δ 7.54 – 7.44 (m, 5H), 7.43 – 7.35 (m, 1H), 7.14 (ddd, $J = 9.3, 4.6, 1.1$ Hz, 2H), 6.95 (t, $J = 7.5$ Hz, 1H), 6.07 (ddt, $J = 16.6, 10.0, 6.6$ Hz, 1H), 5.14 (qdd, $J = 3.2, 2.6, 1.5$ Hz, 2H), 3.48 (d, $J = 6.6$ Hz, 2H).

BM30B

^1H NMR (400 MHz, CDCl_3) δ 7.54 – 7.44 (m, 5H), 7.39 (ddd, $J = 8.7, 5.4, 2.1$ Hz, 1H), 7.08 (dt, $J = 6.3, 2.0$ Hz, 2H), 6.92 (d, $J = 8.1$ Hz, 1H), 5.97 (ddt, $J = 16.8, 10.0, 6.7$ Hz, 1H), 5.15 – 4.98 (m, 2H), 3.36 (d, $J = 6.7$ Hz, 2H).

Appendix C: Chapter 4

PS Coat

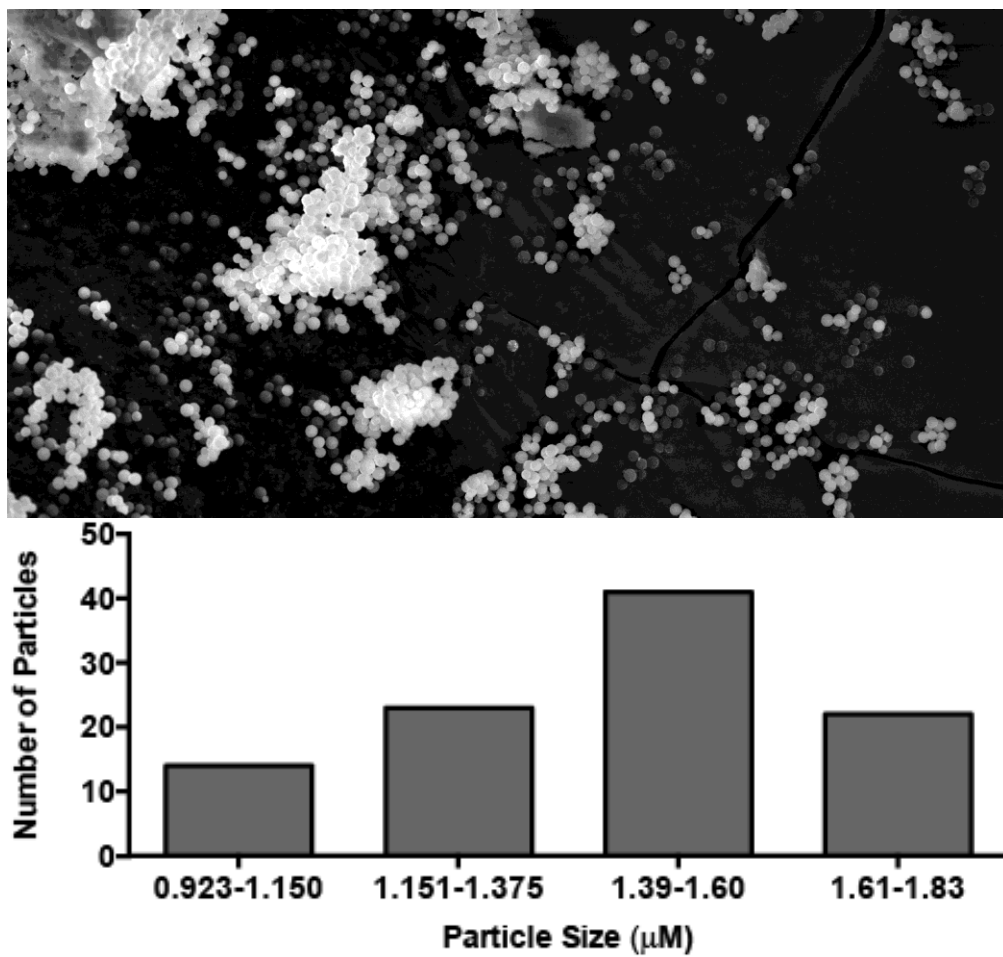


Figure C1. SEM image of coated PS particle 1,677x with histogram of particle size distribution.

PS Coat continued

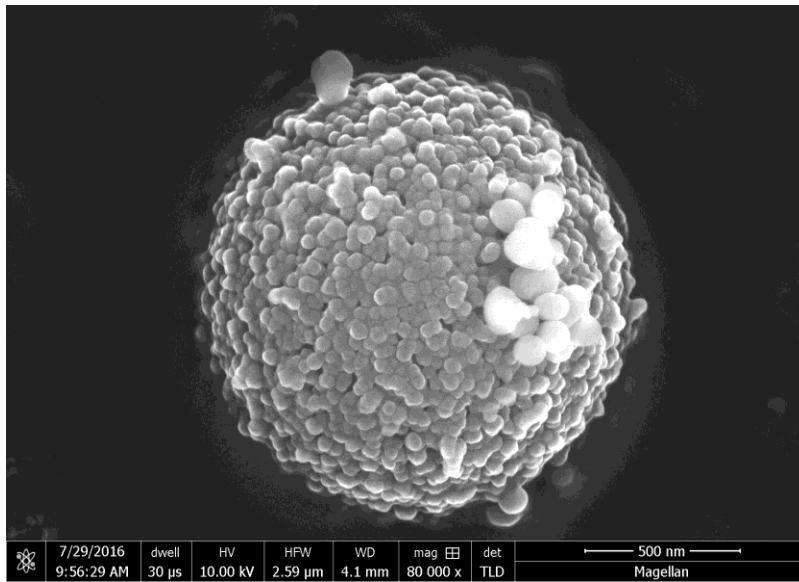


Figure C2. SEM image of coated PS particle 80,000x.

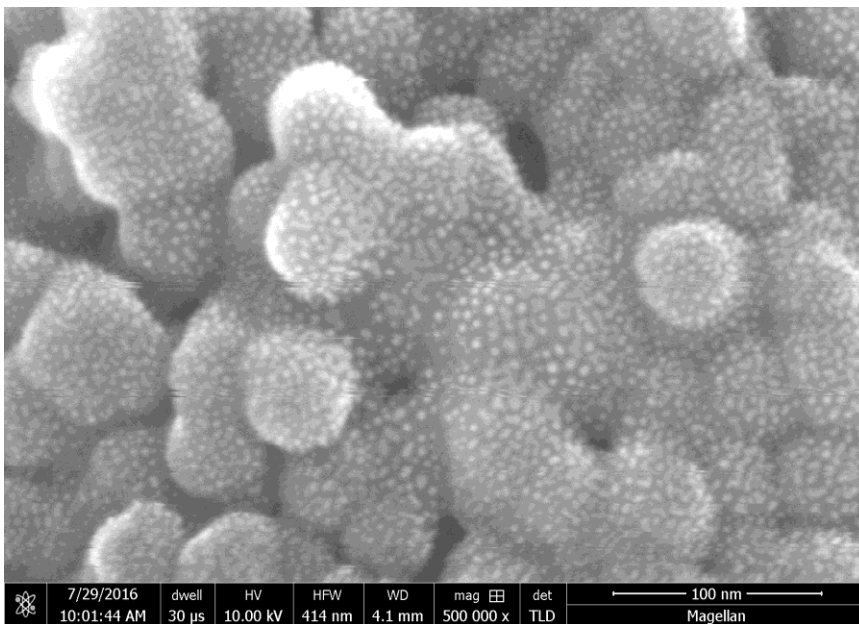


Figure C3. SEM image of coated PS particle 500,000x.

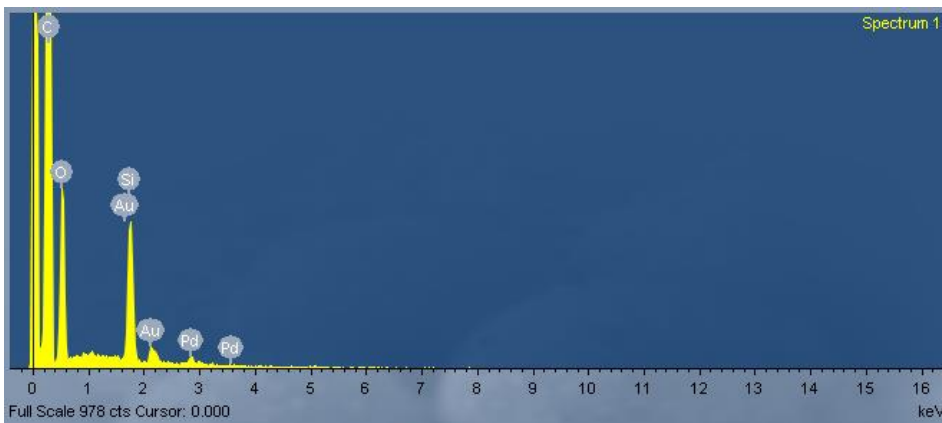


Figure C4. EDS data of coated PS particles sputtered with Au/Pd.

PS

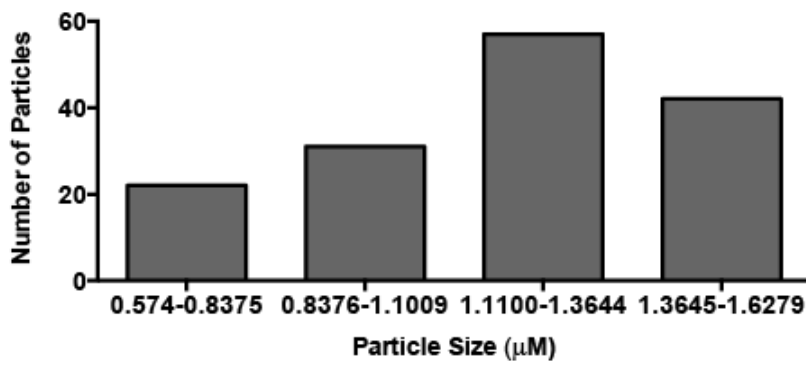
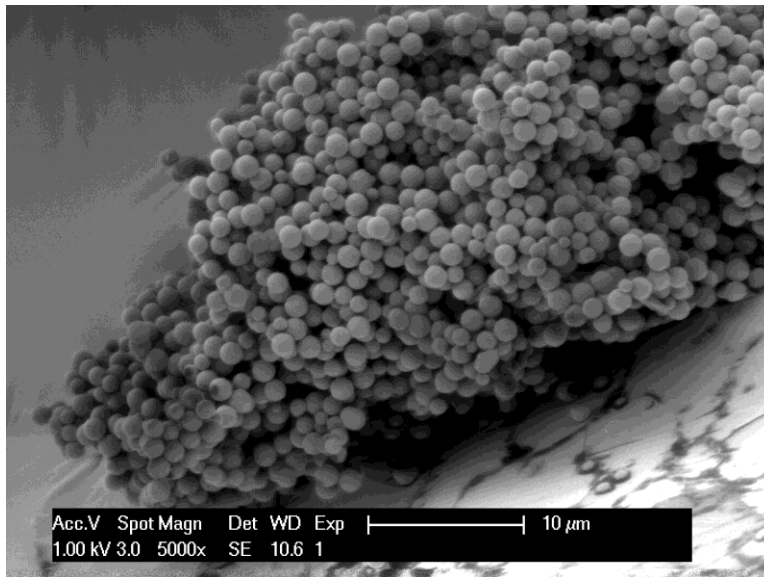


Figure C5. SEM image of PS particle 5,000x with histogram of particle size distribution.

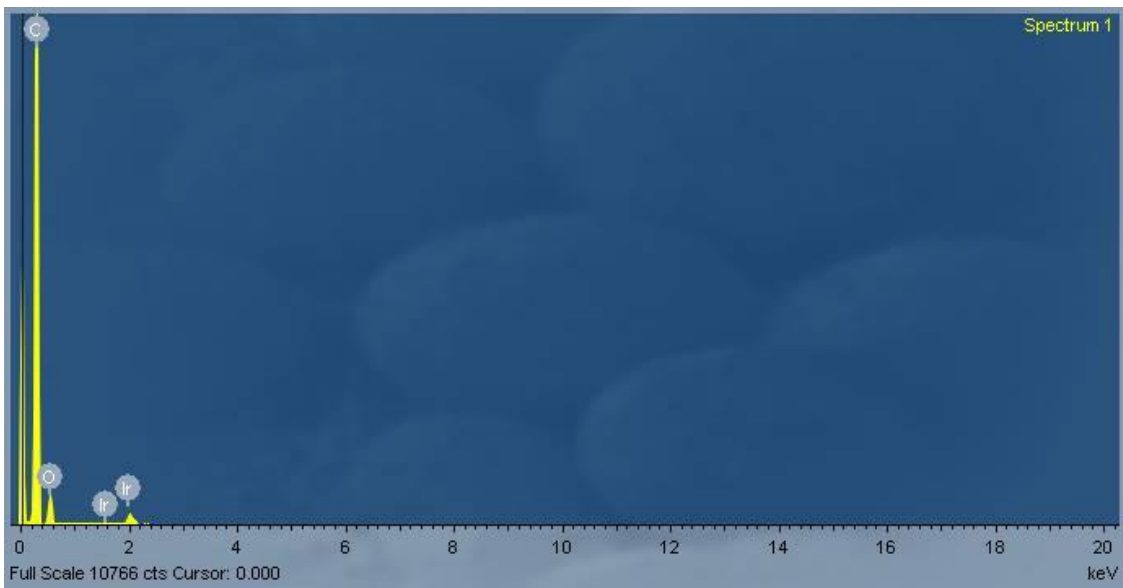


Figure C6. EDS data of PS particles sputtered with Ir.

PMMA Coat

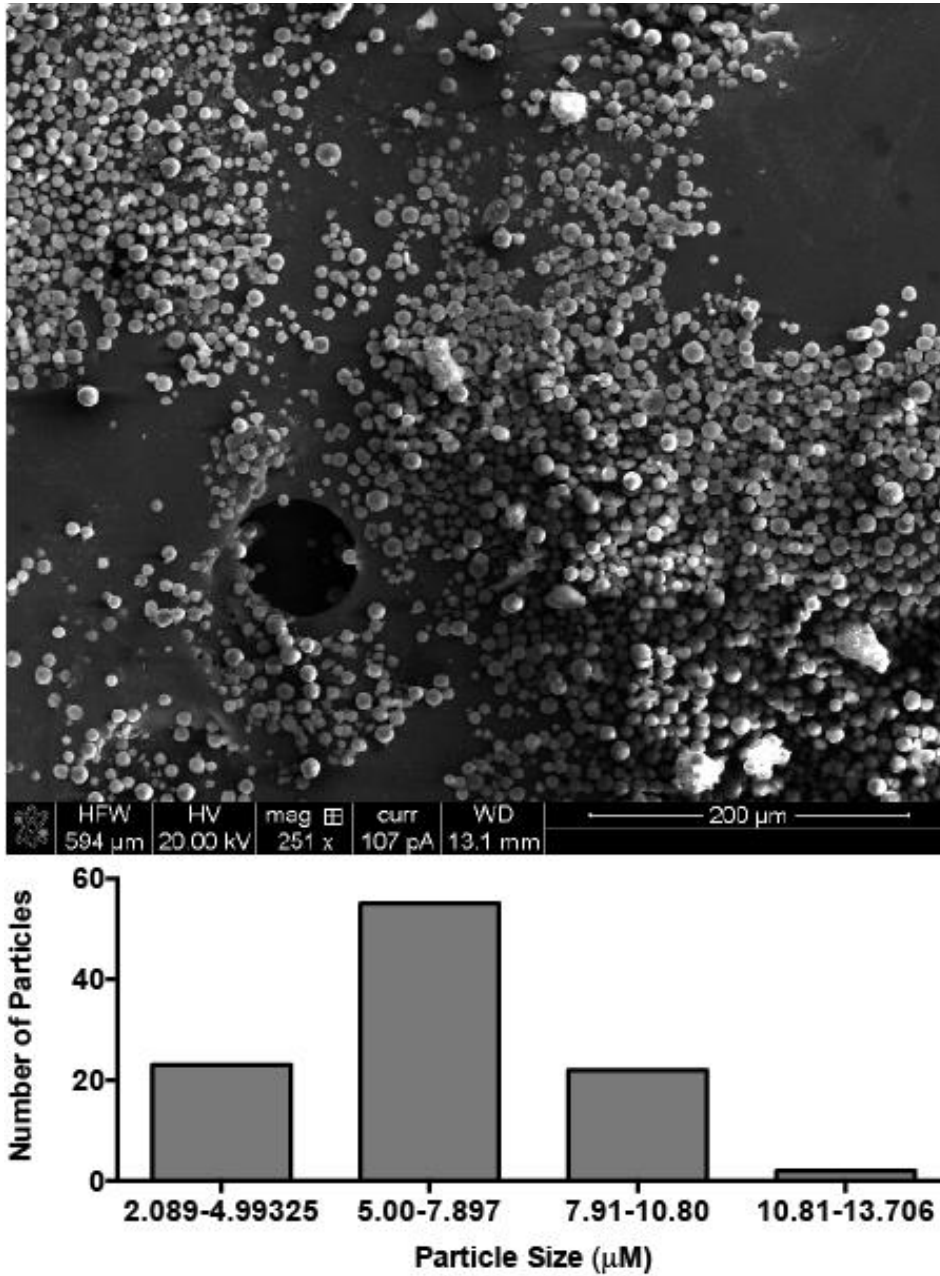


Figure C7. SEM image of coated PMMA particle 251x with histogram of particle size distribution.

PMMA Coat continued

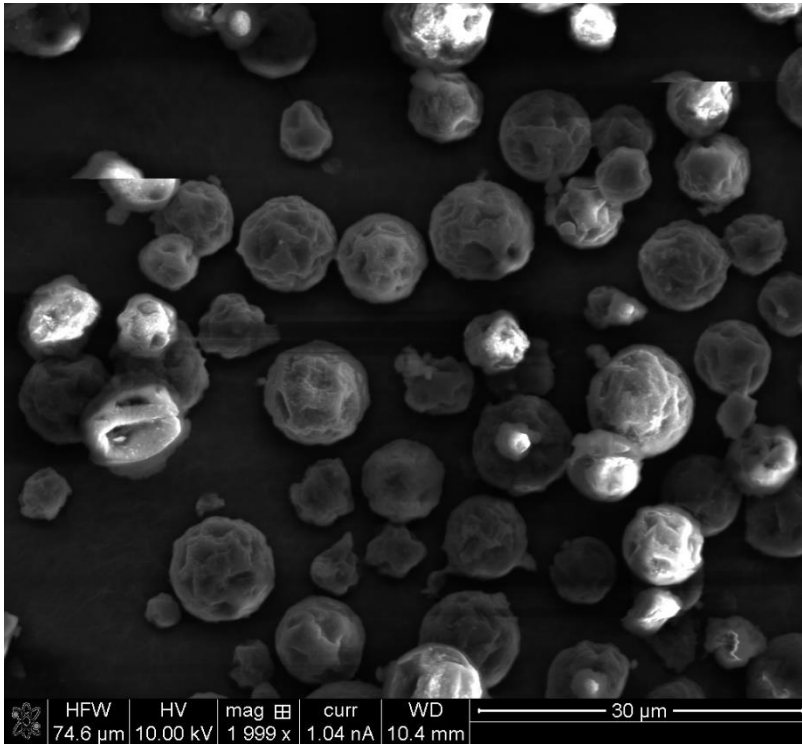


Figure C8. SEM image of coated PMMA particle 1,999x.

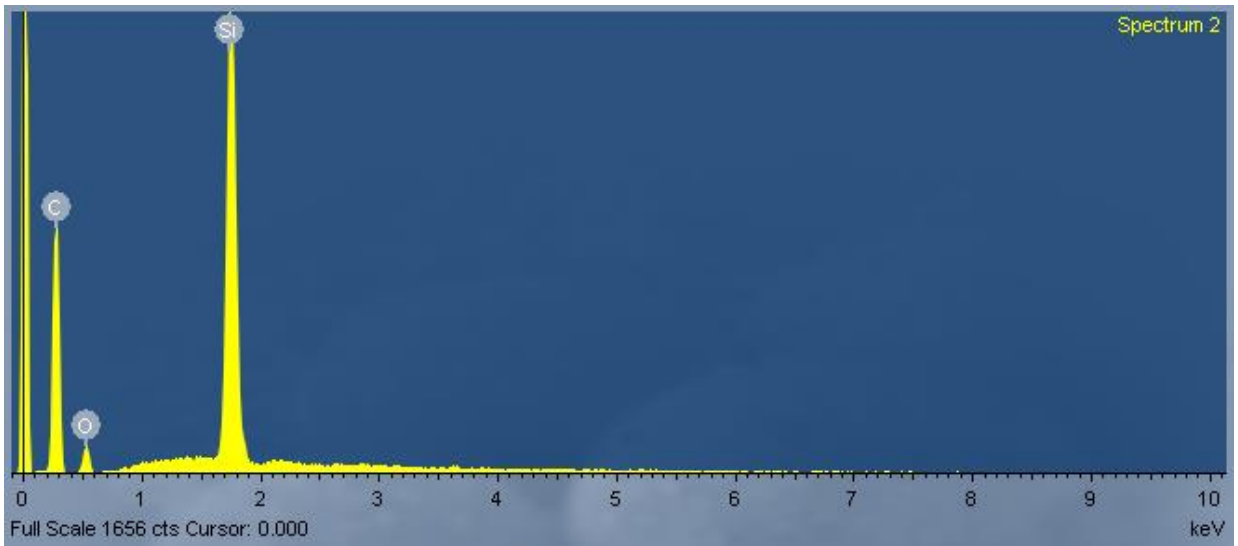


Figure C9. EDS data for coated PMMA particles.

PMMA

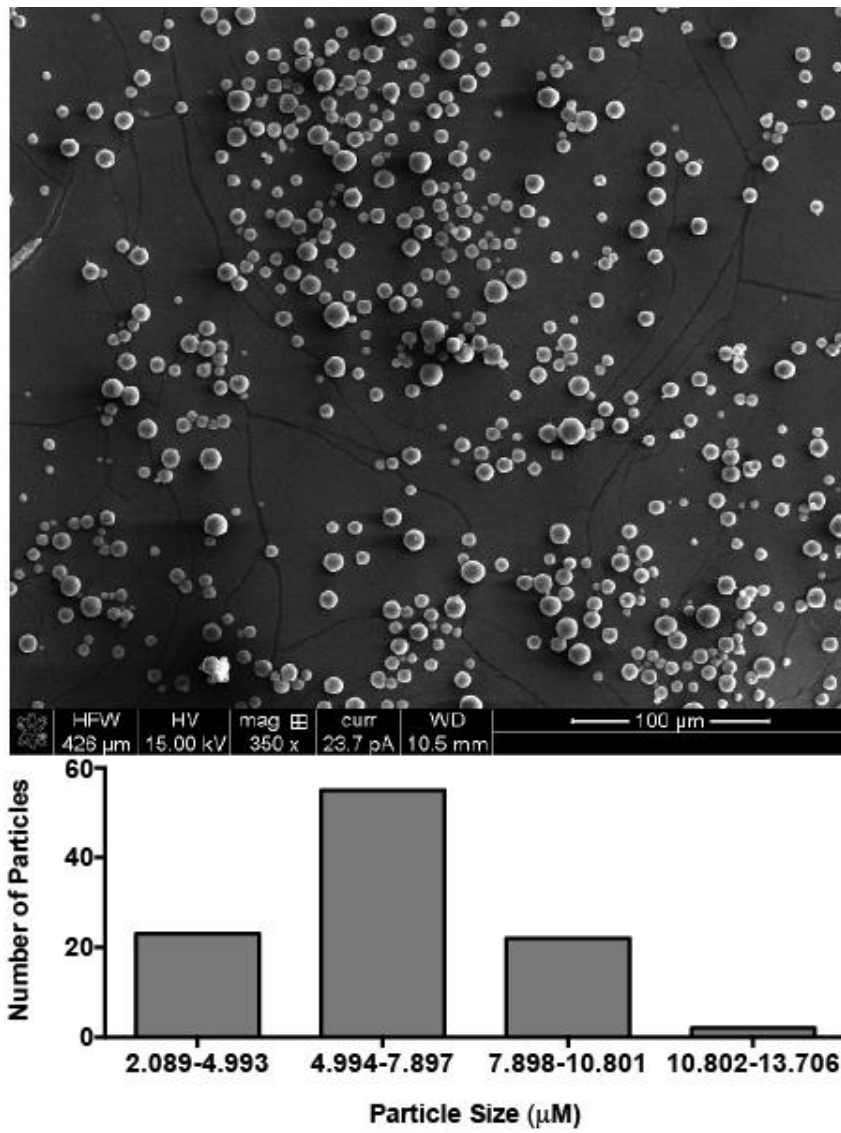


Figure C10. SEM image of PMMA particle 350x with histogram of particle size distribution.

PMMA continued

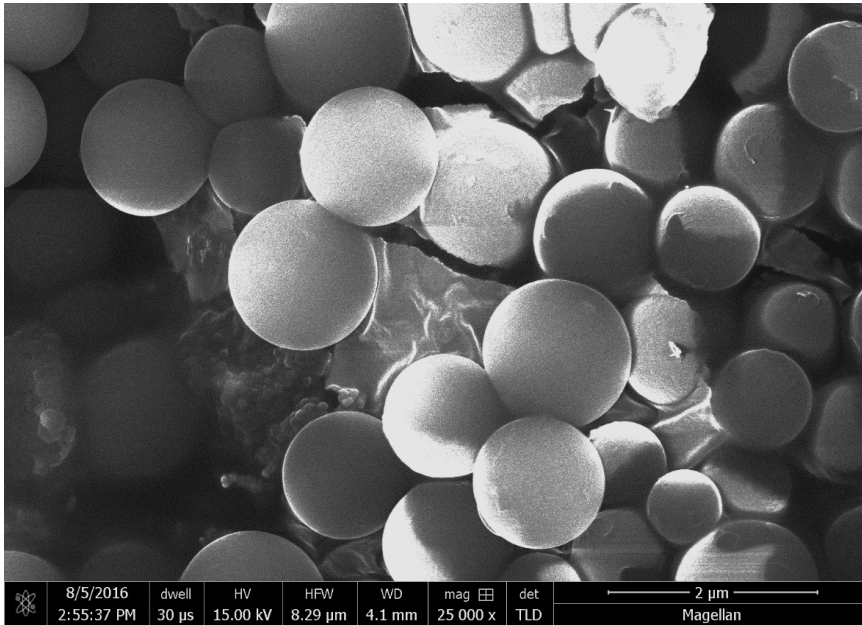


Figure C11. SEM image of PMMA particle 25,000x.

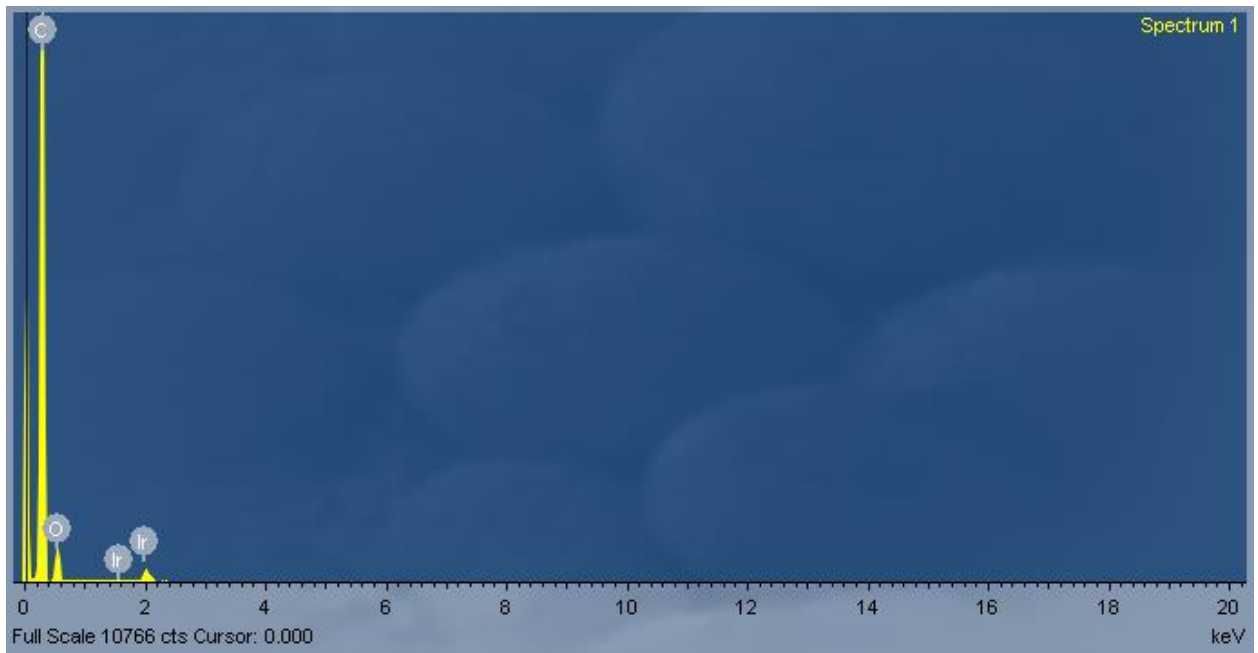


Figure C12. EDS data of PMMA particles sputtered with Ir.

PLGA Coat

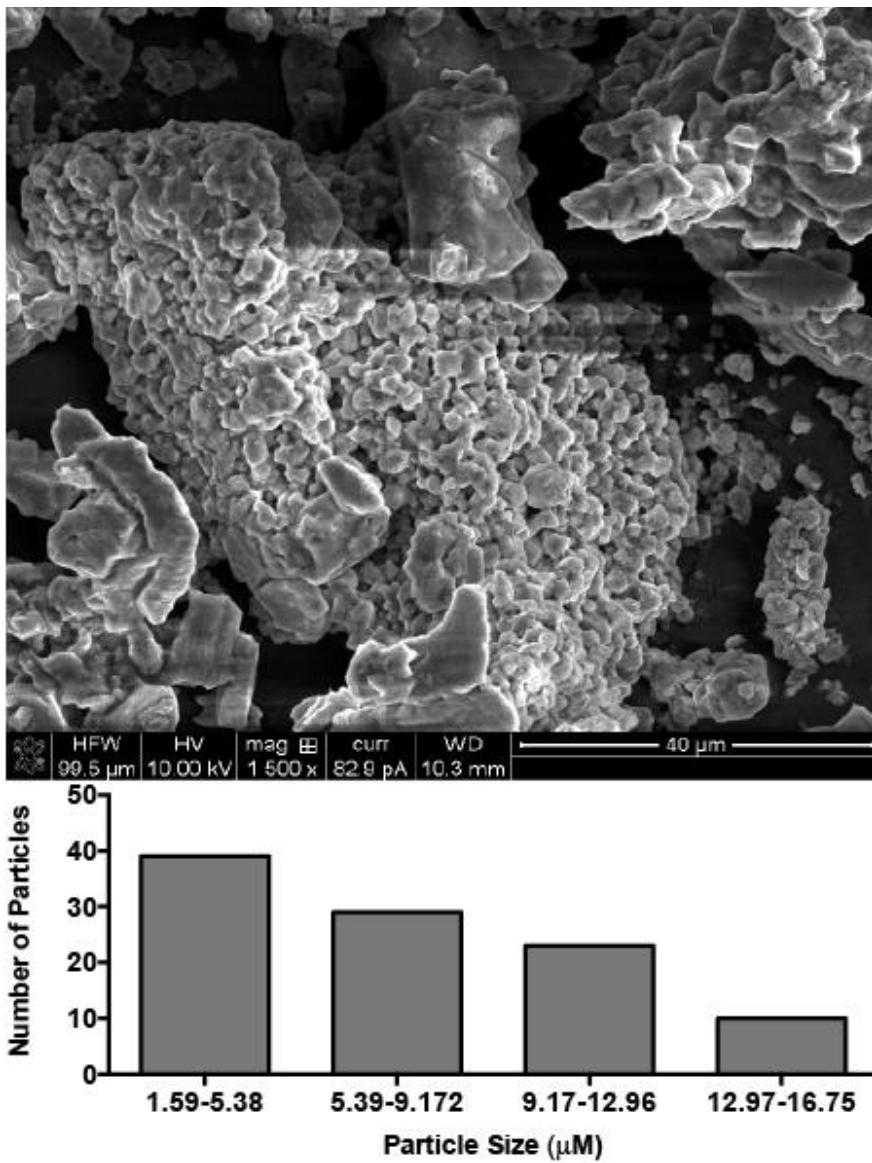


Figure C13. SEM image of coated PLGA particle 1,500x with histogram of particle size distribution.

PLGA Coat continued

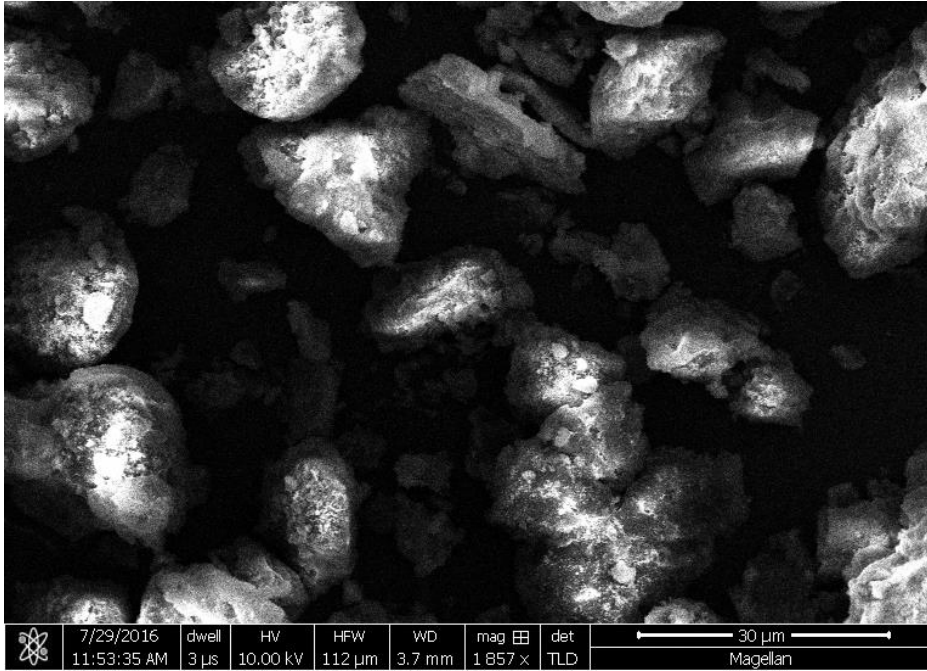


Figure C14. SEM image of coated PLGA particles 1,857x.

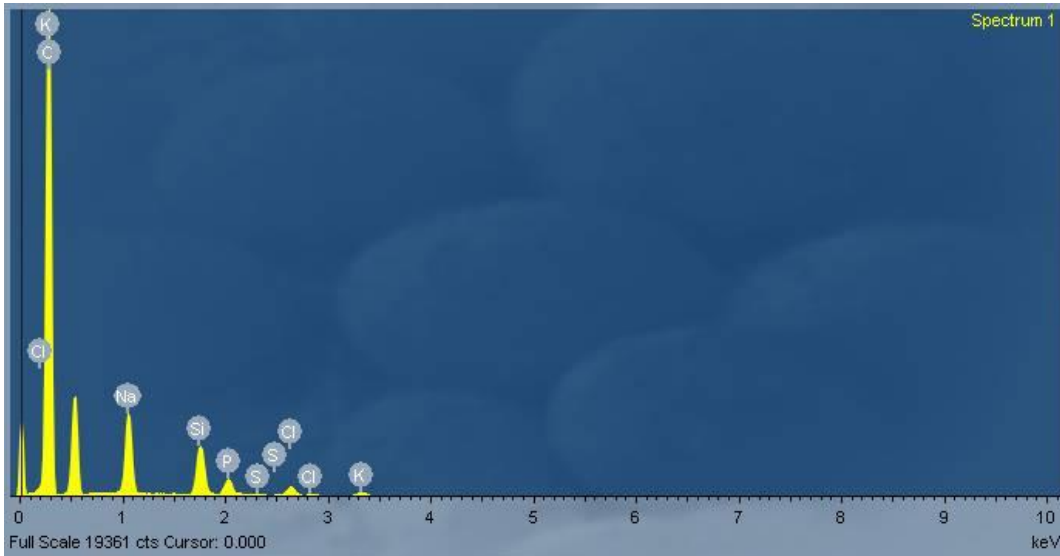


Figure C15. EDS data of coated PLGA particles prepared in a solution of PBS.

PLGA

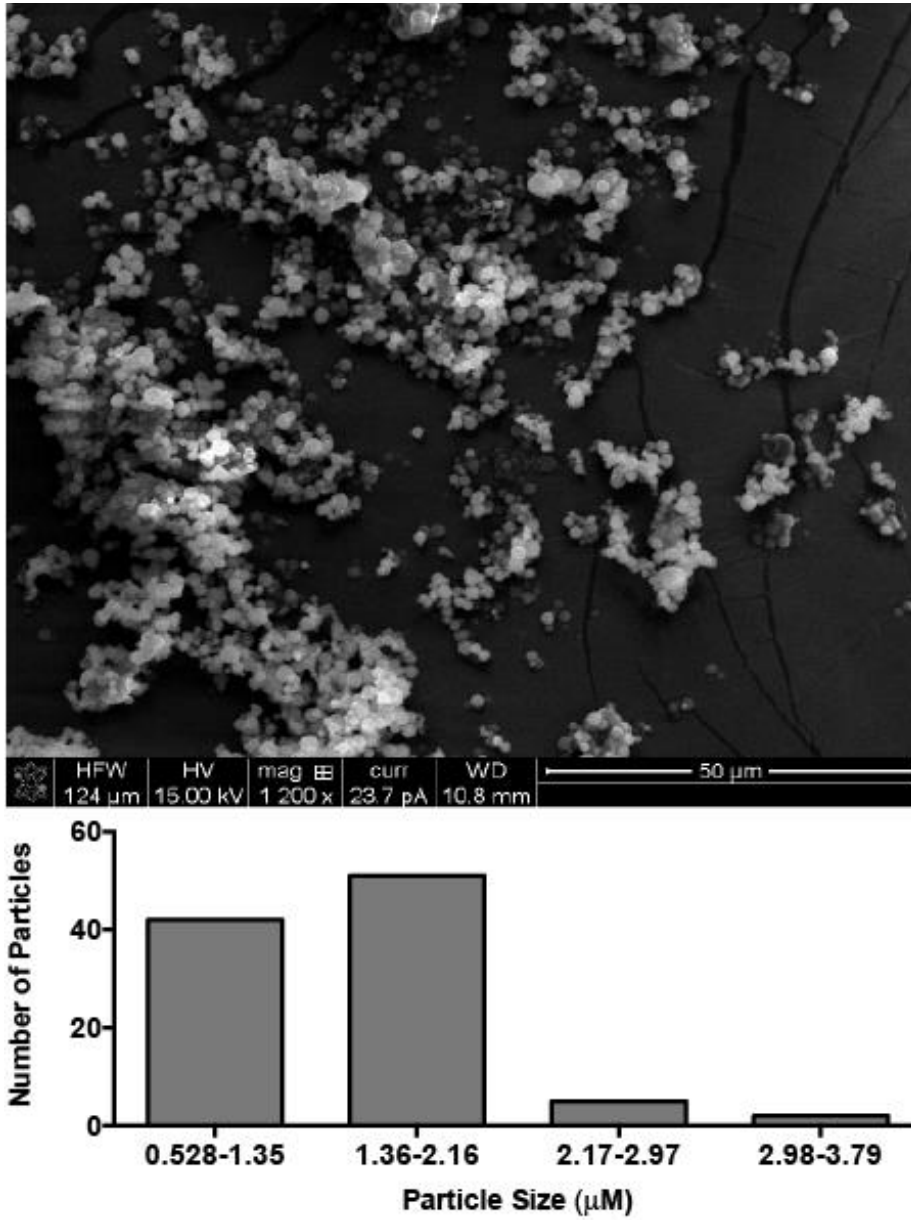


Figure C16. SEM image of PLGA particle 1,200x with histogram of particle size distribution.

PLGA coat continued

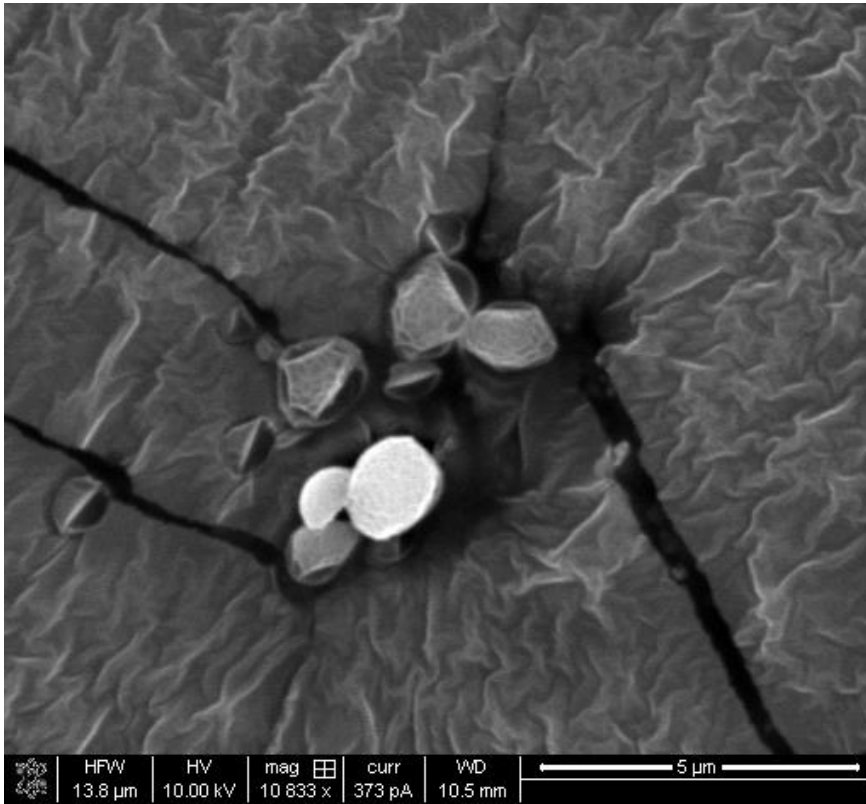


Figure C17. SEM image of PLGA particles 10,833x.

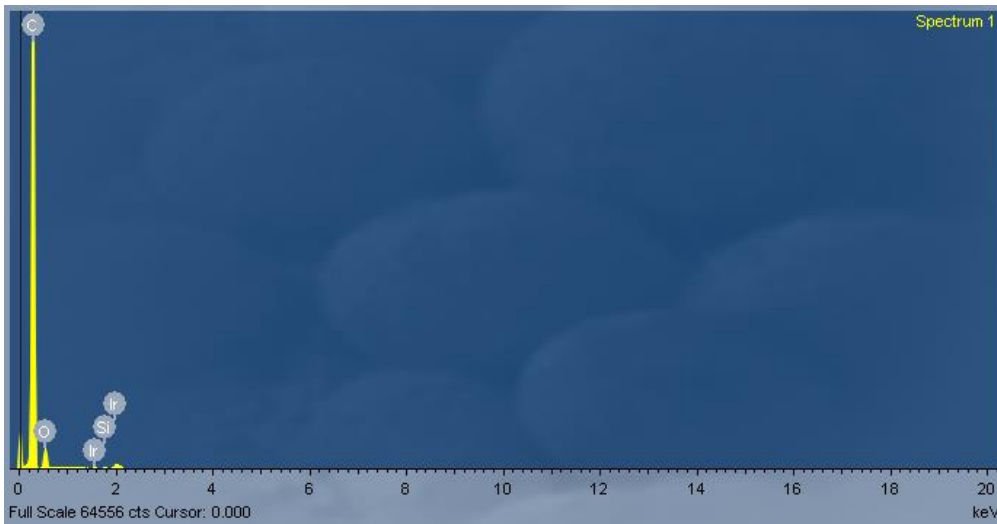


Figure C18. EDS data of PLGA particles sputtered with Ir.

PE Coat

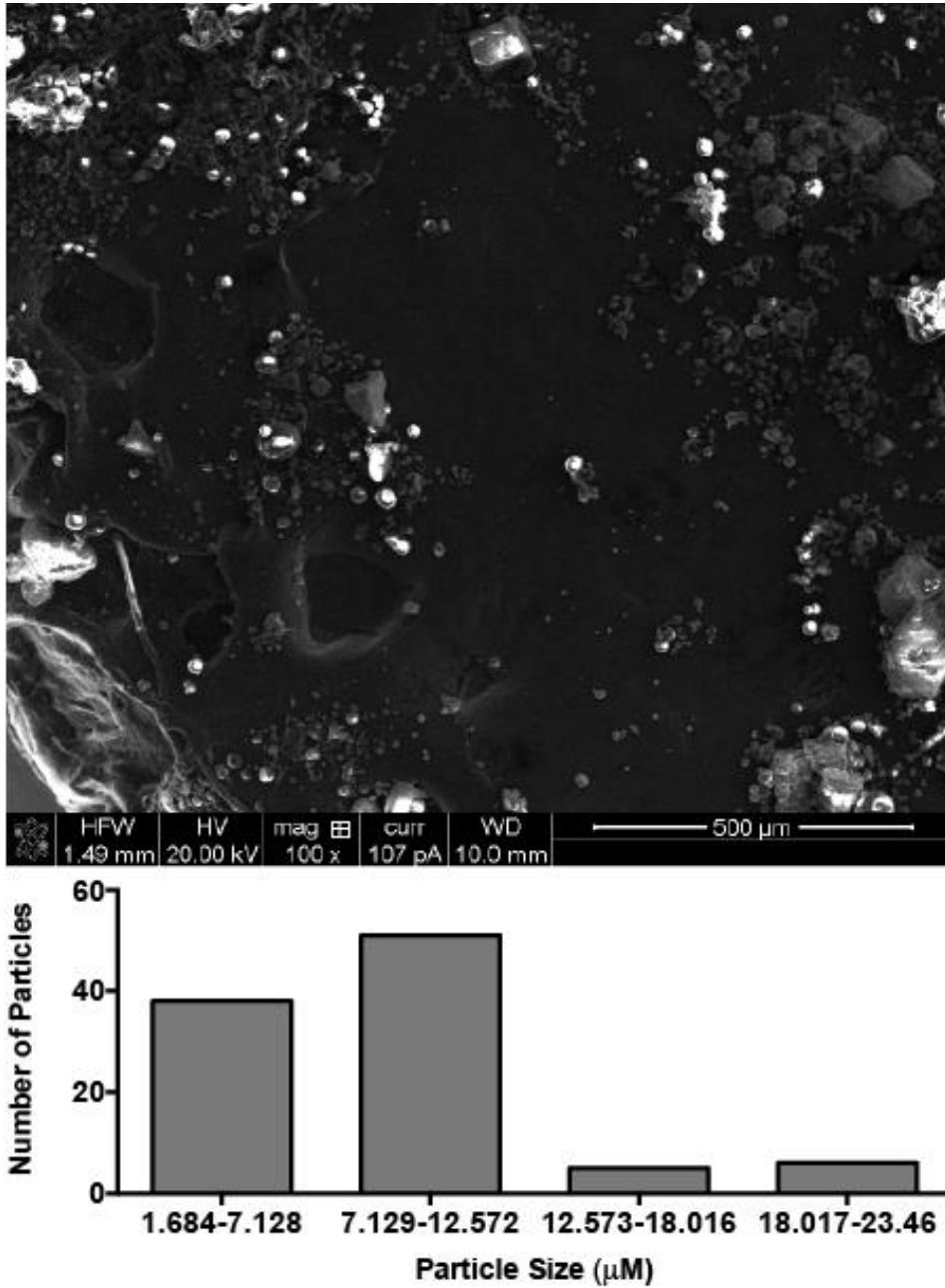


Figure C19. SEM image of coated PE particles 100x with histogram of particle size distribution.

PE coat continued

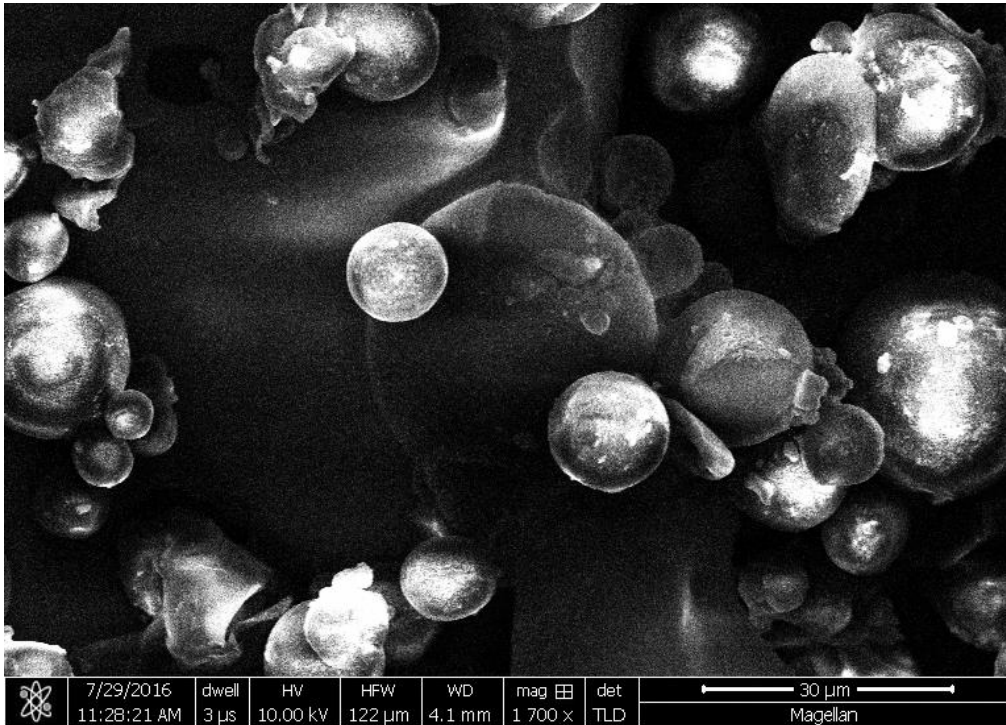


Figure C20. SEM image of coated PE particles 1,700x.

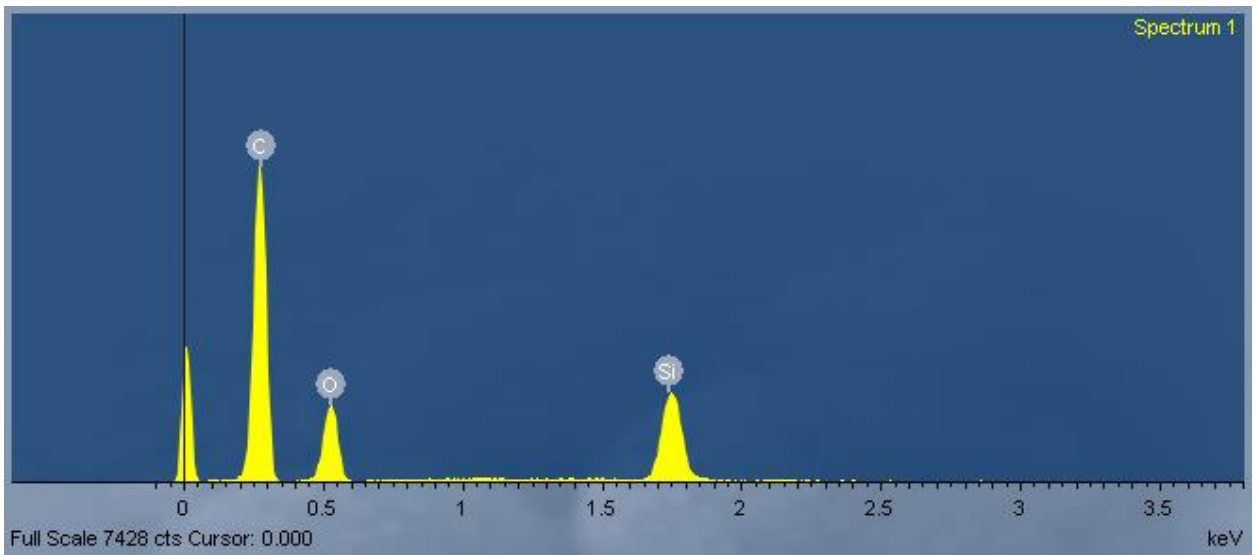


Figure C21. EDS data of coated PE particles.

PE

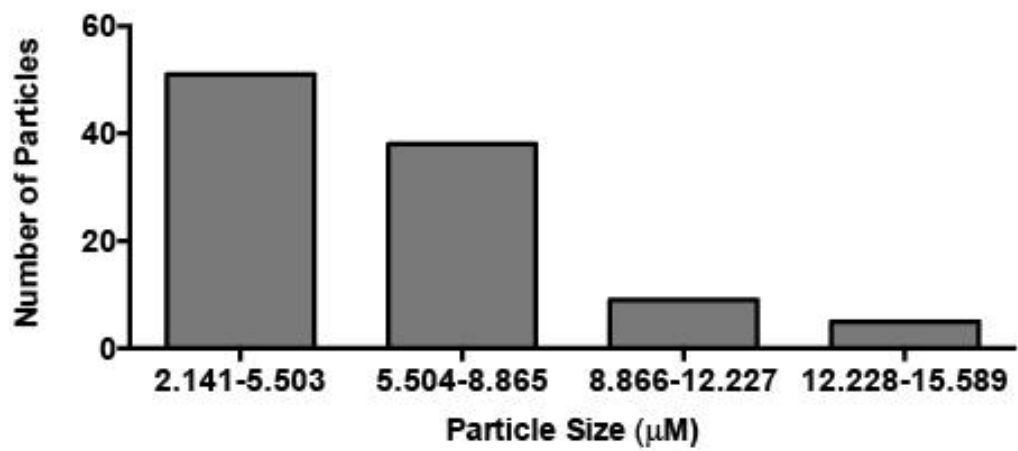
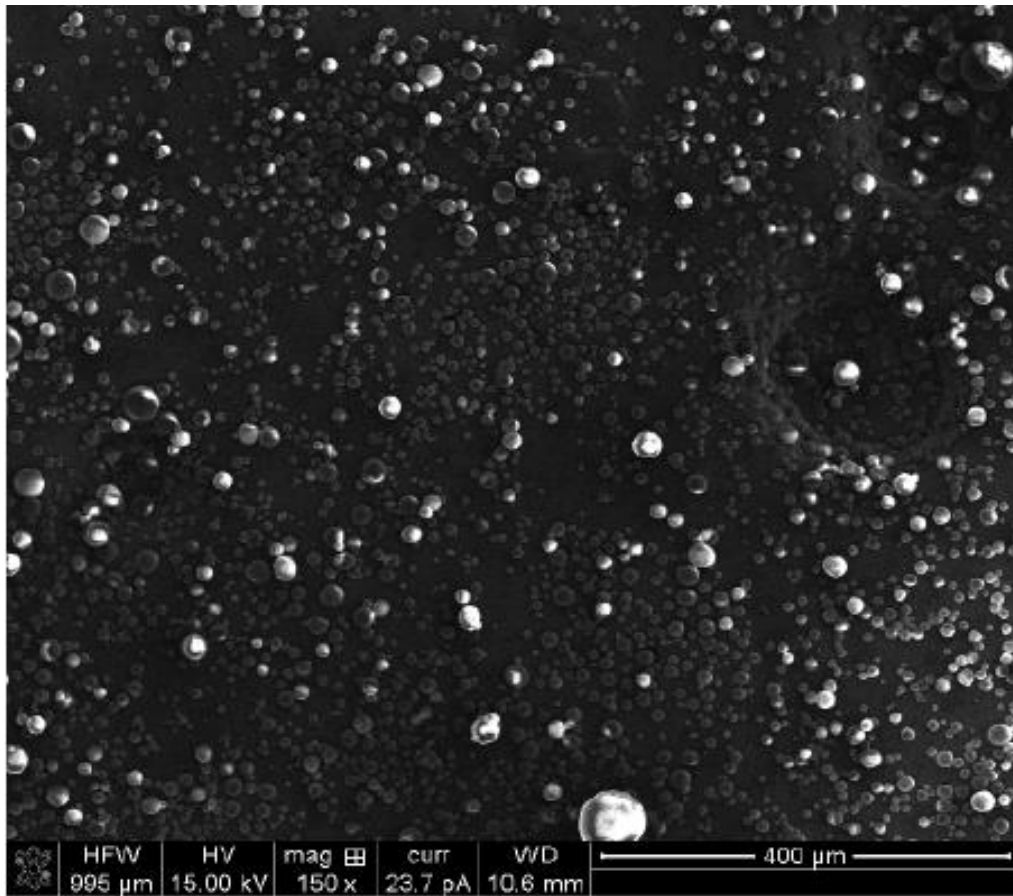


Figure C22. SEM image of PE particles 150x with histogram of particle size distribution.

PE continued

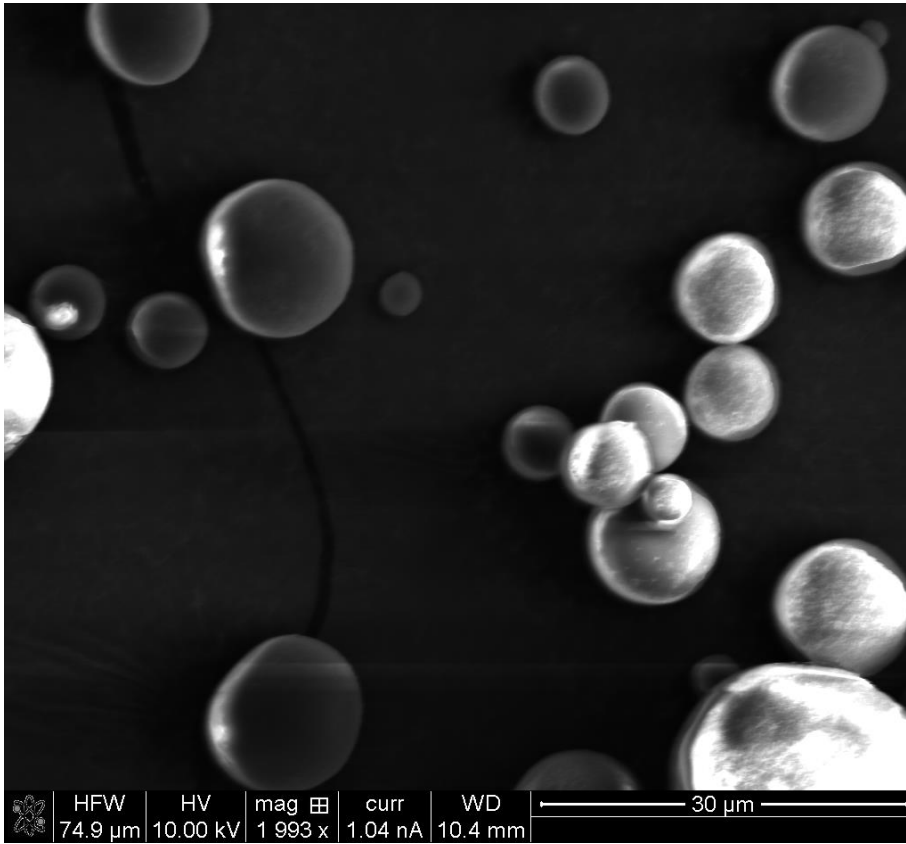


Figure C23. SEM image of PE particles 1,993x.

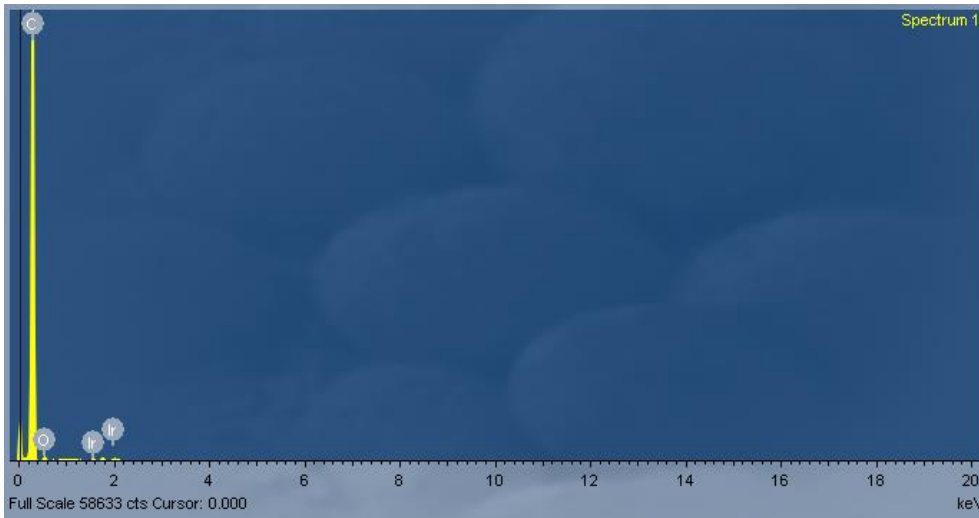
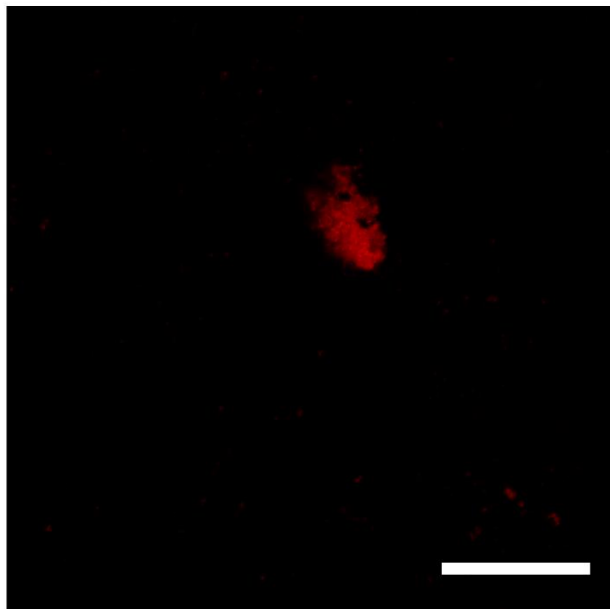


Figure C24. EDS of PE particles sputtered with Ir.

Particle	Size (micron)	Zeta Potential (mV)	Silicon (EDS)
PS	1.36	0.396	No
PS coat	1.62	-22.9	Yes
PMMA	4.94	0.316	No
PMMA coat	7.21	-23.8	Yes
PLGA	3.19	-0.833	No
PLGA coat	5.14	-2.02	Yes
PE	4.57	-21.2	No
PE coat	7.35	-33.8	Yes

Table C1. Table of DLS, Zeta potential and EDS data.

Fluorescence



Merge

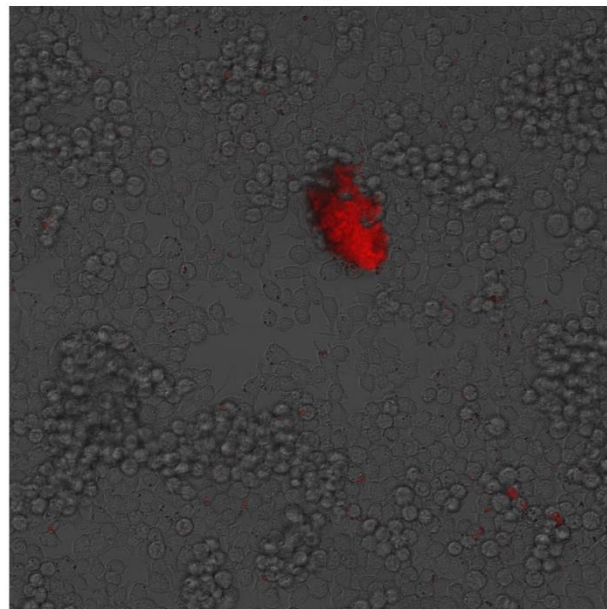


Figure C25. Confocal microscopy image of PS-CpG beads at 20x magnification. Scale bar:
100 μm .

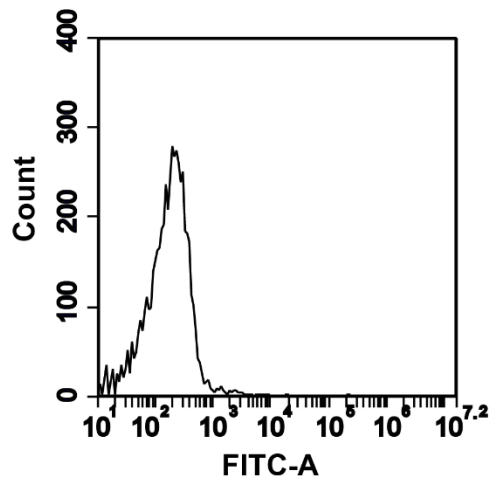


Figure C26. Flow cytometry plot of unlabeled PS particle.

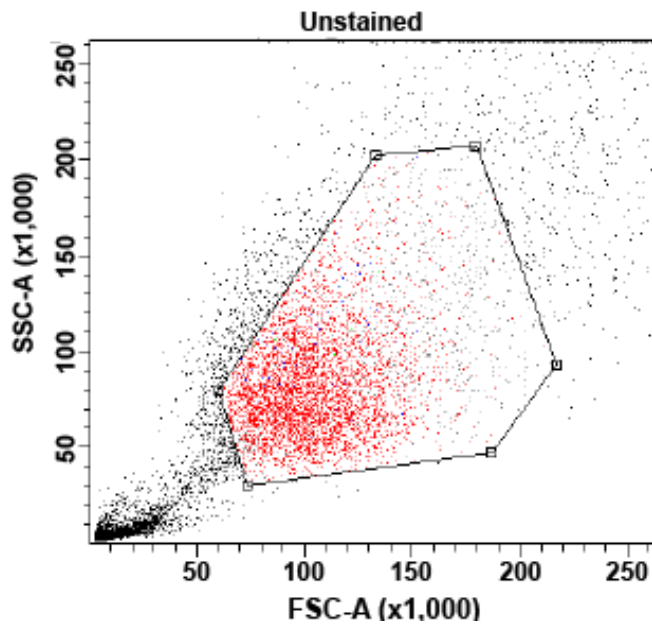


Figure C27. Flow cytometry gating for cells vs. beads using forward scatter vs. side scatter.

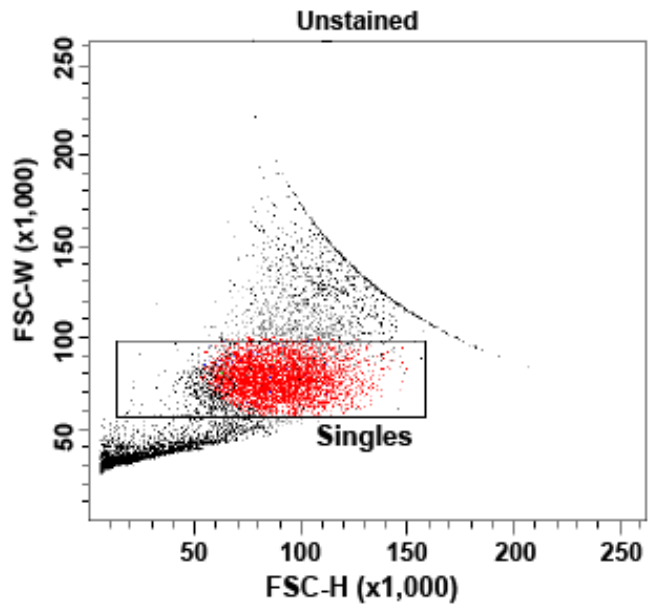


Figure C28. Forward scatter height vs. forward scatter width was used to distinguish single cells. Gating from figure S27 was applied prior to doublet discrimination.

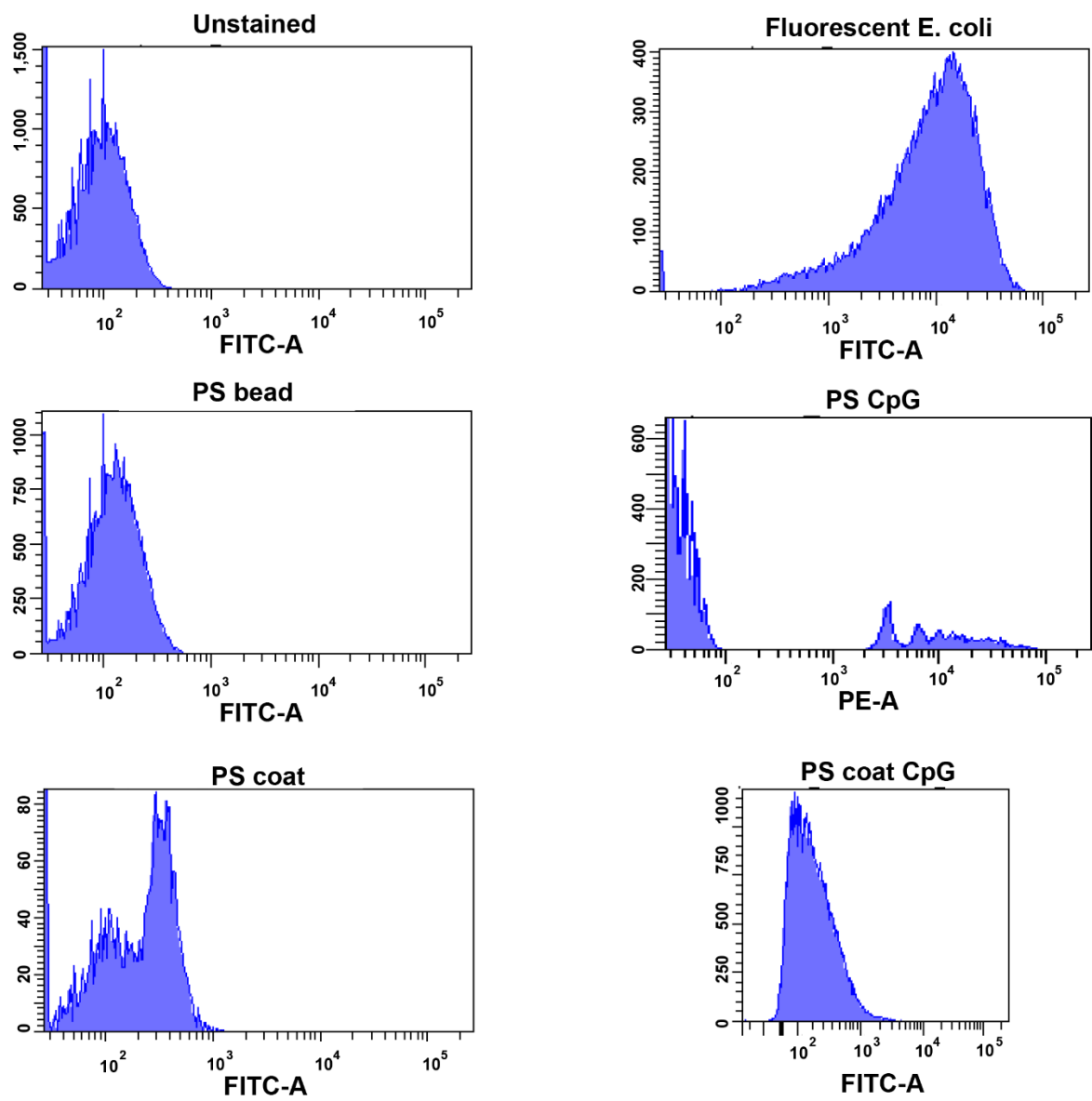


Figure C29. Flow cytometry histograms showing fluorescence of unstained and fluorescent E.coli (top), PS bead and PS-CpG (middle), and PS coat and PS coat functionalized with CpG (bottom).

Appendix D: Chapter 5

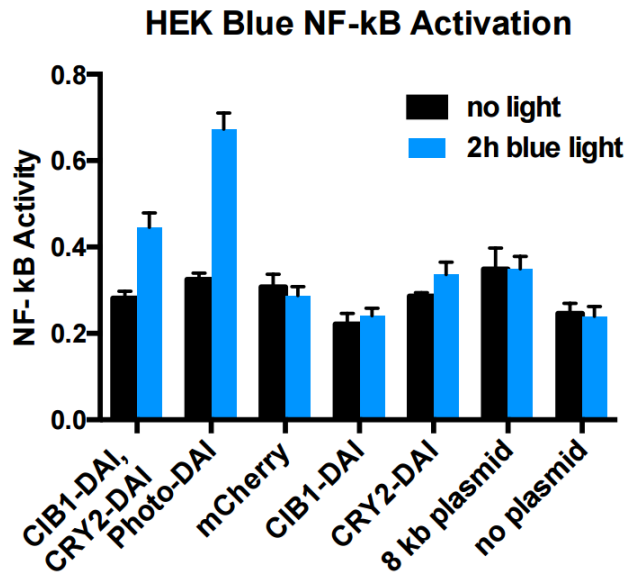


Figure D1. Photo-DAI activity in HEK Blue cells.

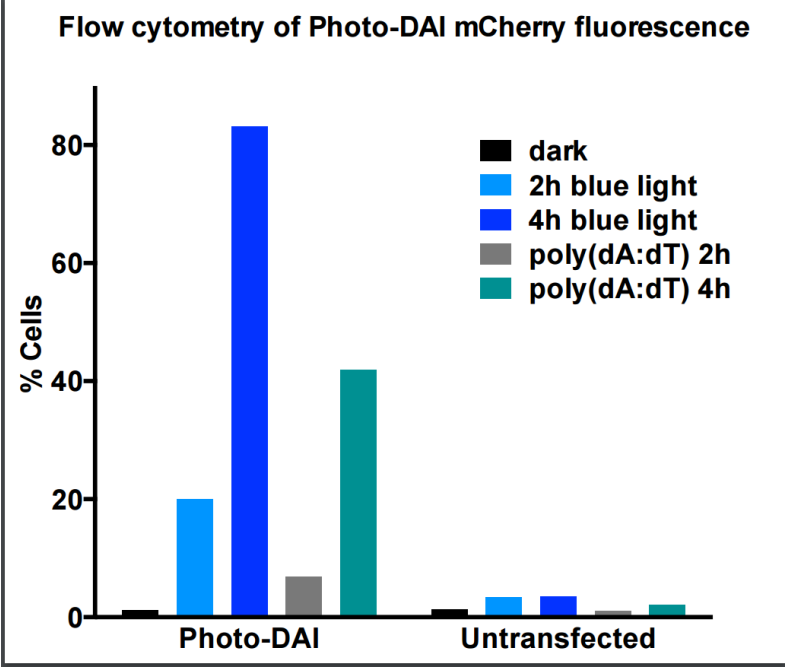


Figure D2. Flow cytometry analysis of mCherry fluorescence from photo-DAI activation using light or 100 ng/ mL poly(dA:dT).